

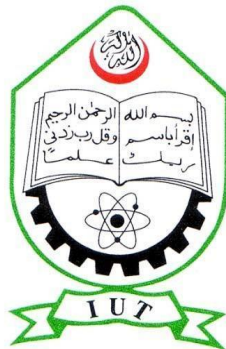
Design of a Highly Sensitive Photonic Crystal Fibre Sensor for Detecting Biochemical Analytes

by

Fariba Tabassum Dola (190021303)
S M Azmain Awsaf (190021315)
Jubair Mahamud Apon (190021333)

A Thesis Submitted to the Academic Faculty in Partial Fulfillment of the requirements for the Degree of

BACHELOR OF SCIENCE IN ELECTRICAL AND ELECTRONIC ENGINEERING

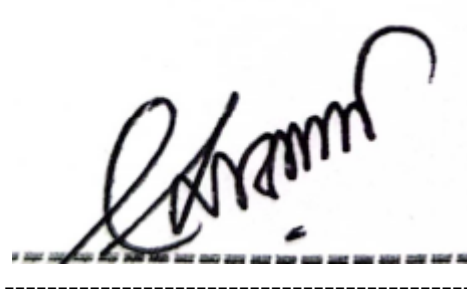


Department of Electrical and Electronic Engineering
Islamic University of Technology (IUT)
Gazipur, Bangladesh

June 2024

Design of a Highly Sensitive Photonic Crystal Fibre Sensor for Detecting Biochemical Analytes

Approved by:



A handwritten signature in black ink, appearing to read 'Rakibul Islam', is written over a dashed horizontal line. Below the dashed line is a solid horizontal line.

Prof. Dr. Mohammad Rakibul Islam

Supervisor and Professor,
Department of Electrical and Electronic Engineering,
Islamic University of Technology (IUT),
Boardbazar, Gazipur-1704.

Date:

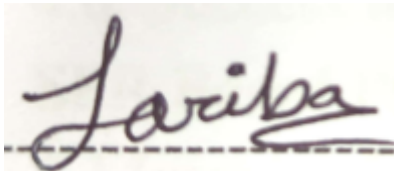
DECLARATION OF AUTHORSHIP

We, Fariba Tabassum Dola (190021303), S M Azmain Awsaf (190021315), and Jubair Mahamud Apon (190021333), hereby declare that the thesis called “DESIGN OF A HIGHLY SENSITIVE PHOTONIC CRYSTAL FIBRE SENSOR FOR DETECTING BIOCHEMICAL ANALYTES” and all the information contained therein are the results of our efforts and original contributions.

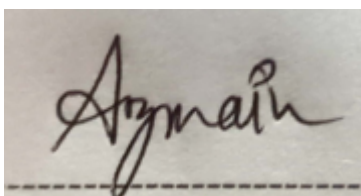
We confirm that:

- This work has been completed in partial fulfillment of the prerequisites for the Bachelor of Science in Electrical and Electronic Engineering degree at the Islamic University of Technology.
- The contents of this thesis have never before been submitted to a university to earn another degree.
- When consulting published work by others, we consistently provide due credit to the sources

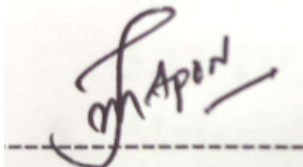
Signatures of Students:

A handwritten signature in black ink on a light-colored background, reading "Fariba". The signature is written in a cursive style and is positioned above a horizontal dashed line.

Fariba Tabassum Dola
Student ID: 190021303

A handwritten signature in black ink on a light-colored background, reading "Azmain". The signature is written in a cursive style and is positioned above a horizontal dashed line.

S M Azmain Awsaf
Student ID: 190021315

A handwritten signature in black ink on a light-colored background, reading "Jubair Apon". The signature is written in a cursive style and is positioned above a horizontal dashed line.

Jubair Mahamud Apon
Student ID: 190021333

Table of Contents

1. Background	
1.1 Background	11
1.2 Problem Statement	13
1.3 Research Objective	13
1.4 Motivation	14
1.5 Thesis Framework	
2. Literature Review	17
3. Photonic Crystal Fiber	
3.1 Introduction	22
3.2 PCF in Brief	22
3.2.1 Classification of PCF	23
3.2.2 High Index Guiding Fibers	23
3.2.3 The Bandgap effect	24
3.2.4 Hollow-Core and Solid-Core Fibers	24
4. Surface Plasmon Resonance	
4.1 Introduction	25
4.2 Working Principle of SPR	25
4.3 Reason of Interest in SPR Technology	26
4.4 Implementation of SPR	26
4.5 Advantages of SPR	26
4.6 Success Rate and Drawbacks	27
5. SPR Based PCF Sensors	
5.1 Introduction	27
5.2 Prism based Sensor	28
5.3 Internal Sensing based Sensor	28
5.4 D-shaped Sensor	28
5.5 External Sensing based Sensor	29
5.6 Plasmonic Material Silver based Sensor	29
5.7 Bimetallic Silver-Graphene based Sensor	29
5.8 Bimetallic Silver-Gold based Sensor	30
5.9 Bimetallic Silver-TiN based Sensor	30
5.10 Plasmonic Material Gold based Sensor	30
5.11 Bimetallic Gold-TiO ₂ based Sensor	30
5.12 ITO based Sensor	31
6. Material Characterization and Mathematical Formulation	
6.1 Introduction	31
6.2 Characterization of Materials	32

6.2.1 Silica (SiO ₂)	32
6.2.2 Air	35
6.2.3 Gold	35
6.3 Performance Parameters	36
6.3.1 Confinement Loss (CL)	37
6.3.2 Amplitude Sensitivity (AS)	37
6.3.3 Wavelength Sensitivity (WS)	37
6.3.4 Resolution	38
6.3.5 Birefringence	38
6.3.6 Full Width at Half Maximum (FWHM)	38
6.3.7 Figure of Merit (FOM)	39
6.3.8 Sensor Length	39
6.3.9 Temperature Sensitivity	39
6.3.10 Resolution (Temperature)	40
6.3.11 Strain Sensitivity	40
7. Proposed Design	
7.1 Introduction	41
7.2 Structural Modelling	42
7.3 Experimental Setup	43
7.4 Sensor Structure	45
7.5 Structure Optimization	45
7.6 Thickness of Gold Layer Optimization	46
7.7 Air Hole Diameters Optimization	47
7.7.1 Bigger Air Hole Optimization	47
7.7.2 Smaller Air Hole Optimization	49
7.8 Performance of the Sensor with Optimized Parameters	50
7.8.1 Scope of analyte RI detection:	50
7.8.2 Maximum Wavelength Sensitivity:	52
7.8.3 Minute Wavelength Resolution:	53
7.8.4 High Amplitude Sensitivity:	53
7.8.5 Regression Analysis of our Proposed Design:	54
8. Fabrication of The Sensor	
8.1 Introduction	55
8.2 Fabrication Method	56
8.3 Fabrication of our Proposed Design	56
8.4 Fabrication Tolerance of our Proposed Design	57
8.5 Comparative Study of our Proposed Design	58
8.6 Conclusion	60
9. Demonstration of Outcome Based Education	
9.1 Introduction	61
9.2 Course Outcomes (COs) Addressed	61

9.3 Aspects of Program Outcomes (POs) Addressed	65
9.4 Knowledge Profiles (K3-K8) Addressed	69
9.5 Complex Engineering Problems and Their Solutions	70
9.6 Socio-Cultural, Environmental, And Ethical Impact	72
Socio-Cultural Impact	72
Environmental Impact	72
Ethical Considerations	72
9.7 Attributes of Ranges of Complex Engineering Problem Solving (P1-P7) Addressed	73
Depth of Knowledge Required	74
Range of Conflicting Requirements	74
Depth of Analysis Required	74
Familiarity of Issues	74
Extent of Applicable Codes	74
Extent of Stakeholder Involvement and Conflicting Requirements	75
Interdependence	75
9.8 Attributes of Ranges of Complex Engineering Activities (A1-A5) Addressed	75
Range of Resources	75
Level of Interaction	76
Innovation	76
Consequences for Society and the Environment	77
Familiarity	
References	77

ACKNOWLEDGEMENTS

"In the Name of Allah, the Most Beneficent, the Most Merciful. All the praises and thanks be to Allah, the Lord of the 'Alamin (mankind, jinns and all that exists)."

We are grateful to ALLAH (SWT), the most benevolent and kind to provide us the health strength and ability to research and write this dissertation.

We extend our cordial gratitude to our honorable thesis supervisor Prof. Dr. Mohammad Rakibul Islam, Department of Electrical and Electronic Engineering, Islamic University of Technology for his constant support, unwavering patience, and nurturing guidance. His experience, mentorship, and fruitful contributions were critical to the efficacy of our thesis. We are very grateful for his contributions to the conceptual investigations, pertinent efforts, and overall thesis book drafting.

We express our heartfelt appreciation to our friends and families, especially our parents for their continuous support and dedication towards our life, which has played a pivotal role in our journey towards accomplishing our goals. Their constant encouragement has been instrumental in shaping us into the individuals we are today, and without their steadfast belief in us, our achievements would not have been possible.

ABSTRACT

We proffer in this research a distinctive, facile to fabricate, and highly sensitive photonic crystal fiber (PCF) biosensor based on the phenomenon of surface plasmon resonance (SPR). Our prototype has a strategic pattern of circular air holes inside the fiber, which leads to a superior sensing performance. The evaluation of all the sensor characteristics has been discharged by employing the finite element method (FEM) of COMSOL Multiphysics. The gold (Au) layer just around the fiber acts as the plasmonic material. After the optimization of all the fiber parameters, we derived a maximum amplitude sensitivity (AS) and wavelength sensitivity (WS) of 2202.64 RIU^{-1} and $140,500 \text{ nm/RIU}$, respectively, with a maximum sensor resolution 7.11×10^{-7} for wavelength and 4.54×10^{-4} for amplitude. Moreover, the maximum figure of merit (FOM) procured was 2285. The overall analyte sensing range is from refractive indices 1.31 to 1.40, and the sensor has a fabrication tolerance limit of $\pm 5\%$ for the gold layer variation and $\pm 2.5\%$ for both of the air holes. With its enhanced performance in terms of sensitivity, we believe that this SPR-based PCF biosensor can potentially contribute to the detection of unknown analytes and in applications of medical diagnostics.

List of Figures

Figure 1.1: A biosensor's schematic representation.....	13
Figure 3.1: Cross-sectional view of a Photonic Crystal Fiber.....	30
Figure 3.2: Cross-sectional view of (a) Solid Core Fiber, (b) Hollow Core Fiber.....	32
Figure 4.1: A light is impacted by a prism on a metal film and the reflected beam is captured and analyzed	33
Figure 5.1: Internal Sensing based Sensors.....	37
Figure 5.2: D-shaped Sensors.....	39
Figure 5.3: (a) External Sensing based sensor, (b) Silver based sensor, (c) Silver-Graphene based sensor, (d) Silver-Gold based sensor.....	40
Figure 5.4: (a) Silver-TiN based sensor, (b) Gold based sensor, (c) Gold-TiO ₂ based sensor, (d)ITO based sensor.....	42
Figure 6.1: Intrinsic losses of silica	44
Figure 6.2: Silica RI as a function of light wavelength (temperature 25 °C).....	55
Figure 6.3: Silica RI as a function of temperature (light wavelength 600 nm).....	46
Figure 6.4: Silica RI as a function of strain (light wavelength 600 nm, temperature 25°C).....	47
Figure 6.5: Air RI as a function of light wavelength.....	47
Figure 6.6: Gold RI as a function of light wavelength.....	48
Figure 6.7: Representation of Full Width at Half Maximum.....	51
Figure 7.1: Structural Model of the Proposed Design.....	55
Figure 7.2: EM field dispersal of (a) Core Mode (b) SPP Mode.....	58
Figure 7.3 : Loss Curve for Gold Layer Optimization.....	59
Figure 7.4: Amplitude vs Wavelength Sensitivity for Gold Layer Optimization.....	59
Figure 7.5: Loss Vs. Wavelength Curve due to Bigger Air Hole Optimization.....	61

Figure 7.6: Amplitude Sensitivity Vs. Wavelength Curve due to Bigger Air Hole Optimization.....	61
Figure 7.7: Loss Vs. Wavelength Curve due to Smaller Air Hole Optimization.....	62
Figure 7.8: Amplitude Sensitivity Vs. Wavelength Curve due to Smaller Air Hole Optimization.....	63
Figure 7.9: Loss Vs. Wavelength Comparison according to RI.....	66
Figure 7.10: Amplitude Sensitivity Vs. Wavelength Comparison for different RI.....	67
Figure 7.11: Regression Analysis of the Proposed Design.....	68
Figure 8.1: Loss Vs Wavelength for 5% Variation of the Gold Layer thickness.....	71
Figure 8.2: Loss Vs Wavelength for 2.5% Variation of the Small Circle Diameter.....	72

List of Tables

Table 6.1: Sellmeier Constants.....	35
Table 7.1: Scope of Analyte RI Detection.....	53
Table 8.1: Comparative Study between the existing works and our proposed design.....	68

List of Acronyms

AI	Amplitude Interrogation
ALD	Atomic Layer Deposition
AS	Amplitude Sensitivity
AZO	Aluminium doped Zinc Oxide
CL	Confinement Loss
CVD	Chemical Vapor Deposition
DNA	Deoxyribonucleic Acid
DWDM	Dense Wave Division Multiplexing
EM	Electro-Magnetic
EML	Effective Material Loss
FEM	Finite Element Method
FOM	Figure of Merit
FWHM	Full Width at Half Maximum
HDPE	High Density Poly Ethylene
IR	Infra-Red
ITO	Indium Tin Oxide
m-RNA	Messenger RNA
PBG	Photonic Band Gap
PCF	Photonic Crystal Fiber
PML	Perfectly Matched Layer
PMMA	Poly Methyl Methacrylate
RI	Refractive Index
RIU	Refractive Index Unit

RNA	Ribonucleic Acid
RW	Resonance Wavelength
SPP	Surface Plasmon Polariton
SPR	Surface Plasmon Resonance
SPW	Surface Plasmon Wave
TiN	Titanium Nitride
TIR	Total Internal Reflection
TM	Transversely Magnetic
WI	Wavelength Interrogation
WS	Wavelength Sensitivity

CHAPTER 1

INTRODUCTION

1.1 Background

A biosensor is an analytical device that integrates a biological sensing element (enzyme, antibody, or nucleic acid) with a physical transducer (mass, optical, or electrochemical), where the resultant signal is further turned into an electronic one (figure 1.1). [1]. Biosensors' application field has expanded tremendously in recent years as a result of its strong and sophisticated research potential. Biosensors may be classified into six types depending on the signal transduction method: mass, optical, magnetic, electrochemical, thermal, and micromechanical sensors. The optical sensors [2–5] are the most amazing breakthroughs in sensing applications. Optical biosensors have specific benefits over conventional profiling methods used to monitor and analyze molecular interactions. It is the most prevalent sort of biosensor that has caught the researcher's interest. The biosensor has been referred to as an analytical device that integrates a biological sensing element (enzyme, antibody, or) for the past couple of decades due to its wide range of applications in various established fields such as drug discovery, healthcare, food quality control, biotechnology industry, and environmental safety monitoring [6]-[10]. It has immediate sensing capabilities, making it a highly efficient and modern sensor. Furthermore, the sensors' compact size, high sensitivity, accuracy, immunity to external disturbance, and cost-effectiveness have made them a popular choice among the research community.

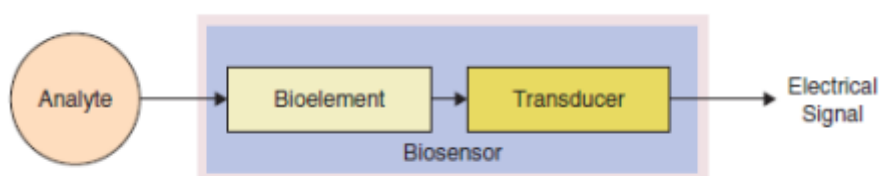


Figure 1.1: A biosensor's schematic representation

Corning Glass Works created optical fiber in 1970. Then, GaAs semiconductor lasers were developed to transmit light across fiber optic networks. Following that, in 1975, the initial fiber optic framework was developed, which used GaAs semiconductor lasers. The second age of fiber optic communication began in the mid-1980s, when scientists experimented with InGaAsP semiconductor lasers. With technological advancements, fiber optic communication has now reached its fifth age, with correspondence frameworks using the DWDM (Dense Wave Division Multiplexing) approach to increase data speeds. Optical biosensors are mostly dependent on the strength of light or magnetic fields produced by biological interactions. The primary operating concept of this biosensor is to convert incident light rays into electrical signals capable of detecting the strength of electromagnetic waves and sensing changes in the related analyte. The scientists used a variety of methods, including interferometry (reflectometric white light interferometry [11] and modal interferometry in optical waveguide structures [12]), fluorescence spectroscopy [13], spectroscopy of guided modes of optical waveguides (grating coupler [14], resonant mirror [15]), and surface plasmon resonance (SPR) [6], [16]. This optical technology may be classified into two types based on its sensing methodology. The first is a label optical biosensor, which comprises fluorescence-based biosensors that need several detection techniques. This technique also includes washing processes and reagent additions. However, it has several disadvantages, such as toxic waste, reduced efficiency, short-term stability, time consumption, biomolecule degradation, and so on. The other one is well-known for its label-free technology. It can provide real-time monitoring without the requirement for labeling. Furthermore, this technology may provide a signal directly without the need for additional probes with labels to deliver the signals [17, 18]. SPR, resonant mirrors, and interferometers use label-free technologies to improve accuracy and efficiency. SPR-based optical sensors have played a significant role in the advancement of fiber-optic communication. Over the last few decades, surface plasmon resonance-based biosensors have had a significant influence on a wide range of real-world applications. Surface plasmons are described as the development of a quantized TM (transversely magnetic) p-polarized electromagnetic wave caused by the coupled oscillation of electrons occurring at the metal-dielectric contact [19]. Surface plasmon resonance occurs when the incident wave's wave vector matches that of the surface plasmon [20]. SPR is primarily caused by the incidence of a transverse magnetic (TM) wave, which excites electrons at the metal-dielectric contact. As a result, a surface plasmon wave (SPW) emerges and propagates across the core-cladding area. In this case, at a specific wavelength, leaky

core mode couples with surface plasmon polariton (SPP) mode. This wavelength is referred to as resonance wavelength λ (RW), and the condition is known as the phase-matching condition [21]. The analyte refractive index (RI) influences the SPP mode and phase-matching state, and a little change in the ambient RI might cause the RW to diverge to a higher or lower wavelength. Thus, the analyte may be precisely recognized by observing the variation of the resultant RW while considering various analyte RI [22]. SPR-based optical sensors have piqued the interest of researchers due to their distinct and well-established properties, high resilience, small and uncomplicated probe construction, and increased sensitivity. Because of its favorable nature, SPR sensors are being examined in a variety of domains, such as preserving water quality and food safety. Because of their advantageous behavior, SPR sensors are being investigated in a variety of fields, including water quality monitoring, food safety observation, glucose inspection, medical diagnostics, real-time monitoring, gas detection, biosensing, strain sensing, and temperature sensing [6]-[10], [23]-[27]. Furthermore, SPR technology enables the combination of nano-electronic and nano-photonics components, resulting in ultra-compact optoelectronic devices [28], [29]. The study of SPR-based biosensors began in 1983 when Liedberg et al. developed SPR biosensors in the domains of gas detection and biosensing [23] and described the prism-coupling approach. Prism-based SPR sensors use the point cross-examination approach. However, the prism-based SPR sensor is unsuitable for use in distant sensing since it has several optical and mechanical components, making the sensor unwieldy in size. To address these limitations, researchers have replaced the prism with fiber, which has gained popularity due to promising properties such as atypical dispersion, high nonlinearity, endless single-mode behavior, label-free detection, adjustable high birefringence, and high integrity and portability [30], [31]. Thus, fiber-based sensors are appropriate for distant sensing. Following extensive study, an upgraded version of the sensor is developed, known as a photonic crystal fiber (PCF)--based SPR sensor. It has higher sensitivity and lower resonance peaks than conventional fiber-based sensors [32–37], resulting in greater accuracy when detecting an unknown analyte. Furthermore, the PCF-based sensors may certainly claim a greater authority on the transient field by adjusting structural factors like pitch, the bore of the air holes, and the total count of various shaped rings and air cavities.

1.2 Problem Statement

Researchers are interested in SPR sensors due to its potential for many sensing applications and promising properties. SPR-based optical sensors have been studied extensively. Sensors primarily use two types of sensing systems. The traditional kind of PCF sensor is internally metal-coated, which involves coating the metal film internally [38]. The drawbacks of this technique include the time-consuming process of emptying and refilling the fiber. Furthermore, the thin interior coating complicates manufacture and structural design. It requires additional procedures and maintenance to function optimally, making it unsuitable for easy sensing. A D-shaped PCF sensor with enhanced construction is proposed to overcome obstructions. However, this sort of sensor increases manufacturing complexity [39]. To get a correct output, the flat piece requires precise polishing, making the production process both challenging and costly.

The contemporary sensing technique is the externally metal-coated PCF, which places the metal coating outside the fiber. Gold, silver, and aluminum are the most often utilized plasmonic materials for sensing processes. Oxidation of plasmonic materials in an aqueous environment can reduce sensing accuracy [40]. The placement and size of air holes impact the sensor's manufacturing complexity and cost. To summarize, the limitations of previously described SPR-based sensors are:

The drawbacks of previously published SPR-based sensors are summarized below:

- Complex design
- Fabrication challenges
- Increased confinement loss
- Weak evanescent field
- Inaccurate sensing behavior
- Expensive costing

1.3 Research Objective

The optical sensors' initial phase focused on the transmission sector. However, the most recent EML value (0.009) is the lowest [41]. Further reducing the value is pointless since it will complicate the design structure. The same scenario applies to confinement loss and other factors. As a result, the transmission field has reached saturation, leaving little room for

improvement. Researchers are shifting their focus away from transmission applications in favor of SPR, which offers more promising research options.

Our research aimed to explore the impact of innovative PCF biosensor designs based on SPR.

The research goals are as follows:

- Measure amplitude sensitivity (AS) and wavelength sensitivity (WS) as refractive index changes the wavelength range.
- Conducting extensive literature review on SPR sensors.
- Using plasmonic materials outside of the PCF structure improves detection accuracy and performance.
- Analyzing the impact of tiny parameter changes on performance and graphics.
- Simulated various parameters by varying the thickness of fiber layers, including gold, titanium dioxide (TiO₂), and analyte.
- Comparison of our proposed PCF-SPR sensors with other sensors from various journals.

1.4 Motivation

Researchers have emphasized the benefits of SPR-based PCF sensors. The sensitivity of this sensor depends on the evanescent field sent toward the cladding region through the core. This causes free electrons to oscillate, resulting in SPW along the metal-dielectric surface. When phase matching occurs, even little changes in analyte RI can have a significant impact. Changing the RI causes oscillations in RW, which may be shown graphically. SPR is considered an unexplored field. This sector has significant potential for additional development. As a result, scientists continue to work to maximize its utility. These biosensors offer sensitive, compact, and high-frequency monitoring without the need for time-consuming sample preparation. These sensors have a wide range of applications, including biochemistry, biotechnology, healthcare, and security. This technique's versatility allows for wide-ranging ramifications. Therefore, it's important to prioritize the development of this technology. This sensor's proven analytical process produces accurate results in a few minutes, unlike prior sensors that were sensitive, time-consuming, and costly to maintain. These biosensors can detect bacteria, viruses, antibodies, DNA, mRNA, RNA, hormones, hemoglobin, and proteins. Future research potential includes applications in electronics,

physics, medical analysis, and software, indicating promising behavior. Currently, SPR is considered the most promising scientific field.

1.5 Thesis Framework

This thesis report is constructed with eleven distinct chapters. A brief synopsis of the upcoming ten chapters is provided in this section.

Chapter 2; provides a full examination of PCF and its categories. This part also examines the historical context. The reasons for the development of PCF-based sensors, as well as their superiority over alternative approaches, are discussed here. Finally, the methodology, approach, and software used to generate the graph and simulations are described.

Chapter 3; provides a brief introduction of SPR technology. Here, information on the operating principle of SPR is mentioned. This chapter also provides an overview of the evanescent field, SPP, SPW, resonance, and SPR-based sensor application.

Chapter 4; offers an analysis and thorough information on SPR-based PCF sensors and why they have become a popular choice among the researcher community. Different types of sensors, such as prism-based, D-shaped, and sensors based on multiple sensing approaches (internal and external), are also discussed. This article compares many types of sensors that use the plasmonic materials gold and silver, as well as the need for additional coatings (graphene, TiN, and TiO₂).

Chapter 5; discusses the fundamental concepts and equations that are important for optimization and analysis. The Sellmeier equation (for silica RI), the Drude-Lorentz model equation (for gold RI), and the equation for TiO₂ RI are all defined. Important criteria for maximizing sensor performance include FOM, amplitude sensitivity, confinement loss, wavelength sensitivity, resolution, birefringence, 7 sensor length, strain, and temperature sensitivity, all of which are described in this chapter.

Chapter 6: discusses the design and theoretical modeling of an SPR-based PCF, including parameter optimization, dispersion characteristics, sensor calibration, sensor length

expansion, resolution, linearity, double resonance, DPSS performance, and comparison to previous work.

Chapter 7: The manufacturing of the sensor is proposed here. The article discusses the stack and draw approach and CVD technology.

Chapter 8: This chapter concludes the thesis book. A summary of future goals has been offered.

Chapter 9: Description of the CO-PO attributes of the thesis is provided in this section.

CHAPTER 2

LITERATURE REVIEW

In the field of optical communication and bio-sensing, SPR based PCFs have proven to be immensely effective for myriad applications[17][18]. When a photon beam falls on the core of the PCF, the electromagnetic field reaches the region of the cladding in a partial manner due to which the surface electrons on the plasmonic materials get excited upon the interaction of the evanescent field with the plasmonic metal surface. When the frequency of the evanescent field matches with the frequency of the oscillation of the electrons on the surface, resonance phenomenon is created which gives rise to a CL peak. At resonant condition, highest energy transfer occurs between the core mode and the SPP mode and the real part of their refractive indices matches. A shift in the position of the peak at the resonant wavelength occurs when the variation of the RI of the analyte is observed. This propagates the way for a wide range of analyte detection using SPR-PCF sensors. The effectiveness of PCF-SPR sensors in the THz regime has paved the way for enhanced bio-sensing and improved THz waveguide propagation applications. The numerical study and proposition of a hollow-core PCF optical cancer detection sensor using Finite Element Method (FEM) in the COMSOL Multiphysics v5.5 environment have been performed that displays an extremely high RS of 99.9314%, 99.9257%, 99.9169%, 99.9277%, 99.9243%, and 99.9302%, with a reduced effective material loss of $8.09 \times 10^{-5} \text{ cm}^{-1}$, $8.79 \times 10^{-5} \text{ cm}^{-1}$, $9.88 \times 10^{-5} \text{ cm}^{-1}$, $8.55 \times 10^{-5} \text{ cm}^{-1}$, $8.96 \times 10^{-5} \text{ cm}^{-1}$, and $8.24 \times 10^{-5} \text{ cm}^{-1}$ for breast cancer type-2, cervical cancer, skin cancer, adrenal gland cancer, blood cancer, and breast cancer type-1 respectively at a frequency region of 3.0 THz, while displaying an extremely low confinement loss of $6.1 \times 10^{-10} \text{ dB/cm}$ [19]. A sectored circular PCF having topas as background material has been proposed that displays an average sensitivity is 92.14% and CL value of $2.308 \times 10^{-9} \text{ cm}^{-1}$ along with EML values of 0.009598/cm for RI=1.33, 0.009620/cm for RI=1.34, 0.009624/cm for RI=1.35, 0.009658 cm^{-1} for RI=1.36, 0.009694 cm^{-1} for RI=1.37 at 1.5 THz frequency[20]. Moreover, Rahman et al. conducted the numerical investigation of a with octagonal hollow-cored PCF structure surrounded by symmetrical air holes in the cladding capable of improving the identification of all tested blood components (RBC, hemoglobin, WBC, plasma, and water) by nearly 99 % with the attainment of a negligible CL value of 10–16±1 dB/cm at 4.5 THz operating frequency[21]. Furthermore, 19 Rahman et al. again

proposed a PCT geometry with polarization maintaining attributes while displaying extremely low EML of 0.013/cm and 0.020/cm in modes of x and y-polarization, respectively, a flattened dispersion value of ± 0.020 ps/THz/cm and ± 0.065 ps/THz/cm at frequency of 1 THz in the x and y-polarization modes respectively, and detecting liquid chemicals, such as, methanol, ethanol, benzene, and cholesterol, and air pollutants, such as, dioxin, cyanide, hydrogen sulfide, and nitrogen oxide [22]. Islam et al. have proffered a sensor with hexagonal outlined porous cladding with vacant core with high bi-refrindex value, capable of detecting cyanides at THz regime, utilizing Zeonex as the material in the background; the numerical investigation of the proposed sensor being performed using FEM exhibits very high sensitivity of 99.75%, extremely small confinement loss of 0.5×10^{-13} cm^{-1} , and a considerably low and flat dispersion of 0.12 ps/THz/cm[23]. Furthermore, a PCF sensor based on optical fiber with rectangular air holes in both the core and cladding has been demonstrated by Khan et al. which depicts low loss and increased sensitivity for the detection of volatile impurities in Ethanol with the highest efficacy. The simulation performed for the mentioned sensor using FEM exhibited RS of 99.15%, 99.36%, and 99.41% with confinement loss values of 5×10^{-17} dB/cm, 2×10^{-16} dB/cm and 1.17×10^{-17} dB/cm, Effective Material Loss (EML) of 0.00065 cm^{-1} , 0.00085 cm^{-1} , and 0.00068 cm^{-1} for Ethanol, Methanol, and Benzene respectively at 2.2 THz frequency band[24]. The experimentation of a Zeonex based hexagonal packing PCF sensor with a wheeled structure for porosities of 85%, 90%, and 98% in the regions of 0.2 to 2.0 THz has been performed; the sensor is capable of detecting cow and camel milk with RIs of 1.3459 and 1.3423 respectively and has shown the highest sensitivity of 81.16% and 81.32%, EML constituting values of 0.033013 cm^{-1} and 0.03284 cm^{-1} , trivial values of CL of $8.675 \times 10^{-18} \text{ cm}^{-1}$, $1.435 \times 10^{-18} \text{ cm}^{-1}$ for camel and cow milk respectively, a high value of 81.573% for core power fraction, and 0.256 as the numerical aperture value[25]. Moreover, a hexagonal cladding structured, Topas-based PCF sensor with hollow core and air cavities structured with square shapes in both the core and the cladding, investigated through FEM in COMSOL v5.3a software is presented by Islam et al. showing sensitivity of 99.39% for RBC, 99.27% for hemoglobin, 99.12% for WBC, 99.03% for plasma, and 98.79% for water, least CL of 1.124×10^{-15} dB/cm for RBC, 9.557×10^{-16} dB/cm for hemoglobin, 7.242×10^{-15} dB/cm for WBC, 1.114×10^{-16} dB/cm for plasma, and 2.515×10^{-15} dB/cm for water in y-polarization with optimized design conditions in the 2-5 THz frequency range along with optimal characteristics, such as, low EML, high bi-refrindex, increased effective area, extensively low and flattened dispersion, and large divergence of beam[26]. 20 Moreover, a PCF

biosensor with two hollow air cavities of square shape enclosed by four air channels of rectangular shape residing in the region of cladding has been proposed for an effective detection of amino acids using THz waves and the scrutiny of the sensor's characteristics applying FEM in COMSOL Multiphysics has depicted extremely high RS with values of 99.97% for phenylalanine, 99.98% for tryptophan and histidine, 99.95% for methionine, and 99.93% for lysine, extremely trivial CL values of $4.72 \times 10^{-22} \text{ cm}^{-1}$ for tryptophan along with other mentionable optical propagation properties, such as, low EML, enlarged effective modal area, and flat dispersion with near-zero value for optical design parameters at 3.4 THz frequency[27]. A fabrication-friendly hexagonal shaped THz PCF-based chemical sensor with a core that's hollow and air lattices that are symmetrically hexagonal in the cladding section that exhibits extensively elevated performance in THz regime (almost 99% at 3 THz) for the detection of ethanol, methanol, water, and benzene has also been proffered and the numerical investigation has been performed using FEM in COMSOL Multiphysics v.5.3a[28]. Furthermore, another Topas based PCF sensor with six head star structure, hexagonal shaped hollow core, and fabrication feasibility has been proposed by Mou et al. for methanol detection, which displays extensively high sensitivity of 98.4%, extremely low CL of $3.34 \times 10^{-19} \text{ cm}^{-1}$, and very low material absorption loss of 0.002 cm^{-1} at 3 THz operating frequency[29]. The performance analysis of an octagonal shaped hollow cored sensor having cladding structure with eight head stars for cholesterol detection in THz frequency regions using FEM in COMSOL Multiphysics has been performed and the proposed sensor displayed very high sensitivity of 98.75 %, CL as low as $3.14 \times 10^{-20} \text{ cm}^{-1}$, and EML value as low as 0.0008 cm^{-1} at the frequency of 2.2 THz [30]. A PCF design with octagonal shaped cladding design for THz transmission has been presented that exhibits an EML as low as 0.007 cm^{-1} at 0.5 THz frequency, an extremely high birefringence value of 0.06, a value of about $4 \times 10^{-6} \text{ m}^2$ for effective area, a value of 70 % for core power fraction with a diameter of 290 micro meter for the core having a core porosity of 80% at the frequency regime of 1.6 THz, and a flattened dispersion of variation $0.3 \pm 0.1 \text{ ps/THz/cm}$ within 0.7–2.1 THz which is a significantly large frequency range of [31]. Besides, Islam et al. proffered a PCF design with slotted core with unsymmetrical air holes structures for the achievement of a high modal bi-refrindex of 0.0911 and air holes arranged compactly in five hexagonal layers in the cladding region to attain a low EML value of 0.025 cm^{-1} .; the design exhibited core power fraction value of 52%, CL as low as $1.05 \times 10^{-13}/\text{cm}$, and a flat dispersion of $0.65 \pm 0.05 \text{ ps/THz/cm}$ in the 0.5 to 1.6 THz frequency range[18]. A fabrication 21 friendly PCF structure with a square core and four symmetrical air fragments in the cladding section

arranged in a circular manner suitable for THz sensing and waveguide application has been demonstrated by Mou et al. where the structure displays extremely low EML of 0.009 cm^{-1} , near zero 0.35 ps/THz/cm flattened $\pm 0.05 \text{ ps/THz/cm}$ dispersion for waveguide operation at 1 THz, an enhanced effective area of $9.56 \times 10^{-7} \text{ m}^2$, and a core power fraction as high as 53.159% at optimal design conditions. Additionally, the PCF design is capable of detecting toxic environmental pollutants with an incredible proportion of 91.5 %, 89.8 %, 89 %, 89.5 %, and 89.6 % for dioxin, toluene, hydrogen sulfide, nitrogen dioxide, and sodium cyanide respectively[32]. Rahman et al. have proposed another Topas based PCF geometry where core and cladding are compartmentalized by a few number of rectangles with air fragments of core and cladding arranged in a circular manner for ease of fabrication; numerical investigation using FEM in COMSOL Multiphysics v.5.3a depicted an extensively low EML of 0.0153 cm^{-1} , extremely flat dispersion of $\pm 0.010 \text{ (ps/THz/cm)}$, an ultra-low confinement loss of 0.0014 cm^{-1} at optimum 1 THz operating frequency, and an extensively flattened dispersion variation of $\pm 0.01 \text{ (ps/THz/cm)}$ [33]. Furthermore, Islam et al. have proposed a hollow cored Zeonex based PCF structure with an enhanced level of cladding asymmetry introduced by using a brick-like structure with identical square shaped air cavities and numerical investigation of the proposed fibre using FEM in COMSOL Multiphysics v.5.3 showed very high sensitivities of 98.6%, 98.7%, 98.8%, 98.83% and 98.9%, and ultra-low confinement loss of $5.5 \times 10^{-9} / \text{cm}$ for RI=1.33, $3.25 \times 10^{-9} / \text{cm}$ for RI=1.34, $1 \times 10^{-9} / \text{cm}$ for RI=1.35, $7.75 \times 10^{-10} / \text{cm}$ for RI=1.36, and $5.5 \times 10^{-10} / \text{cm}$ for RI=1.37 at optimal design conditions along with other favorable propagation characteristics, such as, enlarged effective modal area, very high birefringence, and an extremely low EML[34]. Rahman et al. has presented another air cored 450 rotational square lattice PCF design for THz waveguide which gives very low EML values of 0.016 cm^{-1} and 0.013 cm^{-1} at 1 THz and 0.8 THz respectively, and an average core power fraction of around 40 % for core porosity of 81% in the frequency range of (0.6 to 1.8) THz with the highest core power fraction being 58.88%[35]. A porous core rotate hexagonal PCF structure has been proposed for the purpose of increasing the efficiency and reliability of THz transmission and the numerical analysis of the design using FEM and PML displayed an ultra-low EML of 0.049 cm^{-1} , an extremely high power fraction of 43% at an operating frequency of 1 terahertz, around zero extensively flat dispersion, and single mode properties[36]. Similarly, a Topas based PCF design consisting of only rectangular slots has been presented whose numerical analysis using 22 FEM demonstrated significant properties, such as, a flat dispersion of $0.22 \pm 0.01 \text{ ps/THz/cm}$, a low value of EML ranging from $0.009 / \text{cm}$ to $0.01 / \text{cm}$ in the range of frequency of

0.77–1.05 THz, a high birefringence, single mode operation, and extremely low confinement loss which ensures the efficient transmission of THz signals by preserving their polarization[37]. For the purpose of application in THz range, a hybrid cored, fabrication friendly PCF with only circular air holes in the core and the cladding has been proffered that exhibits an extremely low confinement loss of 10^{-3} cm^{-1} , an extensively low EML of 0.035 cm^{-1} due to the bulk absorption loss of Topas, a flat dispersion with an almost zero value of 0.07 ps/THz/cm for operation in single-mode[38]. Again, with a view to ensuring polarization maintaining applications in THz transmission, a PCF geometry potentially to be fabricated by implementing the capillary stacking and sol-gel technique and consisting of octagonal cladding structure has been investigated for THz wave guidance that concurrently depicts a significant birefringence value in the 0.8-1.05 THz frequency range with single mode operation, the birefringence value being ~ 0.043 at 0.73 THz operating frequency due to the prevailing unsymmetrical structure in the core arising by the coexistence of both elliptical and circular air holes, and a trivial EML value of $0.044/\text{cm}$ [39]. A PCF design with elliptical array shaped core with rectangular cladding has also been proposed for the purpose of polarization maintenance and multi-channel communication of THz waves; the simulations from the proposed design using FEM displayed a high birefringence value of 0.063 at 1.5 THz due to asymmetry of air holes in both core and cladding, an EML as low as $0.06/\text{cm}$ at 0.6 THz, an extremely flat dispersion variation of plus minus 0.02 ps/THz/cm in the 1.05–1.5 THz frequency range due to compact geometry and different air hole sizes in the cladding, and 46% as the core power fraction value at 1.1 THz for y polarization[40]. Another Zeonex based PCF design with Kagome lattice, diamond shaped core with porous structure has been proffered for the purpose of both polarization maintenance and biomedical imaging applications in THz regime whose numerical analysis using FEM shows a high numerical aperture of 0.48, a high birefringence value of 0.039, a negligible EML of $0.078/\text{cm}$ at 1.1 THz, a flattened dispersion of $1.07 \pm 0.05 \text{ ps/THz/cm}$, and a CL as low as $1.39 \times 10^{-4} / \text{cm}$ for 30 % porosity at x-polarization mode[41]. For the purpose of efficient THz transmission, a porous-core circular PCF, also termed as PCCPCF, has been designed, was simulated using full vector FEM and PML, and its outcomes were a low EML value of 0.043 cm^{-1} , an acutely high core power fraction of 47%, an overly flattened dispersion variation of 0.09 ps/THz/cm , and a confinement loss with a trivial value 23 of $10^{-2.5} \text{ cm}^{-1}$ along with single mode operation properties[42]. Moreover, for THz wave guidance, a Topas based hybrid porous core octagonal lattice PCF has been numerically investigated using full vector FEM and displays an EML as low as 0.04 cm^{-1} , maximum core power fraction of 50.4% at a core

diameter of 350 μm and operating frequency of 1 THz at 81% porosity, and an acutely flattened dispersion of 0.10 ps/THz/cm within the frequency range 0.95–1.15 THz[43]. For polarization maintaining guidance of THz waves, an investigation of the numerical properties of slotted-porous core microstructure polymer fiber was performed that showed a high modal birefringence of ~ 0.08 because of the existing asymmetry inside the core introduced by rectangular slotted air holes, a very low EML of $\sim 0.08 \text{ cm}^{-1}$ for 35 % porosity and core diameter of 350 μm at 1 THz frequency, a flat dispersion value of $0.85 \pm 0.05 \text{ ps/THz/cm}$ for y-polarization in the frequency range of 1.16-1.5 THz[44]. Additionally, a porous-core octagonal photonic crystal fiber (PC-OPCF) is proposed for THz transmission that displays a low EML value of 0.047 cm^{-1} , a power transmission of 49% through core air holes, and a flattened dispersion variation of 0.15 ps/THz/cm at 1 THz operating frequency and a core diameter of 345 μm when its numerical analysis has been done in COMSOL Multiphysics v4.2, and making it an efficient medium for THz wave transmission[45]. A novel PCF Biosensor with high sensitivity in the region covering the visible and near infrared (IR) bands and fabrication-friendliness is proposed in this study which comprises a singular lattice layer of hexagonal shape comprising air-slots of only circular structure. The suggested design has an x-polarization mode sensor resolution of 2.4×10^{-6} , a peak WS of $41,000 \text{ nmRIU}^{-1}$, and a maximum AS of 1072.5 RIU^{-1} [46]. Recent years have seen a substantial increase in interest in the use of photonic crystal fibers to detect alcohol in beverages. Islam et al. proposed a novel Zeonex-based PCF for alcohol detection, which exhibited remarkable characteristics in the terahertz frequency band. The fiber was characterized using the FEM, and results of simulation showed a remarkable RS value of 88.6%, as well as a very low EML of 0.0222/cm, and negligible CL of $3.63 \times 10^{-11}/\text{cm}$ at 1.9 THz operating frequency[46]. Using comparative analysis of AS as the metric of sensitivity, the first study that suggested a biosensor for identification of blood components in the frequency regions comprising the near-infrared and visible spectrum bands demonstrates higher AS of 5078.99 RIU^{-1} . In this case, Al-doped ZnO is taken into consideration as a plasmonic material to boost sensor performance and design extensibility [47]. SPR based PCF sensors have made incredible progress during the past ten years. Islam et al. [30] presented a straightforward circular SPR-24 PCF sensor with x-polarization mode. The proposed sensor's maximum AS and WS values are 1757.3 RIU^{-1} and $32,000 \text{ nmRIU}^{-1}$, respectively. The design they have proposed also depicts a significantly low value sensor resolution value of 1.428×10^{-6} , 587.2 as FOM value, and maximum birefringence of 0.004. New directions in sensing research have been made possible by the coupling of PCF sensors with plasmonic materials. Due to its stability

and chemical inertness, gold is a material that is highly favored in the plasmonic field. Because they may be made using common methods like stack and draw and still offer great sensitivity, simple and easily constructed structures are very desirable. Islam et al. presented a number of unique solid core photonic crystal fibers in their study that are intended to take advantage of the surface plasmon resonance (SPR) phenomena. These fibers were designed with a specialized circular cladding structure that not only made manufacturing them easier but also improved their sensing capacities[48]–[50]. The geometric properties of the photonic crystal fiber (PCF) can affect the sensor's performance since they have a direct bearing on how the plasmonic layer surface interacts with the evanescent field. The square lattice design is widely regarded as the easiest to construct lattice structure. The insertion of annular airholes in the square lattice has shown to be a noteworthy improvement in the context of biosensors, demonstrating outstanding sensitivity and resolution[48]. Specifically, for biological sensing applications, a unique structure with two arrays of six small airholes on each side and two arrays of two large airholes on each side displayed higher sensitivity. When compared to other structures, this particular design produced a higher level of sensitivity, making it an attractive option for biomedical sensing applications[49]. The addition of airholes with the same radius has considerably simplified the production of the biosensor design. With this design decision, the core mode and plasmonic mode may more easily couple, which facilitates efficient coupling and results in high amplitude and wavelength sensitivity. The regularity in the size of the airholes ensures the biosensor's reliable and optimal performance[50]. The use of a hexagonal lattice structure with a greater quantity of rods in the context of surface plasmon resonance (SPR)-based photonic crystal fibers (PCFs) enables additional versatility in design for both the core and cladding. This structural design gives the PCF more control over its optical properties and capabilities, allowing for better performance in SPR applications for sensing. The greater the number of rods, the easier it is to manipulate the modal properties and interact with the plasmonic layer, resulting in both increased sensitivity and efficiency of the PCF- SPR sensor[46], [51]–[54]. In the biosensor's cladding region, an intelligent arrangement of air holes, including hexagonal- 25 shaped groups and v-shaped configurations, has been applied[51]. The development of four channels for efficient light transmission from the core to the plasmonic mode is facilitated by these air holes of a specified dimension. The cladding's clustered pattern of circular-shaped air spaces contributes to improved plasmonic effects. The use of an Al-doped ZnO (AZO) coating as the plasmonic material improves the performance and flexibility of the design of the sensor. The modified design has better amplitude sensitivity, resolution, and FOM. The inclusion of an

extraneous AZO layer to the sensor construction improves design flexibility and optical tuning that outperform the metal films used traditionally[52]. The use of a TiO₂ coating and a novel twin spider core arrangement in a biosensor design led to better gold adhesion to the fiber[53]. An unusual structure consisting of two clusters that are V-shaped generating the shape of an eye is used in the cladding section of one design. These clusters have a symmetrical arrangement along a horizontal line in the opposite direction. A thin gold layer with an island pattern of development is used to improve the sensor's performance. A carefully aligned ring-shaped layer is also used to decrease surface exposure effects[55]. One sensor can sense analyte, magnetic field, and temperature by the virtue of a new trigonal cluster-based configuration of circular air holes within the fiber that enables effective interaction with the environment[56]. In a study, a square lattice and solid core SPR-based PCF sensor with extremely low loss and appropriate sensitivity are proposed and examined. Along with its ability for magnetic field and temperature detection, the sensor also exhibits an exceptionally high external strain sensitivity of 4.00 pm / $\mu\epsilon$ [57]. In a study, a dual cluster and dual array design is used for the suggested structure. In order to successfully direct the electromagnetic (EM) wave to the surface and improve the overall sensing performance, the air holes within the fiber are strategically placed[58]. There are significant gains in performance metrics with the suggested PCF design, which has elliptical air holes and a perfectly circular shape[59]. When the elliptical, rectangular, and circular air holes that were developed are compared, it is found that they produce the best outcomes. In one study, the central airhole was purposefully chosen to be rectangular rather than the more typical circular shape in order to create birefringence. This innovative design decision causes asymmetry in the structure of the photonic crystal fiber, which results in an altered reaction to polarization and increased birefringence[60]. To induce birefringence in the photonic crystal fiber, another design comprises hexagonally arranged clusters of circular airholes in the cladding, as well as a rectangular airhole in the middle[61]. It is noteworthy how PCF-SPR sensors are applied in communication. In a D-shaped PCF with a micro-opening, a unique broadband single polarization filter has been successfully developed using SPR[62]. The advancement of SPR-26 PCF has found a new direction with the implementation of double resonance using two plasmonic materials[63]. The simultaneous use of two materials using localized surface plasmon resonance has been used to enhance the detection range of the sensor. In this work, we have proposed an LSPR based PCF sensor that uses the concurrent application of gold and GZO in order to create two peaks at two distinct wavelengths. The evolution of two peaks occurs due to the splitting of the evanescent field as it interacts with the surface

plasmons. Our proffered sensor introduces a broadened working range both in the ultra-violet and the visible spectrum range which was never observed in any of the literatures stated above. Therefore, the uniqueness, efficacy, and novelty of the sensor for the diverse biosensing field can be strongly established.

CHAPTER 3

PHOTONIC CRYSTAL FIBER

3.1 Introduction

Photonic-crystal fiber (PCF) is a kind of optical fiber with superior waveguiding capabilities. It outperforms ordinary optical fibers in terms of light confinement. PCF applications include fiber optic interchanges, fiber lasers, non-linear devices, high-control transmission, gas sensors, and data transmission at THz frequencies. PCFs consist of a microstructured arrangement with undoped silica as the backdrop material and air holes throughout the fiber. The core is the center portion, whereas cladding refers to the surrounding area. However, this study does not just employ silica as the backdrop material [42]. Crystal fibers like Teflon [43], PMMA [44], TOPAS [45], [46], and HDPE [47] are widely utilized. TOPAS is considered the best material for waveguide propagation due to its exceptional water barrier qualities [46] and biosensing capabilities [48]. Birefringence is an important characteristic for sustaining polarization in porous fiber sensing applications [49].

The core and cladding areas of a PCF significantly impact fiber performance. The honeycomb cladding construction was first proposed by J. Laegsgaard et al. [50]. As design freedom and fabrication capabilities improved, the number of designs expanded significantly. Efficiently executed designs include square [51], hexagonal [52], octagonal [53], spiral [54], and circular [55]. Porous core fibers have received significant attention for their capacity to sustain low EML (effective material loss), high birefringence, and greater power into the core area [57]. Photonic crystals may be used to create a diverse range of PCF designs with positive outcomes.

3.2 PCF in Brief

A traditional optical fiber has a core with a greater refractive index than its cladding. Doping a high refractive index material in the core area increases its refractive index compared to silica cladding. Germanium is commonly used to enhance the refractive index of the core, whereas fluorine is typically used to lower it.

Photonic Crystal Fiber is a low-loss dielectric media made out of a periodic pattern of small air holes that run the whole length of the fiber [58]. PCF's core traps light, providing a more efficient waveguide for photons than ordinary optical fibers. PCF has a solid silica core that guides the optical signal. The core is encircled by a periodic air-hole array in the cladding. Since the effective cladding index is lower than the core refractive index, light may be steered by total internal reflection down the silica fault core. Air-holes contribute to low index cladding, and the core is often made by creating a bigger air hole or eliminating one from the center. PCFs may be designed with many parameters such as core radius, number of rings, air hole diameter, and pitch. Modulating these factors can improve the guiding qualities of optical fibers, which are influenced by the refractive index. Modulating these parameters can improve the guiding qualities of optical fibers, as the refractive index of PCFs is affected by design freedoms [59].

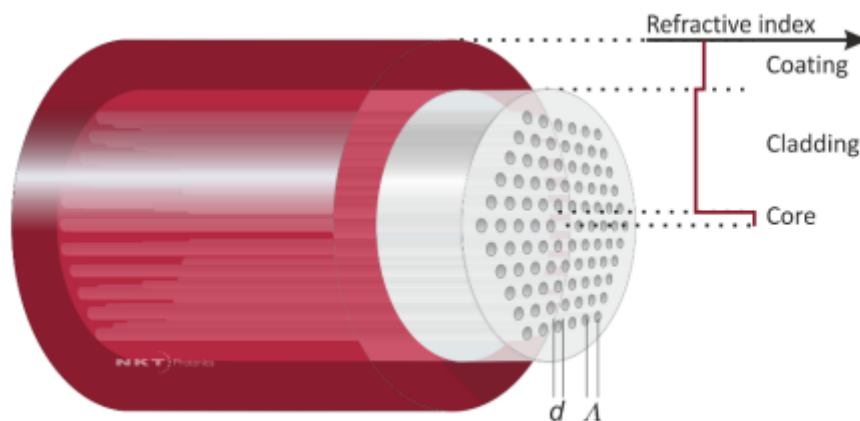


Figure 3.1: Cross-sectional view of a Photonic Crystal Fiber

3.2.1 Classification of PCF

Traditional fiber optics have a continuous difference in refractive indices between the core and cladding regions. Refraction allows light waves to readily move over the core area. However, increasing the distance of propagation leads to increased transmission loss. To improve communication quality over long distances, we recommend using repeaters and amplifiers. Photonic crystal fibers (PCF) have superior wave-guiding capabilities because

light waves are confined within the core area, unlike typical optical fibers. Photonic crystal fibers benefit from increased flexibility and lower manufacturing costs due to their backdrop material. PCFs have a superior manufacturing method than regular optical fibers. Photonic crystal fibers are commonly divided into two classes:

- **Index-Guiding Fibers:** These fibers have a solid core, similar to traditional ones. Total internal reflection causes light waves to become trapped within the core.
- **Photonic Bandgap (Air Guiding) Fibers:** These fibers have periodic microstructures and a low index material core. The core has a lower refractive index than the cladding area composed of photonic crystals. Light waves are steered via fibers using photonic bandgap, which differs from total internal reflection.

3.2.2 High Index Guiding Fibers

M-TIR is the acronym for total internal reflection in optical fibers.

The structure consists of a high-index core made of pure silica and a low-refractive index microstructure. Photonic crystal fibers vary from standard optical fibers due to their very wavelength-dependent cladding. The high dependence of the refractive index on wavelength allows for the fabrication of unending single-mode fibers that support just one mode regardless of wavelength. We can readily change the dispersion characteristics of optical fibers, allowing for the construction of irregular dispersion at visible wavelengths. Photonic crystal fiber technology can generate coherent super-continuum due to its tiny cores and comparable phase-matching conditions to existing sources. Optical fibers with large mode-field widths may now have controlled refractive-index profiles, allowing for better beam-quality guiding and amplification.

3.2.3 The Bandgap effect

This optical fiber differs from M-TIR guiding fibers in terms of mechanism and qualities. PBG fibers' cladding area is strategically micro-structured to create photonic bandgaps. Light rays of particular wavelengths cannot flow through the fibers. PBG fibers develop core areas by producing defects in their structure, allowing light to easily propagate. The faulty region

forms a low index guiding core, allowing light to readily travel through. Photonic bandgap fibers provide significant advantages over typical fibers because to their low index-guiding properties, opening up new possibilities. This technology allows us to route light waves via air or any appropriate gas through the fiber material.

3.2.4 Hollow-Core and Solid-Core Fibers

One of the unique types of photonic bandgap fibers is the hollow-core fiber. The electromagnetic field is limited to an air-filled core. Air-core fibers, like other photonic bandgap fibers, only guide light in a narrow spectrum. Fibers typically guide about 1550 nm and have a common bandwidth of 200 nm. The anti-guiding core area is underneath this one. Guided light waves via hollow cores have several uses, including high power delivery without fiber damage, gas sensing, and low-loss guiding across vacuums. Hollow core fibers offer unique advantages over regular fibers. They are more helpful because of their low susceptibility to bending, Kerr effect, temperature fluctuations, and Faraday effect.

Furthermore, they possess strong dispersive features, such as anomalous dispersion values. The dispersion of photonic bandgap fibers is mostly determined by wave-guide dispersion, since the material inside the core has a minor role. Another form of photonic bandgap guiding fibers is solid-core PBG fibers. This type of fiber contains a solid core and high-index areas embedded in silica coating. These fibers can only transmit light waves within a specific spectral range. Filtering with a core doped with rare earth material, such as Yb, allows for easy amplification and lasing at a newer wavelength with lower fiber gain (12). The laser community benefits from the combination of doped-solid-core photonic bandgap fiber and its dispersive properties, opening up new options.

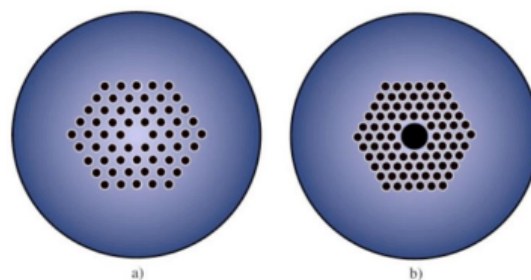


Figure 3.2: Cross-sectional view of (a) Solid Core Fiber, (b) Hollow Core Fiber

CHAPTER 4

SURFACE PLASMON RESONANCE

4.1 Introduction

Surface plasmon resonance (SPR) occurs when the frequency of photons and electrons on a surface matches. A surface plasmon resonance (SPR) sensor detects variations in the refractive index at a specific spot. This biosensor focuses on measuring fabric adsorption onto flat metal surfaces, such as gold or silver, or metal nanoparticles.

4.2 Working Principle of SPR

SPR procedures energize and distinguish collective motions of free electrons (known as surface plasmons) in which light is focused onto a metal film through a glass crystal, and the resulting reflection is recognized at a specific angle of propagating light, forming a faint line within the reflected beam containing a wealth of data. A shift in the reflectivity bend indicates an atomic official event occurring on or near the metal film, or a conformational change within the atoms bonded to the film. Analysts may think about atomic official events and official energy without having to worry about a name.

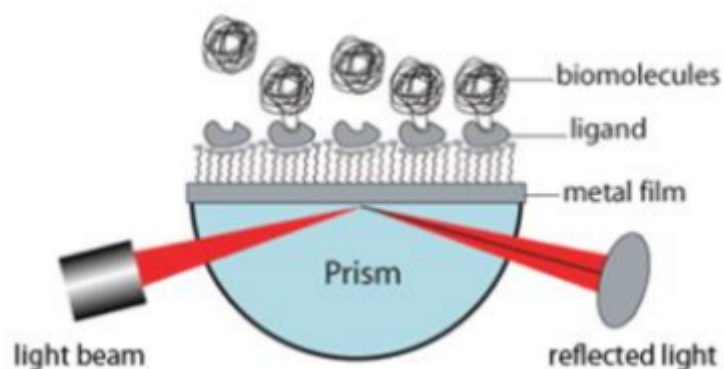


Figure 4.1: A light is impacted by a prism on a metal film and the reflected beam is captured and analyzed

4.3 Reason of Interest in SPR Technology

SPR-based biosensors have gained popularity among researchers due to their high robustness, sensitivity, and proven properties. Potential applications for SPR technology include food safety, protection, medical testing, bimolecular analyte detection, and medical diagnostics [60]. PCF-enabled SPR modes are popular for sensing applications due to their ability to adjust optical characteristics by design, lightweight nature, and tunable birefringence. [20], [61]-[65].

4.4 Implementation of SPR

SPR can be utilized in a variety of applications. SPR is often used in medical diagnostics, such as for hepatitis B virus.

SPR has also been used to identify biomolecules. SPR has been used to analyze many biological substances. Viruses in blood samples may readily be detected. SPR detects molecular interactions in real-time and without labeling. Traditional sensors require labels for detection and only offer information on binding specificity and affinity. SPR, on the other hand, provides information on specificity, affinity, kinetics, thermodynamics, and concentration of interactions for various compounds. The existence of hazardous gasses in a complicated combination. This biosensor enables quick and cost-effective detection of presence in complicated mixtures.

4.5 Advantages of SPR

SPR technology has improved the accuracy and ease of tracking limited activity on a subatomic level compared to other bio-detecting devices available. Here are some of the key advantages of adopting surface plasmon resonance.

- SPR detects contrasts in the refractive record, eliminating the requirement for a label. Real-time observations can reveal bio-subatomic collaboration among proteins, DNA/RNA, and tiny particles.

- SPR investigations need small sample sizes with negligible test results. By using less expensive materials, researchers and medical practitioners may make surface plasmon reverberation more accessible and cost-effective.
- SPR allows for the reuse of sensor chips. Sensor chips play a crucial role in bio-detection and immediately impact the data. It's crucial to note that sensor chips may be reused, as their efficiency and execution rely heavily on them.
- Surface Plasmon reverberation can handle complicated samples, including rough instances, for research purposes. SPR has been utilized for evaluating investigations in several contexts, including serum analysis.
- SPR technique enables real-time monitoring of biomolecule interactions at minimal cost. It has several applications in the pharmacological and therapeutic fields.

4.6 Success Rate and Drawbacks

The high success rate of high sensitivity SPR is a very compelling incentive to use it. Developing small molecule medications is expensive and time-consuming. Due to low success rates of existing sensors, there is a need to develop new methods for measuring activity rapidly and precisely. However, SPR biosensor technology has several downsides as well. Biosensors require active biological molecules to function properly. Biosensors require an active molecule to provide a signal, unlike other analytical methods like mass spectrometry or UV spectrometry, which can define a chemical regardless of its state. However, while biosensor devices are simple to use, they may be challenging to develop and implement. To begin, remember that biosensors rely on the Biosensor equipment and are simple to operate, however planning and conducting an experiment requires considerable biochemistry knowledge.

CHAPTER 5

SPR BASED PCF SENSORS

5.1 Introduction

PCF-based sensors have higher sensitivity and lower resonance peaks than other fiber-based sensors, resulting in greater accuracy when detecting unknown analytes. Furthermore, by adjusting structural factors such as pitch, bore of air holes, and total count of various shaped rings and air cavities, PCF-based sensors may undoubtedly get a deeper understanding of the transient fields. SPR is the recommended approach for achieving the desired sensing qualities. When SPR-based technology combines with benign features, it produces the ideal SPR-based PCF sensors. Such a sensor uses SPR and is activated when light travels through the fiber. As a result, the generated evanescent field falls on the plasmonic metal surface, causing the free electrons to oscillate. Thus, the SPW becomes agitated and moves along the core-cladding area. At a certain wavelength, the SPP mode combines with the core mode to provide phase-matching between two modes with an equal real fraction of effective RI. During this scenario, a sharper resonance peak is obtained at that specific wavelength, which is heavily dependent on analyte RI. As a result, every little change in RI causes the resonance wavelength (RW) to move upward or downward. Thus, an anonymous analyte may be detected by observing the variation of the RW for different analyte RIs. The first level of SPR-based sensors is prism-based and D-shaped sensors. After extensive investigation, PCF sensors were implemented. It has a long history owing to its development process. The plasmonic metal layer and the analyte channel through which the material to be diagnosed are conveyed are retained outside or within the fiber, depending on the kind of sensor. The history, variation, and division of PCF sensors using the SPR method are briefly detailed in the following segments.

5.2 Prism based Sensor

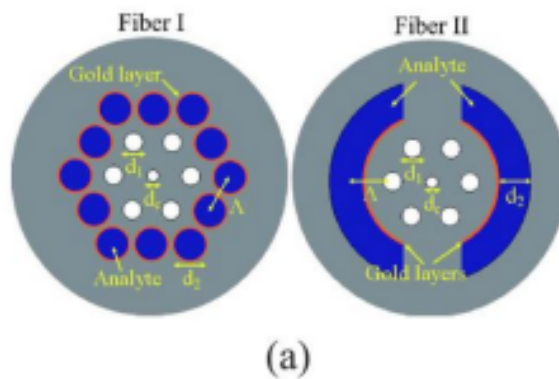
In 1983, Liedberg et al. used a prism-coupled SPR biosensor in biosensing fields to detect unknown gasses [23]. The investigation of SPR-based biosensors began then. In prism-based SPR sensors, light was passed through the prism at a precise angle. When light strikes the

metal surface, a surface plasmon wave (SPW) forms as a result of the metal's active valence electrons absorbing the incident light. Later, it was discovered that prism-based SPR sensors had several limitations, such as inaccuracy in sensing applications and bulkiness in size due to additional sophisticated opto-mechanical elements, rendering them unsuitable for distant sensing [67], [68].

5.3 Internal Sensing based Sensor

The internal sensing type sensor was developed to control obstructions in prism-based sensors. Internal sensing involves coating air pores with metal sheets and packing analytes within them, as seen in Figure 5.1. [67]-[70].

The first type's practical application is challenging due to the difficulty of coating internal fiber holes with metal coatings and filling with analytes. Small holes pose difficulty. Additionally, keeping a consistent thickness of the perforations is not practical for production. Additionally, the process of measuring, emptying, and replacing the fiber takes time. Furthermore, repeated filling and emptying might cause a decline in the sensing capabilities of the sensor.



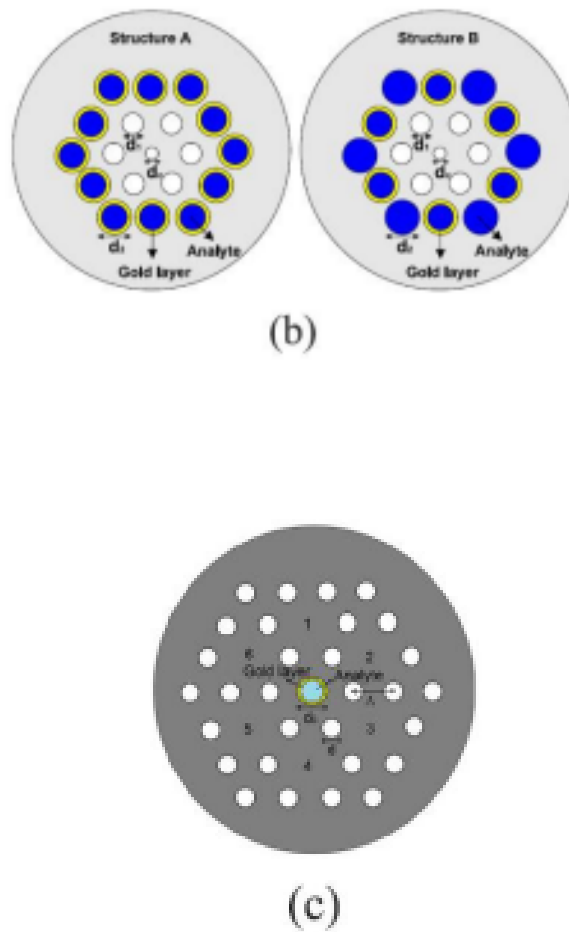


Figure 5.1: Internal Sensing based Sensors

5.4 D-shaped Sensor

D-shaped or exposed-core PCFs can overcome the limitations of prism-based and internal sensing devices [71]-[74]. D-shaped PCFs allow for direct deposit of metal and analyte on the exposed surface, simplifying sensor construction and analyte changes (see figure 5.2). However, the flat section of D-shaped PCFs requires polishing, making production challenging. In fact, this form of sensor requires etching certain sections of the surface, which complicates fabrication and increases cost.

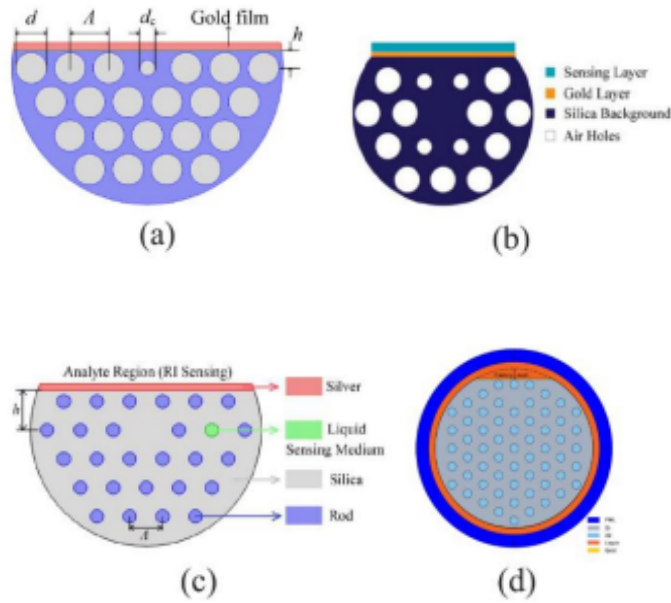


Figure 5.2: D-shaped Sensors

5.5 External Sensing based Sensor

External sensing is the favored approach for analyte detection due to its superior sensing capabilities and ease of manufacture (75, 76). Internal sensing and D-shaped PCF have limitations. It offers possibilities for cleaning and reusing sensors. In contrast to internal sensing, which involves placing the metal coating within the air pores, external sensing does not require any pre-sampling processes. See figure 5.3-a. The sensor clings to the analyte solution and performs as expected within minutes.

5.6 Plasmonic Material Silver based Sensor

The plasmonic material used in the sensor affects the sensing performance strongly. Silver gives a sharper resonance peak which gives beneficial output in terms of FOM. A silver based sensor is shown in figure 5.3 (b) [77]. Though silver is one of the most conductive materials, it is oxidized easily with time in aqueous circumstances. This phenomenon reduces the sensing accuracy and hampers the sensor performance. Due to this chemical instability of silver (Ag) and other limitations [78], it shows an inaccurate sensing performance.

5.7 Bimetallic Silver-Graphene based Sensor

Silver oxidizes in a hydrous environment, resulting in a decrease in sensing accuracy. An attempt to put a lean coating of graphene has been made to control the oxidation problem, which in practice increases the manufacturing cost along with the fabrication difficulties due to additional layers [79]. A sensor utilizing Silver-Graphene coating is depicted in figure 5.3 (c)[79].

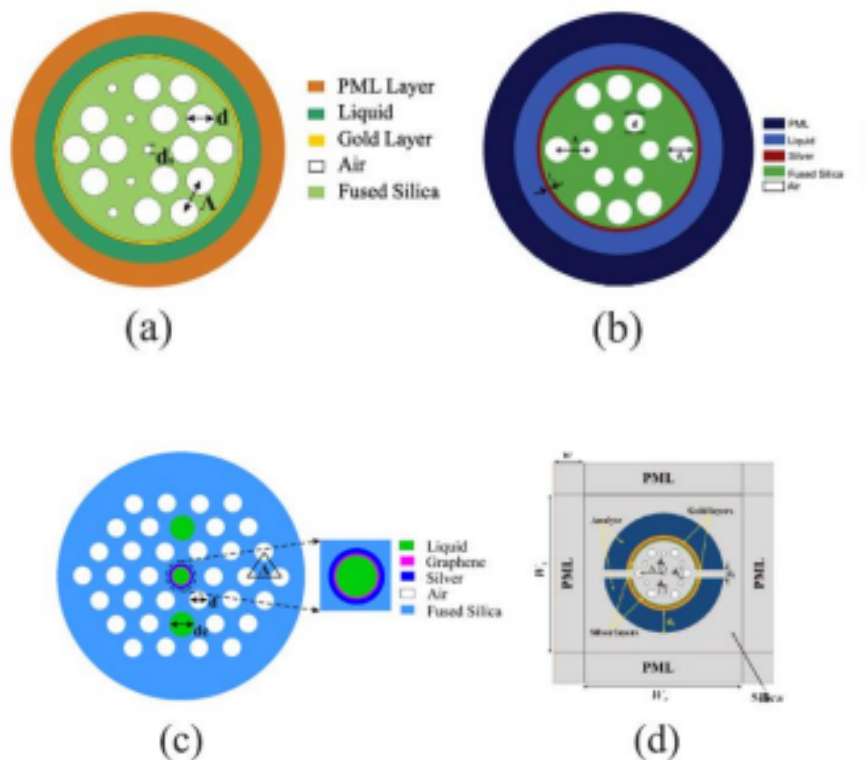


Figure 5.3: (a) External Sensing based sensor, (b) Silver based sensor, (c) Silver-Graphene based sensor, (d) Silver-Gold based sensor

5.8 Bimetallic Silver-Gold based Sensor

This type of SPR-PCF biosensor has two metalized microfluidic slots that are constituted with gold and silver as plasmonic material. This innovative type design was initially proposed by Akowah et al. in 2012. Gold is positioned at the top of the silver to prevent oxidation and other chemicals. The structure (shown in figure 5.3-d) has an easier fabrication process due to large micro-fluidic slots [80].

5.9 Bimetallic Silver-TiN based Sensor

Conventional bimetallic designs have Gold-Silver coating where gold is used as a protective layer. But gold has the disadvantage of broader resonance curves that limit the accuracy of detection. So, the newly proposed bimetallic configuration can be based on silver and TiN (shown in figure 5.4-a). The surface of the operating channel is layered with a silver coating. An additional layer of TiN was utilized to protect the silver layer from oxidation and to maintain chemical stability [81].

5.10 Plasmonic Material Gold based Sensor

Though silver has a sharper resonant peak, it exhibits chemically unstable behavior. Thus, recently gold is popularly used due to its chemical stability and the shift of resonant wavelength by a significant amount, which results in proper detection of the analyte [82], [83]. A large number of researches are done on gold-based biosensors. A sensor utilizing Gold as the plasmonic material is displayed in figure 5.4 (b) [83].

5.11 Bimetallic Gold-TiO₂ based Sensor

In this type of sensor, gold is applied as a thin layer to coat the channel. On top of that, the deposition of a TiO₂ film proliferates the surface plasmonic excitation by assisting the adhesion of gold [84]. The rise in the excitation of surface plasmonic increases the evanescent field. It also has higher RI than the fiber and provides strong coupling between the leaky core guided and the plasmonic mode whenever placed on the glass. Therefore, this layer improves sensing performance. A sensor having Gold-TiO₂ coating is displayed in figure 5.4 (c) [85].

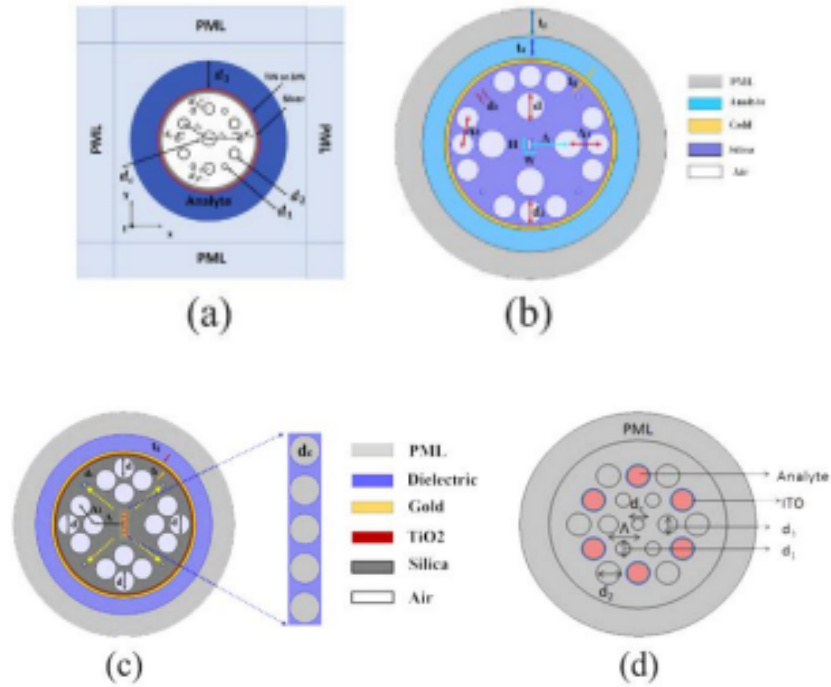


Figure 5.4: (a) Silver-TiN based sensor, (b) Gold based sensor, (c) Gold-TiO₂ based sensor, (d) ITO based sensor

5.12 ITO based Sensor

Using Indium Tin Oxide (ITO), the adjustment of the plasmonic resonance can be performed by varying the inherent characteristics of the materials [38]. Basically, by altering the number of oxygen content and metal atoms, the plasmonic behavior can be controlled. Additionally, ITO is more cost-effective than gold and silver. A sensor utilizing ITO as the plasmonic material is displayed in figure 5.4 (d) [38].

CHAPTER 6

MATERIAL CHARACTERIZATION AND MATHEMATICAL FORMULATION

6.1 Introduction

In this chapter, we have discussed the different materials that are used in designing the SPR-based PCF sensors. Silica (SiO_2), Titanium dioxide (TiO_2), Gold (Au), Aluminium doped Zinc Oxide (AZO), etc., are the materials that are commonly used. Here we have demonstrated the equations that can be used to characterize these materials in simulation platforms. It is to be mentioned that only the refractive index (RI) of these materials is of interest. So we have shown only the RI equations of these materials. In some cases, we have provided the permittivity equations since the square-root of permittivity gives the RI. Then we also discussed in this chapter the parameters that help to determine the sensor performance. These parameters include confinement loss (CL), amplitude sensitivity (AS), wavelength sensitivity (WS), temperature sensitivity, strain sensitivity, resolution, birefringence, figure of merit (FOM), sensor length, etc. The formulas that can be used to calculate these parameters are displayed and explained in this chapter.

6.2 Characterization of Materials:

In this section, the materials characterization equations are discussed. Here we have focused only on the materials we have used in our research works discussed in the upcoming chapters. Note that some materials have a complex effective RI. The effective RI of any material can be represented in the complex form of $n_{\text{eff}} = n + jk$, where n and k denote the RI's real and complex parts.

6.2.1 Silica (SiO_2)

SPR-based sensors are usually fabricated by putting a lamination of plasmonic metal on the surface of a PCF. The PCF can be made of either some glasses or some polymers. Fused

Silica, also known as silicon di-oxide, is vastly preferred as the background material of the PCF. Generally, an undoped version of silica is used. Due to the following advantageous behaviors, silica is given preference over other glasses and polymers [86]:

- One of the essential advantages of silica is its chemical stability. It does not show any hygroscopic behavior.
- Silica exhibits good optical transparency in a wide wavelength range.
- The mechanical strength of silica is remarkable against pulling and bending.
- Silica has deficient scattering and absorption loss (around 0.2 dB/km) in the nearIR spectral region. This characteristic can be realized from figure 6.1.
- At high temperatures, silica can be drawn into fibers.
- Another advantage of silica is that the fusion splicing of silica performs excellently.
- The high damage threshold is another advantageous property of silica.
- Due to this property, silica shows a low tendency of laser-induced breakdown. During the amplification of short pulses in fiber amplifiers, this property plays a vital role.

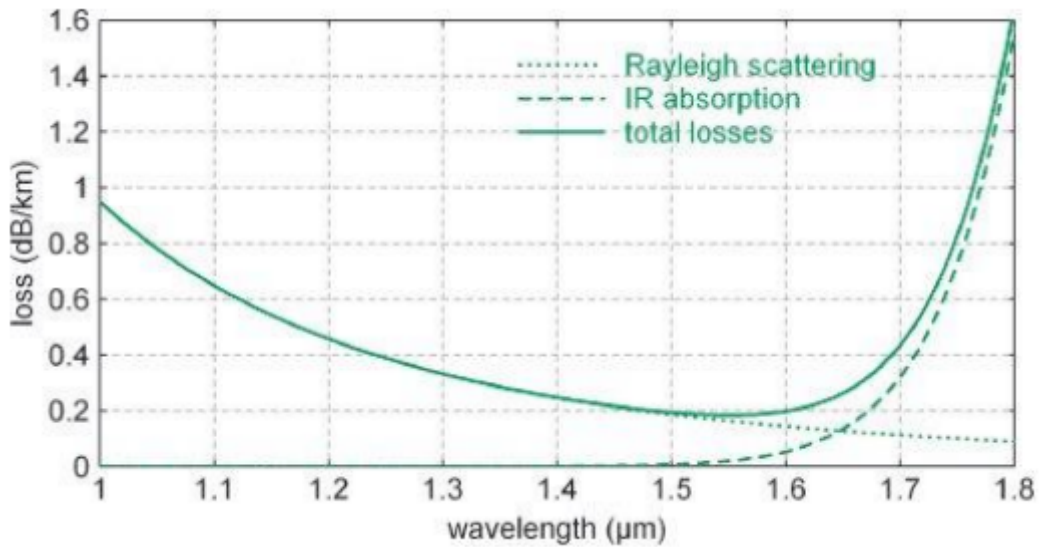


Figure 6.1: Intrinsic losses of silica

The RI property of the fused silica is extracted from the Sellmeier equation given below [9]:

$$n_{silica}(\lambda) = \sqrt{1 + \frac{B_1 \lambda^2}{\lambda^2 - C_1} + \frac{B_2 \lambda^2}{\lambda^2 - C_2} + \frac{B_3 \lambda^2}{\lambda^2 - C_3}} \quad (5.1)$$

Here, n_{silica} represents the RI of silica, and the value of n_{silica} depends on the wavelength of light (λ) and the Sellmeier constants. The Sellmeier constants are listed in table 5.1. It is to be mentioned that equation 6.1 is valid for the wavelength range of 0.22 μm to 3.71 μm [85]. This formula can be used to estimate the silica RI at a constant temperature of 25°C [87]. Figure 6.2 depicts the RI of silica as a function of wavelength. It is visible from figure 5.2 that the complex part of the silica refractive index is always zero. Therefore, the refractive index of silica is always a real number.

Table 6.1 - Sellmeier Constants:

Constant	Value
B_1	0.69616300
B_2	0.407942600
B_3	0.897479400
C_1	0.00467914826 μm^2
C_2	0.0135120631 μm^2
C_3	97.9340025 μm^2

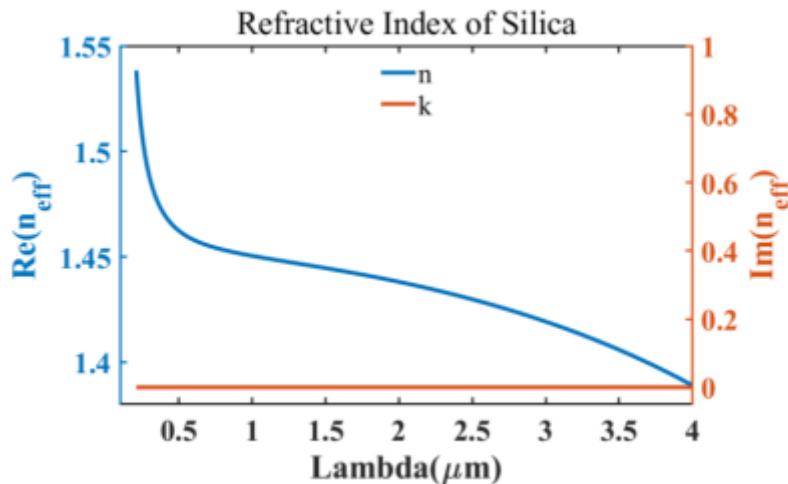


Figure 6.2: Silica RI as a function of light wavelength (temperature 25°C)

When T denotes the temperature in Celsius ($^{\circ}\text{C}$) scale, the temperature-dependent Silica RI n_{silica} can also be estimated using the modified Sellmeier equation given below [25]:

$$\begin{aligned}
n_{silica}^2(\lambda, T) = & (1.31552 + 6.90754 \times 10^{-6} T) \\
& + \frac{(0.788404 + 23.5835 \times 10^{-6} T)\lambda^2}{\lambda^2 - (0.0110199 + 0.584758 \times 10^{-6} T)} \\
& + \frac{(0.91316 + 0.548368 \times 10^{-6} T)\lambda^2}{\lambda^2 - 100}
\end{aligned} \tag{6.2}$$

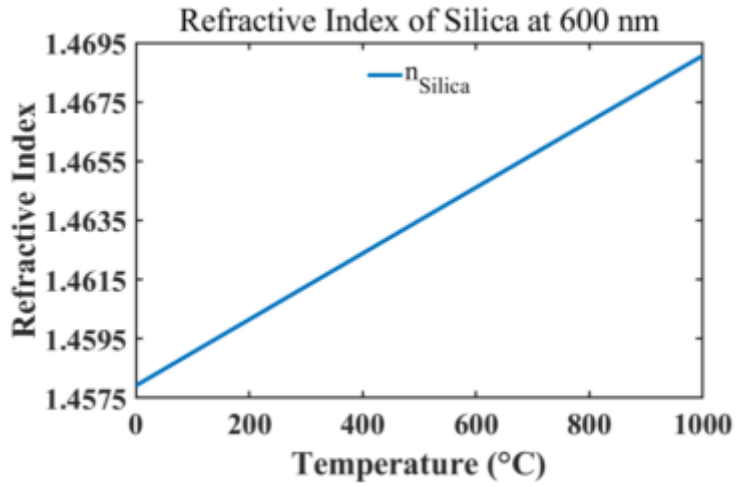


Figure 6.3: Silica RI as a function of temperature (light wavelength 600 nm)

At a constant light wavelength of 600 nm, the silica RI vs. temperature is manifested in figure 6.3. It is realizable from figure 6.3 that the silica RI increases as the temperature is raised. The above two equations evaluate the silica RI when the applied strain is null. However, when the fiber undergoes any amount of strain, the RI of silica changes owing to the Opto-elastic property. The strain-dependent refractive index of Silica for variable applied stresses can be estimated by the following formula [26], [88]:

$$n'_{silica} = n_{silica} [1 - P_e \varepsilon_z] \tag{6.3}$$

where n_{silica} and n'_{silica} are the silica RI without strain and with strain, ε_z denotes the applied strain, and P_e is the elastic-optic constant. It is to be mentioned that P_e has a magnitude of

0.22 for silica [88]. For varying strain in the range of 0-2000 $\mu\epsilon$, the silica RI is exhibited in figure 5.4. It is realizable that silica RI reduces with the increase of strain.

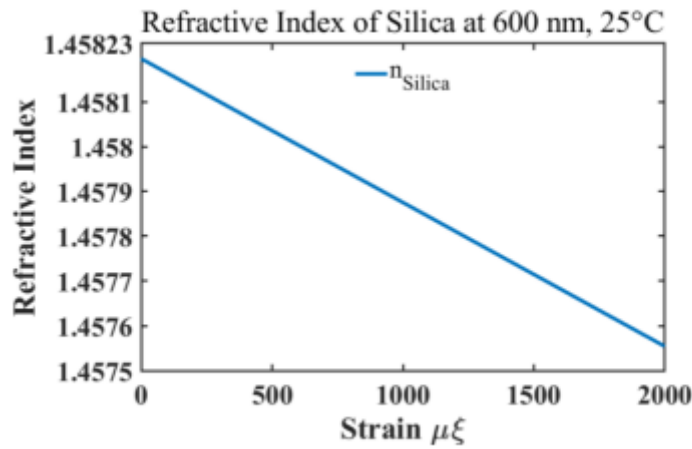


Figure 6.4: Silica RI as a function of strain (light wavelength 600 nm, temperature 25°C)

6.2.2 Air

Air is used to fill up the cavities existing in the PCF. The refractive index of air gets altered as the light wavelength is varied. However, this change is very insignificant, which can be realized from figure 6.5.

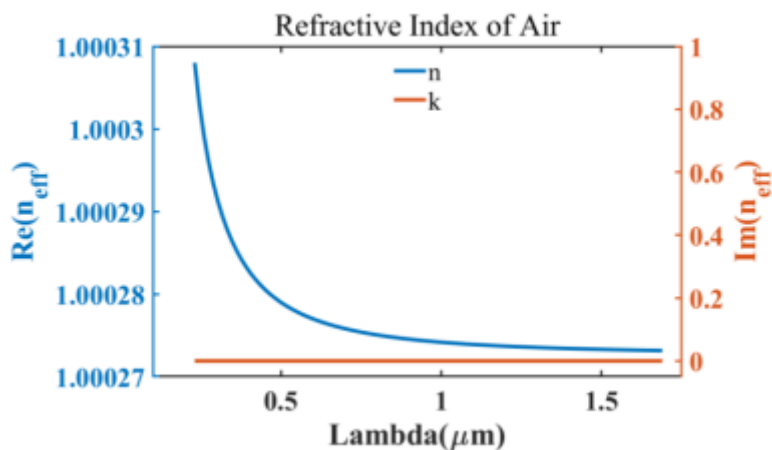


Figure 6.5: Air RI as a function of light wavelength

Figure 6.5 displays the relationship between the air RI and the light wavelength. It is realizable that air RI is always a real value and has a magnitude very close to 1. Therefore, we have considered air RI to be 1 in all our research works.

6.2.3 Gold

Gold is a material that has an atomic number of 79. It is symbolized by ‘Au’ and has a relative atomic mass of 196.96657. The melting point of gold is 1064 °C. We have used gold to laminate the exterior of our SPR sensors. It is vastly used as the plasmonic material due to its advantageous behavior over other plasmonic materials. The advantages that gold provides are [40]:

- Gold is chemically stable and inert.
- Gold does not get oxidized in an aqueous environment.
- A sharp resonant peak and a broad resonance peak shift even in an aqueous environment.
- The dielectric constant of gold can be estimated from the Drude-Lorentz model, and it can be described as below [89]:

$$\epsilon_{Au} = \epsilon_{\infty} - \frac{\omega_D^2}{\omega(\omega + j\gamma_D)} - \frac{\Delta\epsilon\Omega_L^2}{(\omega^2 - \Omega_L^2) + j\Gamma_L\omega} \quad (5.4)$$

In this equation, ϵ_{Au} represents the permittivity of gold, ϵ_{∞} represents the high-frequency permittivity with a value of 5.9673. ω is the angular frequency, ω_D and γ_D are plasma and damping frequencies respectively, where $\omega_D = 4227.2\pi$ THz, $\gamma_D = 31.84\pi$ THz. Moreover, $\Delta\epsilon = 1.09$ is the weighting factor while the oscillator strength is $\Omega_L = 1300.14\pi$ THz, and spectral width is $\Gamma_L = 209.72\pi$ THz.

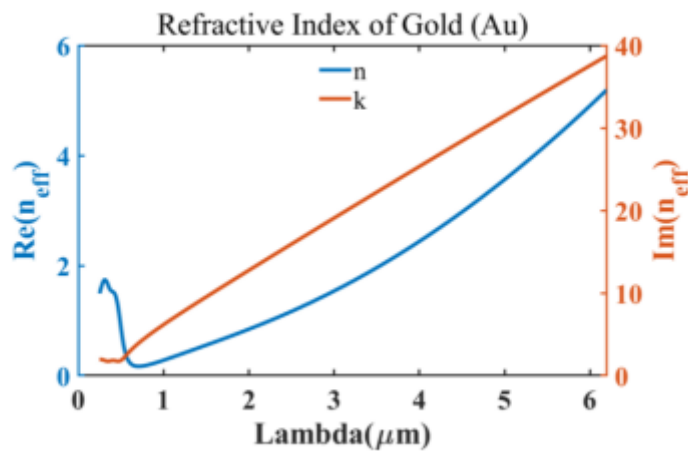


Figure 6.6: Gold RI as a function of light wavelength

It is clear from equation 6.4 that the dielectric constant of gold is a complex number, and it is equal to the squared value of gold RI. So the gold RI can be obtained by square-rooting the dielectric constant, which is another complex value. The real and complex parts of gold RI vs. wavelength curves are plotted in figure 6.6.

6.3 Performance Parameters

In this section, different performance parameters have been discussed that are used to estimate the sensor performance. These parameters include confinement loss (CL), amplitude sensitivity (AS), wavelength sensitivity (WS), resolution, birefringence, figure of merit (FOM), and so on.

6.3.1 Confinement Loss (CL)

Among all performance parameters, confinement loss (CL) is the most critical parameter for measuring sensor performance since it is required to measure all other parameters. The CL indicates the energy that is redirected to SPP mode from core mode. Confinement losses are the losses arising from the modes' leaky nature and the PCF fiber's non-perfect structure. When light is dispatched through the core of the PCF sensor, a portion of the light energy leaks from the core and reaches the metal layer region. The amount of this leaked energy is termed as the 'confinement loss' (CL). The CL can be quantified by the following equation [85], [94]:

$$\alpha = 8.686 \times k_0 \times \text{Im}(n_{\text{eff}}) \times 10^4 \text{ (dB / cm)} \quad (6.8)$$

6.3.2 Amplitude Sensitivity (AS)

The sensor potential can be measured using two methods, known as the amplitude interrogation method (AI) and the wavelength interrogation (WI) method. The variance of loss depth due to analyte RI change can be utilized to detect different unknown analytes. This method of identifying unknown analytes is known as the amplitude interrogation

(intensity-based measurement) method. When $\alpha(\lambda, n_a)$ is the confinement loss at a particular RI of the analyte and $\partial\alpha(\lambda, n_a)$ is the confinement loss difference due to two adjacent analyte RIs the amplitude sensitivity (AS) of a sensor can be determined by using the formula [85], [95]:

$$S_A = -\frac{1}{\alpha(\lambda, n_a)} \frac{\partial\alpha(\lambda, n_a)}{\partial n_a} (RIU^{-1}) \quad (6.9)$$

The AI method measures AS at a constant wavelength, and thus this method is straightforward in terms of practical implementation. It is because it does not require spectral manipulation [96]. That is why this is the most popular method to determine the sensitivity of a sensor. However, this method has a trade-off of being very prone to external noise. A significant amount of external noise may hamper the sensor performance and result in erroneous detection of the analyte. Therefore, additional arrangements are needed to block the external noise, making the implementation of this method expensive.

6.3.3 Wavelength Sensitivity (WS)

Another technique to measure the sensor's performance is the wavelength interrogation (spectral-based measurement) method, where the shift of resonance wavelength is taken into account. The following formula is applied to calculate the sensitivity of a sensor in the WI method [85]:

$$S_\lambda = \Delta\lambda_{peak} / \Delta n_a (nm / RIU) \quad (6.10)$$

where Δn_a and $\Delta\lambda_{peak}$ represent the difference between two neighboring analytes RI and the contrast in their corresponding resonant wavelengths. Usually, this method exhibits a high sensitivity response compared to the AI method [76]. The phase-detection method (WI method) has the advantage of being cost-effective. However, it comes with a tradeoff, which is the complexity of measuring sensitivity [97].

6.3.4 Resolution

Resolution is a parameter that assists in realizing the detection capability of the sensor. The resolution gives an idea about the degree of the slightest modification in RI that can be identified. Assuming the minimum spectral resolution to be $\partial\lambda_{\min}$, and $\partial\lambda_{\text{peak}}$ being the RW shift, the following formula enumerates the resolution [84], [85]:

$$R = \frac{\partial n_a \times \partial\lambda_{\min}}{\partial\lambda_{\text{peak}}} \text{ (RIU)} \quad (6.11)$$

6.3.6 Full Width at Half Maximum (FWHM)

FWHM is the width of the confinement loss curve at the half value of the peak loss. It determines the sharpness of the loss peak. The sharper the loss peak, the better the sensing performance of a sensor. Moreover, FWHM is needed to evaluate the FOM of the sensor. Therefore, FWHM is an important parameter to determine sensor performance. Figure 6.10 gives an idea about how to determine the FWHM. Usually, FWHM is measured on a nanometer scale.

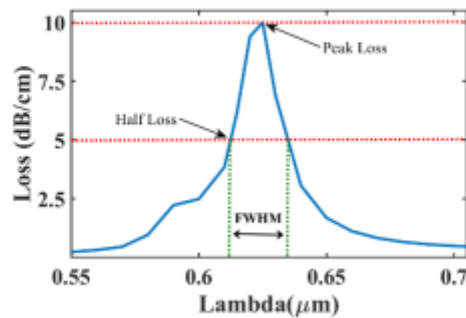


Figure 6.7: Representation of Full Width at Half Maximum

6.3.7 Figure of Merit (FOM)

Besides AS and WS, the sensor efficiency can also be indicated through another parameter known as the figure of merit (FOM). It is simply the ratio of the WS and the FWHM. When

S_λ is the WS, and the FWHM indicates the full width at half-maximum, the FOM can be measured by the following equation [83]:

$$FOM = \frac{S_\lambda (nm / RIU)}{FWHM (nm)} \quad (6.13)$$

The FOM of a highly performable sensor should be of high value, obtained when the sensor's sensitivity increases with the decrease of FWHM [85]. The increased value of WS indicates a higher shift of resonance wavelength. On the other hand, reduced FWHM indicates a sharper resonance peak. Therefore, FOM gives an idea about the overall sensor performance.

CHAPTER 7

PROPOSED DESIGN: DESIGN OF A HIGHLY SENSITIVE PHOTONIC CRYSTAL FIBRE SENSOR FOR DETECTING BIOCHEMICAL ANALYTES

7.1 Introduction

Surface plasmons, the quantized rise of transversely magnetic (TM) p-polarized electromagnetic waves at the metal-dielectric interface due to the combined oscillation of electrons, have revolutionized sensing technologies, particularly through the phenomenon of surface plasmon resonance (SPR).[1] Initially proposed by Kretschmann-Raether, SPR sensors have traditionally relied on bulky prism-based configurations, which, despite their sensitivity, present challenges in terms of size, complexity, and suitability for remote sensing applications. [23]

In response to these limitations, researchers have turned to innovative sensor designs utilizing photonic crystal fibers (PCFs) for SPR sensing. PCFs offer distinct advantages, including high sensitivity, lightweight, low propagation loss, and tunable optical parameters, making them ideal for various sensing applications across multiple domains, including water and food quality control, medical diagnostics, environmental monitoring, and chemical detection. [54-56]

Recent advancements in PCF-based SPR sensors have led to the exploration of diverse measurement schemes such as long-period fiber gratings (LPFG), Fabry-Perot interferometers (FPI), in-fiber modal interferometers, and liquid-filled PCFs.[23] Among these, PCF Bragg gratings (PBG) have emerged as versatile sensing platforms, attracting significant attention for their performance in sensing applications.

Researchers have proposed various PCF structures, including square, octagonal, hexagonal, hybrid, and decagonal geometries, to facilitate core-guided leaky-mode propagation for SPR-based sensing.[35] Two primary categories of SPR-based PCF sensors have been identified: internally metal-coated sensors, where analytes are contained within the fiber

holes coated with metal films, and externally metal-coated sensors, where the metal coating is applied to the outer surface of the PCF.

While internally metal-coated sensors face challenges in fabrication complexity and maintenance, externally metal-coated sensors offer advantages in terms of ease of fabrication, cleaning, and reusability. Gold, silver, and aluminum are commonly used as plasmonic materials in these sensors, each offering unique advantages and challenges. [45]

Notably, aluminum-doped zinc oxide (AZO) has emerged as a promising alternative to gold due to its chemical stability and near-infrared plasmon frequency, making it particularly suitable for biomedical sensing applications. [34] Despite its potential, challenges remain in optimizing sensor performance, including maximizing sensitivity and resolution while minimizing fabrication complexity and material limitations.[47]

In this context, we propose a novel circular-shaped cladding-based tri PCF SPR biosensor design, incorporating thin layers of gold on the outer plane for enhanced sensitivity and flexibility. Through numerical investigations, we evaluate the sensor's performance metrics, including resolution, wavelength sensitivity, amplitude sensitivity, figure of merit, and linearity, aiming to contribute to the advancement of SPR sensing technologies with a practical, commercially viable sensor design.

7.2 Structural Modelling

A sensor's structure has a significant impact on its performance. The sensor's guiding properties are determined by the structural design, which controls the sensor's performance by positioning the air holes inside the core. A hexagonal lattice-based PCF structure with circular air holes and a gold coating is adopted for the external sensing-based SPR sensor. Fig 7.1 shows the 2D cross-section of this sensor. Different diameters (d_1 , d_2) of air holes are utilized for its advantageous behavior. In the cladding region, there are three pentagonal clusters, each consisting of 5 air holes. In each cluster, 3 air holes have diameter ($d=1.15 \mu\text{m}$) and 2 air holes have diameter ($d=1.30 \mu\text{m}$). For convenience, the air holes with $1.30 \mu\text{m}$ diameter are considered as larger holes and the one with diameter $1.15 \mu\text{m}$ is considered as small holes. There are 9 holes with a diameter of $1.30 \mu\text{m}$ and whereas there are 6 holes with a diameter of $1.15 \mu\text{m}$. There is a symmetrical distribution of the holes where in every

segment there are 3 big circles and 2 smaller circles. The prudent disposition of the air holes, having d_1 diameter, assists in forming four channels for the propagation of light from core to plasmonic mode. The fiber is made of fused silica (SiO_2) Gold is chosen due to its chemical stability in aqueous environments and its higher resonance peak. A thin layer of gold, with thickness denoted as t_g , is applied around the cladding section. Although the thickness of the analyte layer is not crucial for sensing performance, a thickness of $1.2 \mu\text{m}$ is chosen arbitrarily for this layer. An artificial PML layer with diameter of $4 \mu\text{m}$ is utilized at the outer portion of the computational area to absorb the scattered field. In a practical sensor, the PML layer is absent as it is employed only for better simulation purposes. So, finally after optimization, regular air hole diameters and gold layer thicknesses were found to be $1.15 \mu\text{m}$, $1.30 \mu\text{m}$ and 20 nm respectively.

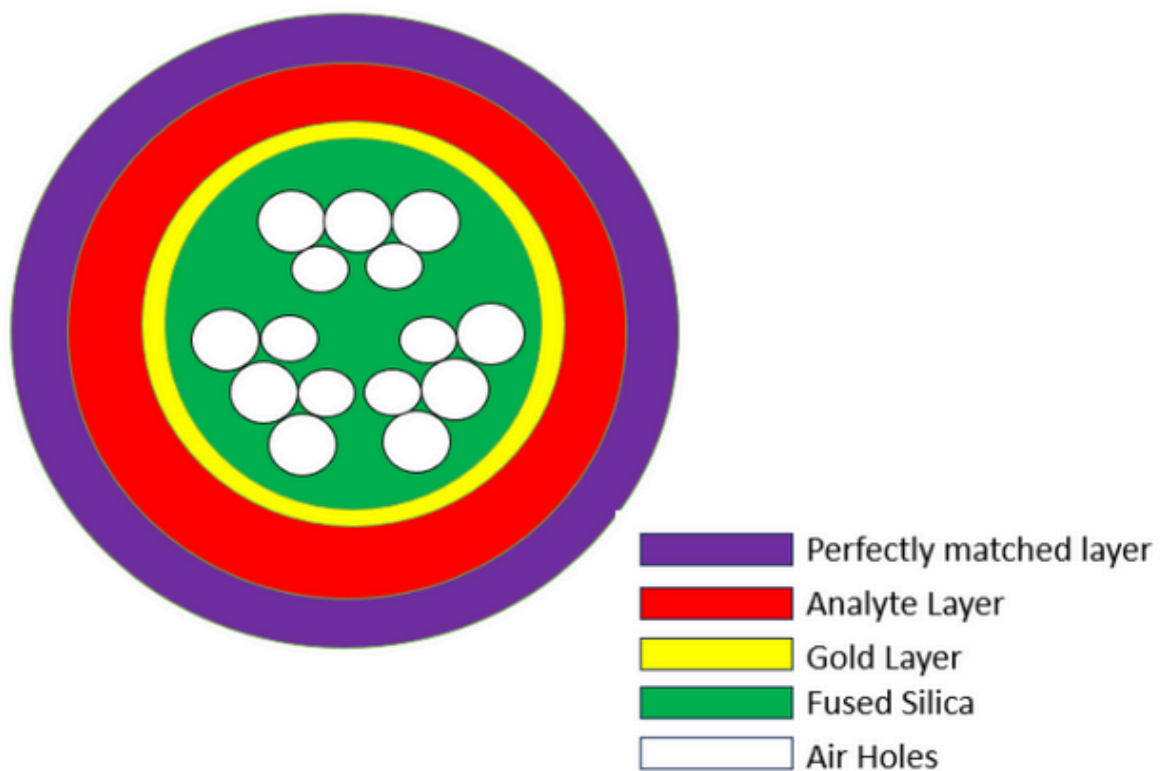


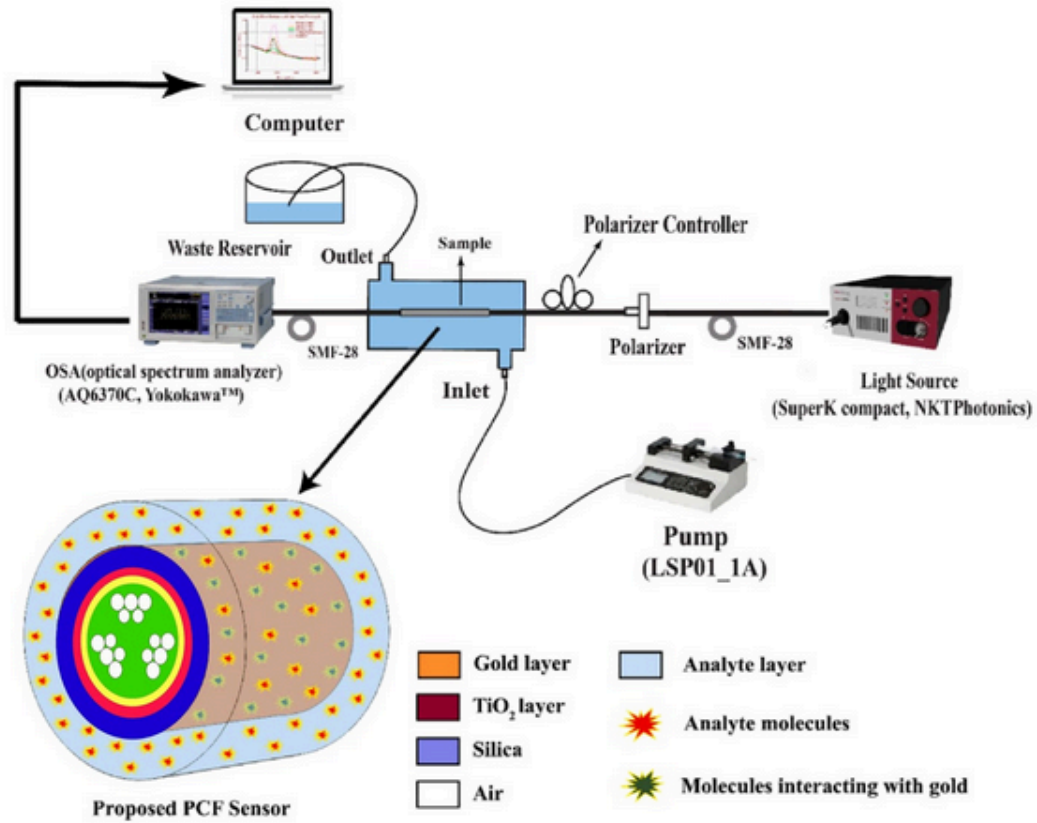
Figure 7.1: Structural Model of the Proposed Design

7.3 Experimental Setup

The experimental arrangement for this sensor begins with the initiation of incident light emitted by a supercontinuum light source with a spectrum spanning from 450 nm to 1600 nm, typically facilitated by the SuperK compact from NKTPhotonics™. This light is then guided through a polarizer, controlled by a polarizer controller, and transmitted via a single-mode fiber (SMF-28) into the sensor. Subsequently, the light passes through the sensor and is directed towards an Optical Spectrum Analyzer (AQ6370C, Yokokawa™) through another single-mode fiber. [54]

To ensure proper coupling between the sensor and the SMF-28, a method called splicing is employed. This splicing process can be conducted using the Vytran FFS-2000 splicer, employing the filament fusion technique, with alignment facilitated manually through translational and rotational adjustments. Alternatively, another splicing method involves connecting the SMF and the PCF by inserting an etched SMF tip into the PCF, boasting a reported coupling efficiency of 84.5%. Additionally, there are various high-efficiency SMF-PCF couplers available for this purpose, enabling coupling efficiencies ranging from 80% to 90%. [100]

In the experimental setup, an analyte channel is strategically positioned to allow for the introduction and extraction of liquid analyte. The analyte is injected into the channel using a programmable micro injection pumper (LSP01-1A, LongerPump™). [67] The outlet of the channel is connected to a waste reservoir for the storage of used analyte. The presence of various unknown analytes causes the resonance wavelength to shift either towards higher or lower wavelengths. [89] These spectral shifts can be detected through the optical spectrum analyzer. Finally, the wavelength peak shifts are analyzed via computer software, displaying the resulting SPR output spectra. [56]



7.4 Sensor Structure

The proposed sensor has been designed using a Finite Element Method (FEM) based software named COMSOL Multiphysics 5.5. Figure shows the 2D overview of the sensor. T_g refers to the thickness of the plasmonic material, that is, the gold layer whereas d_1 and d_2 denote the diameter of the bigger and smaller air hole respectively. We inserted another theoretical parameter: a layer called Perfectly Matched Layer (PML) which is basically a mathematical boundary condition that absorbs the emitted energy. This layer is purely imaginary and used to restrict the computing zone.

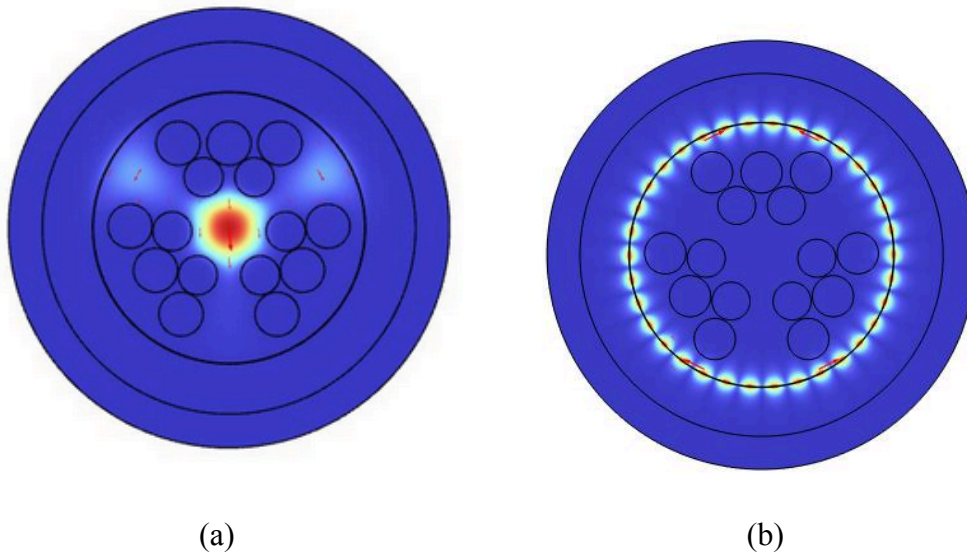


Figure 7.2: EM field dispersal of (a) Core Mode (b) SPP Mode.

7.5 Structure Optimization

We performed our calculation using the Finite Element based method in COMSOL Multiphysics 5.5 software and evaluated the sensor performance on different parameters. We varied the thickness of the only plasmonic material, Gold (Au) layer and the two air holes and observed the effect on loss curves of two neighboring RI. The optimized physical parameters were obtained after maximizing the confinement loss shift, that is, the Amplitude Sensitivity for each parameter. We chose the initial values of the gold layer thickness, diameters of the large air hole and small air holes to be 40 nm, 1.40 μm and 1.20 μm respectively.

7.6 Thickness of Gold Layer Optimization

The production of SPW by the gold film activates the sensing capability within a PCF. Additionally, the TiO_2 film strengthens this capability by generating sufficient electrons on the surface and improving the adhesion of gold to the fiber.[39] Consequently, these layers significantly influence sensor performance. The thicknesses of these films distinctly regulate the RW shift and the CL peak. [121]

Gold layer thickness varied from 15 nm to 45 nm while the other parameters remained fixed at the initial values. At 45 nm, the Amplitude sensitivity lessened. The Amplitude sensitivity increased from $\Delta n/\text{RIU}$ to $\Delta n/\text{RIU}$ for decreasing the gold layer thickness from 25 nm to 20 nm. However, AS decreased as the thickness was further decreased from 20 nm to 15 nm. The

confinement loss vs wavelength curves for three parameters is shown in Fig: 7.3 for RI 1.38 and RI 1.39. Similarly, AS vs wavelength curves for the three parameters is also shown in Fig:. We can see that a thinner gold film (20 nm) facilitates a smooth analyte-evanescent field interaction. However, for a very thin gold layer (15 nm) , the sensitivity drops owing to the CL peak broadening and the skin depth limitation of the surface plasmons. Therefore, 20 nm is determined to be the optimum thickness of the gold film since the highest AS is attained at this thickness. [3]

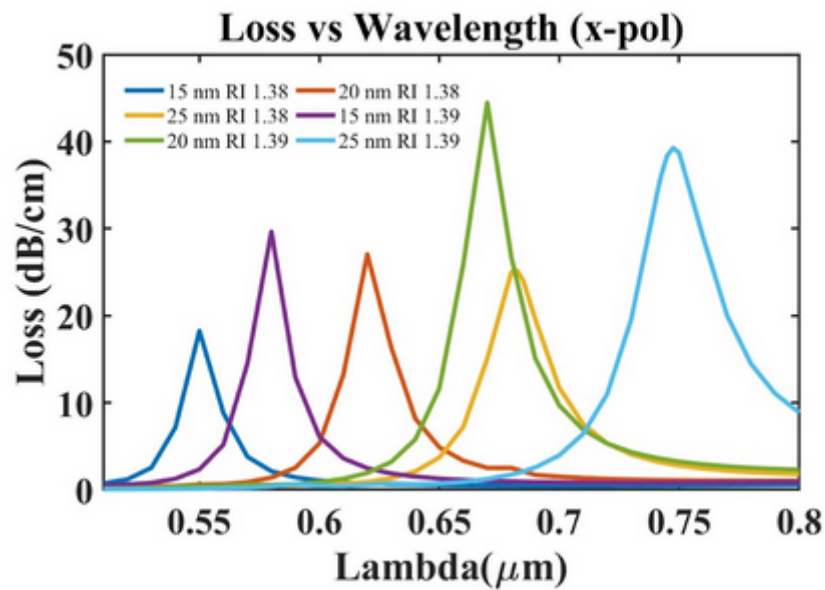


Figure 7.3 : Loss Curve for Gold Layer Optimization

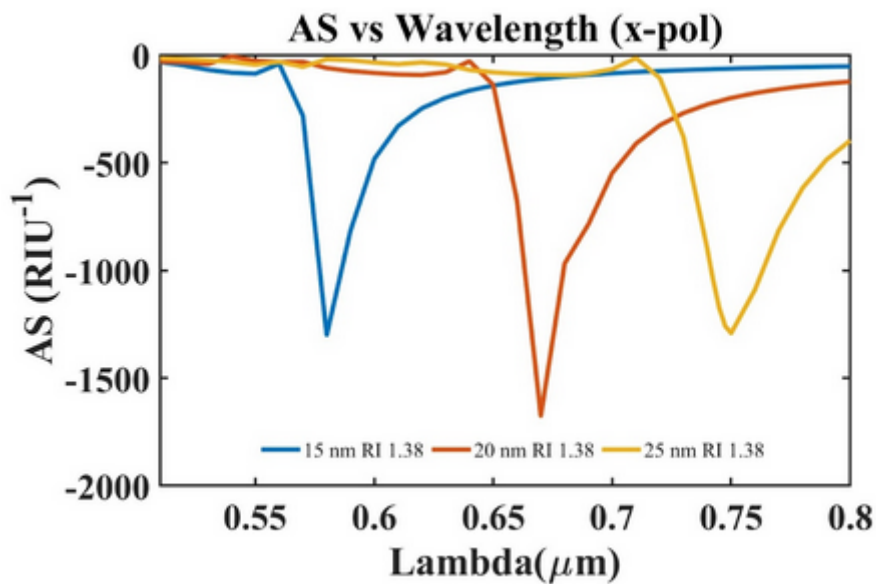


Figure 7.4: Amplitude vs Wavelength Sensitivity for Gold Layer Optimization

7.7 Air Hole Diameters Optimization

Air holes in Photonic Crystal Fiber (PCF) sensors play a crucial role in manipulating light propagation and enhancing sensitivity. They create a photonic bandgap effect, which helps to confine light within the core and improve the interaction with the surrounding environment. This unique structure allows PCF sensors to achieve high precision in detecting various physical, chemical, and biological changes.

7.7.1 Bigger Air Hole Optimization

Air cavities are stationed inside the PCF to incarcerate the light in the core region. These air holes also aid in ushering the light towards the plasmonic layer via specific channels. The diameter of the air hole varied from 1.25 μm to 1.40 μm . The Gold layer thickness was kept at the optimized value of 0.20 nm while the diameter of the small air hole was kept at the initial value of 1 μm . We observe the decrease of confinement loss and decrease of AS for the increment of bigger air hole diameter. On the other hand, shrinking the air holes gives rise to CL and increases the AS due to better guiding of light into the core. The resonant wavelengths are also shifted a little bit as the diameter is changed. We found the maximum AS at 1.30 μm diameter as further decreasing the air hole diameter to 1.25 μm reduced the guiding property of the light into the core mode even after generating greater CL. The downgrading of AS can be explained by the fact that the light cannot interact appropriately with the plasmonic layer due to the shrinkage of the channels towards the metal layer. The variation of loss vs wavelength curve with respect to the change in air hole diameter for RI 1.38 and RI 1.39 is shown in fig: 7.5 and fig: 7.6 shows the variation of AS for three parameters. From the figures, we come to the conclusion that the optimized parameter would be 1.30 μm .

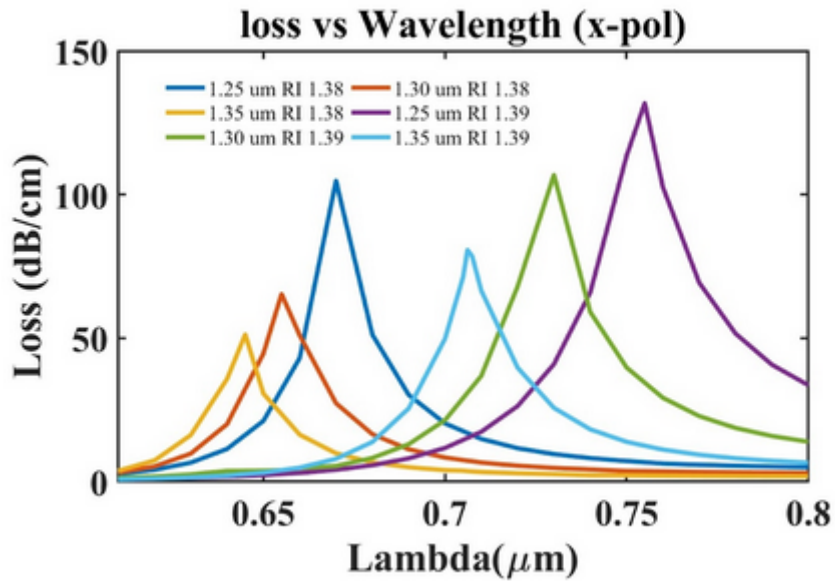


Figure 7.5: Loss Vs. Wavelength Curve due to Bigger Air Hole Optimization

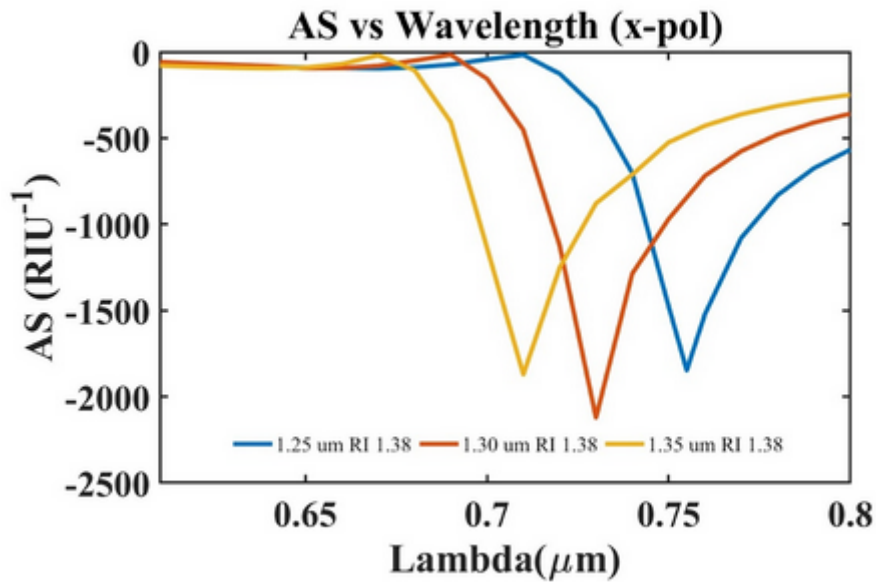


Figure 7.6: Amplitude Sensitivity Vs. Wavelength Curve due to Bigger Air Hole Optimization

7.7.2 Smaller Air Hole Optimization

While keeping the Gold layer at the optimized value of 0.20 nm and the large air hole diameter at optimized value of 1.30 μm, we varied the small air hole diameter from 1 μm to

1.15 μm . Increasing the diameter of the small air hole, we could see significant shifts in the resonant wavelength. We could also see minimal increase of the confinement loss but it meant that AS was increased. At diameter 1.15 μm , we observed an increased RW shift and also CL peak shift. The AS was also maximum at this parameter indicating the best guidance of light. However, we cannot increase the diameter further because that would result in overlapping of the bigger and smaller air holes. This incurs a structural malfunction. The confinement loss curves for three parameters are illustrated in fig: for RI 1.38 and RI 1.39. Change of AS for the change of parameter is also shown in fig: for RI 1.38. We see from the figures that the AS increased from 2121.97/RIU to 2124.6/RIU as we increased the diameter from 1.05 μm to 1.10 μm . We notice the further increase of AS to 2202.64/RIU as we increase the diameter to 1.15 μm , the threshold value. As the value of AS was observed to be maximum in this diameter, we take the optimized value of air hole diameter as 1.15 μm .

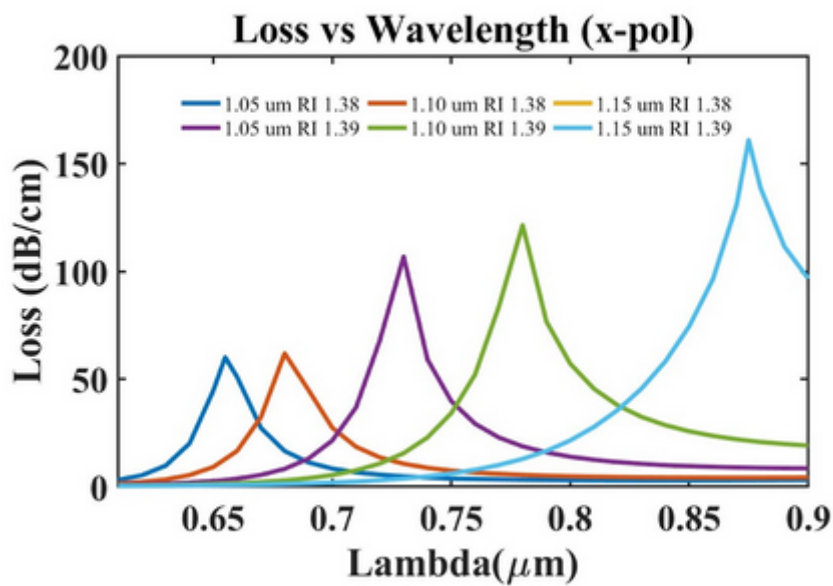


Figure 7.7: Loss Vs. Wavelength Curve due to Smaller Air Hole Optimization

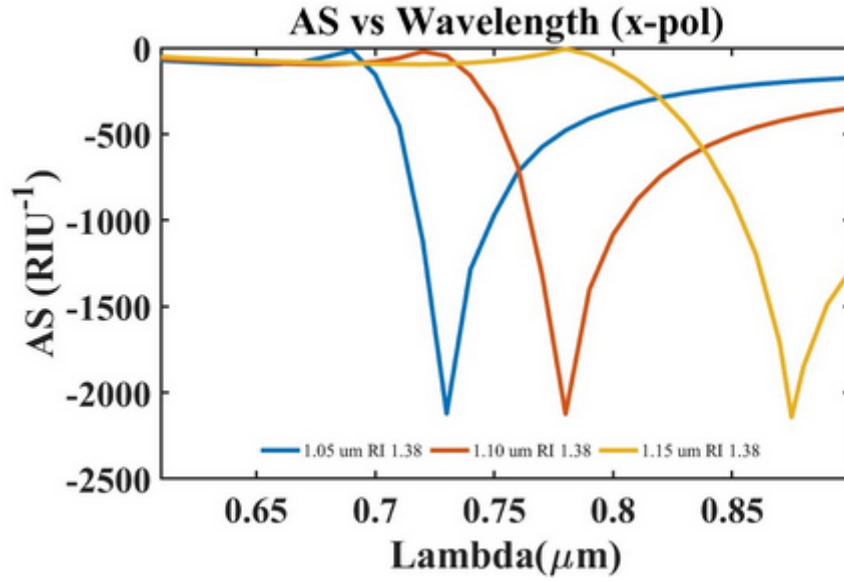


Figure 7.8: Amplitude Sensitivity Vs. Wavelength Curve due to Smaller Air Hole Optimization

7.8 Performance of the Sensor with Optimized Parameters

We measured the performance after simulating with optimized parameters

7.8.1 Scope of analyte RI detection:

In the context of Surface Plasmon Resonance (SPR) sensor analysis, confinement loss refers to the leakage of the evanescent field from the sensing region into the surrounding medium. This loss occurs due to the finite extent of the metal film used in SPR sensors, which affects the sensitivity and resolution of the sensor. Confinement loss is given using the equation:

$$\alpha(\text{db/cm}) = 8.686 \times (2\pi/\lambda) \times \text{Im}(\text{eff}) \times 10^4$$

It is observable that the analyte's RI will and that of the fused silica-covered cladding region slowly converge as RI further increases. The core and SPP modes typically merge at greater wavelengths. As RI decreases, the effective mode index decreases along with it. This also shows that the propagation factors decrease along with RI. We carried out the sensor performance evaluation in the RI range of 1.31–1.40. This range of RI is of the essence

because numerous essential biological agents and biochemical solutions have RI in this range. Some of the prominent analytes that can be identified by our sensor are acetone (1.36), silicone oil (1.403), ethanol (1.36, glucose solution in water (10% solution = 1.3477, 20% solution, = 1.3635), ethylene tetrafluoroethylene (1.403), White Blood Cell (1.36), human liver (1.369), blood plasma (1.35), human urine concentration(1.3415–1.3464), human intestinal mucosa (1.329–1.338), Red Blood Cell (1.40), hemoglobin (1.38), cervical cancer cell (HeLa), skin cancer cell (Basal), blood cancer cell (Jurkat), adrenal gland cancer cell (PC12), breast cancer cells (MDA-MB-231 and MCF-7) (1.36–1.40) and many more. It is noteworthy that the previously reported SPR based biosensors have a sensing range indistinguishable from our sensor. The values of different performance parameters of the sensor at different RI is available in Table 7.1

Table 7.1: Scope of Analyte RI Detection

RI	CL (dB/cm ³)	RW (um)	WS (nm/RI U)	Resoluti on (WS) (x10 ⁻⁶)	AS (RIU ⁻¹)	FWHM	FOM
1.31	8.928	0.525	1100	909.09	214.61	0.0175	62.86
1.32	10.91	0.536	1400	714.26	270.534	0.01937	72
1.33	13.376	0.55	1575	634.92	346.92	0.02	78
1.34	17.1	0.56575	2105	475.06	455.71	0.02125	99
1.35	22.146	0.5868	2820	354.61	601.02	0.02218	127
1.36	29.722	0.615	4000	250	835.86	0.025	160
1.37	41.945	0.655	6500	153.85	1178.08	0.03	216
1.38	66.119	0.72	15500	64.52	2202.64	0.035	442
1.39	165.18	0.875	140500	0.712	148.46	0.06125	2285
1.40	111.77	2.28	-	-	-	-	-

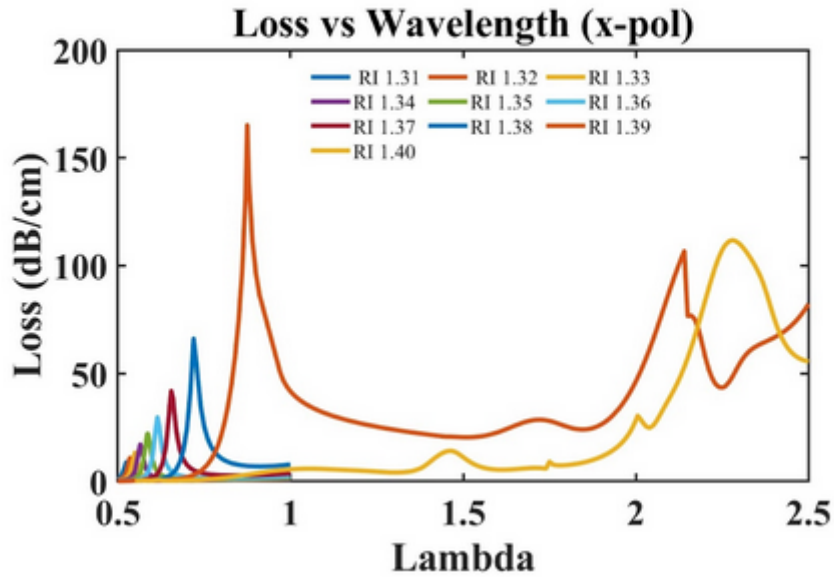


Figure 7.9: Loss Vs. Wavelength Comparison according to RI

We conducted the sensor performance analysis in the RI range of 1.31–1.40 with an interval of 0.01.

7.8.2 Maximum Wavelength Sensitivity

Wavelength sensitivity, sometimes called spectral sensitivity, is a measure of the relative effectiveness of sensing according to wavelength or frequency. Higher Spectral Sensitivity is indicated by greater resonance wavelength changes with minor modification in the RI of the unknown analyte. It is estimated using the wavelength interrogation method using the corresponding formula –

$$\frac{\Delta Peak}{\Delta na}$$

Here, $\Delta Peak$ and Δna successively indicate the distinction between two nearby wavelengths corresponding to resonance and two nearby refractive indices. Due to wavelength variation from 0.875 to 2.28 nm for RI fluctuation from 1.39 to 1.4, our sensor possesses a wavelength sensitivity of 140500 nm/ RIU.

7.8.3 Minute Wavelength Resolution:

The smallest change in a quantity that may be accurately detected is the sensor resolution of a RI sensor. The below equation defines the proposed sensor's detecting capability, which makes it important to calculate the sensor resolution. The use of the wavelength interrogation technique can be applied to evaluate sensor resolution, which can be calculated using Eq. 7, where λ_{\min} indicates the most minute wavelength resolution, which is 0.1 nm. The maximal wavelength resolution was observed to be 7.18×10^{-7} . As a consequence, the proposed sensor is capable of correctly distinguishing a RI disparity on a scale of 10^{-7} .

7.8.4 High Amplitude Sensitivity:

In COMSOL, the Amplitude Sensitivity of a Photonic Crystal Fiber (PCF) sensor is typically analyzed by examining how the amplitude of the transmitted or reflected light changes in response to variations in an external parameter. It is calculated by observing the difference in maximum confinement loss as the analyte RI is varied.

The maximum amplitude of our proposed sensor is 2204.64nm/RIU at RI 1.38 for change of RI from 1.38 to 1.39.

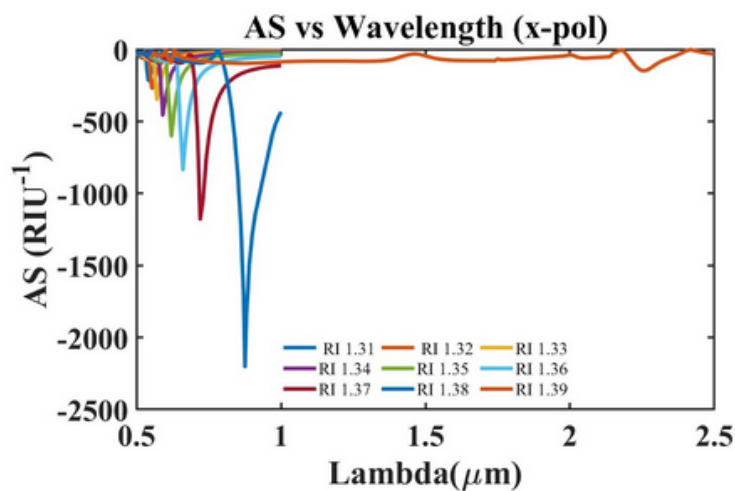


Figure 7.10: Amplitude Sensitivity Vs. Wavelength Comparison for different RI

7.8.5 Regression Analysis of our Proposed Design:

The RW for varying analyte RI is plotted in Fig. 7.11 (a), which also includes the 4th order polynomial fitting curve. The fitting curve, which has the coefficient of determination $R^2 = 0.9973$, can be expressed by the equation $y = A + Bx + Cx^2 + Dx^3 + Ex^4$. Here, x denotes the analyte RI, y symbolizes the Resonant Wavelength (RW). The prominent R^2 value embodies the enhanced performance of the sensor. [11]

The coefficients for the 4th order polynomial fit $y = A + Bx + Cx^2 + Dx^3 + Ex^4$ to the given data points are:

$$A = -1309.46, B = 4962.57, C = -5586.95, D = 2731.11, E = -504.02;$$

Where x is the analyte RI and y is the value of the resonant wavelength in micrometers.

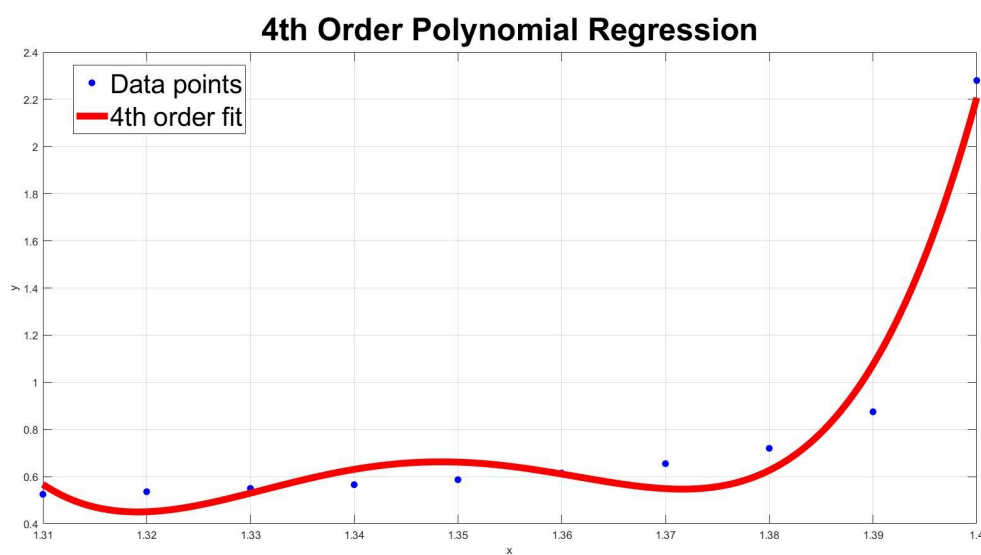


Figure 7.11: Regression Analysis of the Proposed Design

CHAPTER 8

FABRICATION OF THE SENSOR

8.1 Introduction

The effectiveness of an SPR sensor extensively depends upon the feasibility of its fabrication. Therefore, we aim to design the proffered sensor with the least amount of fabrication difficulties possible. Sensors with a difficult manufacturing process should not be prioritized over optical fiber designs with better developed sensing activities and simpler fabrication techniques. Moreover, the ease of fabrication process also contributes to ensuring the cost effectiveness of the sensors. It is to mention that the use of circular air holes in the cladding region helps in reducing the fabrication difficulties of the sensors[38]. The proffered sensor with the desired core structure is fabricated utilizing the Stack and Draw Method after which Chemical Vapor Deposition Technique is used to give the metal layer coating. The fabrication technique and the fabrication tolerance of the proffered sensor has been discussed in detail later in this chapter.

8.2 Fabrication Method

Since hexagonal shaped cores are more fabrication friendly and easy to implement, the rods are arranged in a hexagonal manner, rather than being arranged in D-shape since D-shaped cores are more complex and less symmetric. The capillaries and solid rods will be placed according to the air hole configuration. Depending on the level of confinement needed at the core, the solid rods were chosen. At first, thick-walled capillaries will be chosen 100 times larger than their actual size and these thick-walled capillaries contribute to the transfer of energy from the core to the plasmonic materials. Furthermore, the number of thin-walled capillaries are chosen with a view to ensuring low CL value and increased sensitivity. After that, the cane intermediate preform will be drawn till the suggested measurement accuracies are achieved. Next, a photolithography process consisting of two steps will be implemented for the purpose of creating the gold and GZO layer coatings[109]. The metal layer will first be deposited to the 60 fiber surface utilizing the chemical vapor deposition (CVD) technique[110]. The remaining area will then be etched while the targeted region is masked. This process will be followed at first for gold and when the gold layer will be obtained, the

GZO layer will be obtained following the same procedures. The selected regions comprising the necessary GZO and gold layers will then be masked off once again before the remaining regions are subjected to etching. It is to mention that the sensor layer will be implemented using two pumps, one of them will be for introducing analyte and another one for evacuation[102]. Therefore, the fabrication of the sensor we have proffered is possible by implementing the aforementioned steps.

8.3 Fabrication of our Proposed Design

Fabrication is an important aspect of our proposed sensor since we have conducted a simulation-based study only. [66] The pre-eminent performance of the proposed sensor will have no significance if the sensor is not practically accomplishable. For that reason, we suggest fabrication techniques that can be implemented to forge our sensor at this juncture. We have configured our sensor in such a way so that the stack-and-draw method can be implemented to manufacture the sensor. [89] The circular air holes can be originated by drilling the capillary rods at the preform stage with the help of an ultrasonic mill . [54-60] The preforms can be stacked after drilling, and then they can be drawn using a drawing tower. Solid, thin-wall, and thick-wall rods can be used in the stack to form the different sized air cavities. [32] After assembling the fiber framework, a thin layer of gold needs to be varnished on it. Atomic layer deposition (ALD), wheel polishing, high-pressure microfluidic chemical deposition, and chemical vapor deposition (CVD) methods can be adopted to overlay the fiber with thin gold film. Hence, our sensor can be easily fabricated using existing fabrication technologies. [12]

8.4 Fabrication Tolerance of our Proposed Design

The fabrication techniques of the PCF sensor cannot achieve precise dimensions while manufacturing the sensor. [33] Generally, there is always $\pm 1\%$ or $\pm 2\%$ variations from the desired structure dimensions, which introduces the necessity of fabrication tolerance (FT) analysis. [13] We have done the Fabrication analysis for our sensor by modifying the gold layer thickness by $\pm 5\%$ and the two air hole diameters by $\pm 2.5\%$ from their optimum value for RI 1.36, which allows an extensive range of errors during the fabrication process. Fig. shows that $\pm 5\%$ of the gold layer thickness results in the shifting of the RW. When the

thickness was decreased by 5%, the RW gets reduced to 60.5 μm from the optimized 61.5 μm . [15] When it is increased by 5%, the RW gets shifted to 0.625 μm . So every time, the RW gets changed by 1.62%. This means that the variation of the Wavelength Sensitivity will also be minimal. The peak CL change is slightly more, almost 3.5%, but not enough to change the Amplitude sensitivity by a significant amount.

This CL alteration occurs for all RI, and hence, the relative change in AS is minimal. $\pm 2.5\%$ variation of small circle diameter also changes the RW by not more than 2.4%. The variation of confinement loss is minimal. [77] So, we can say that the AS will be almost unaltered. Thus, we can deduce that due to the error in fabrication, our sensor performance will not differ by more than 3% of the stated values.

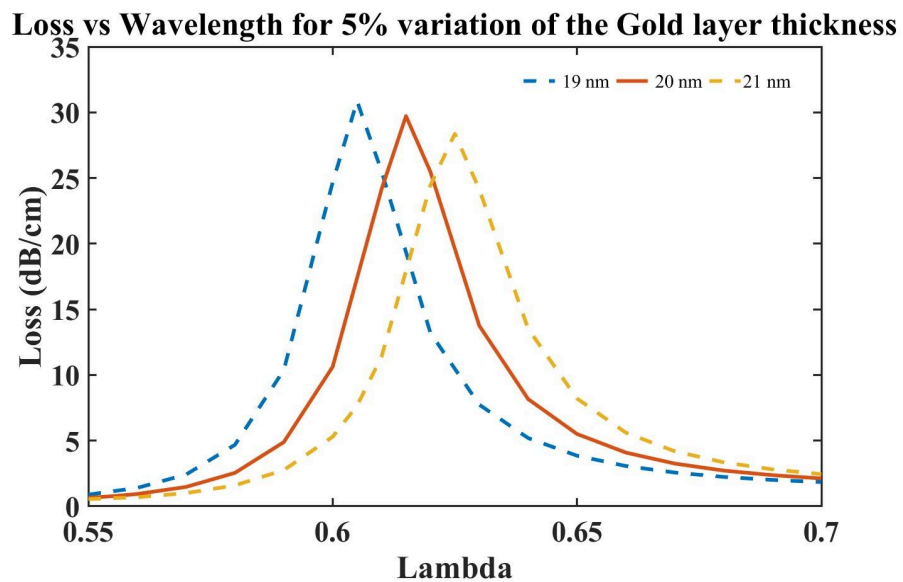


Figure 8.1: Loss Vs Wavelength for 5% Variation of the Gold Layer thickness

Loss vs Wavelength for 2.5% Variation of the Small Circle Diameter

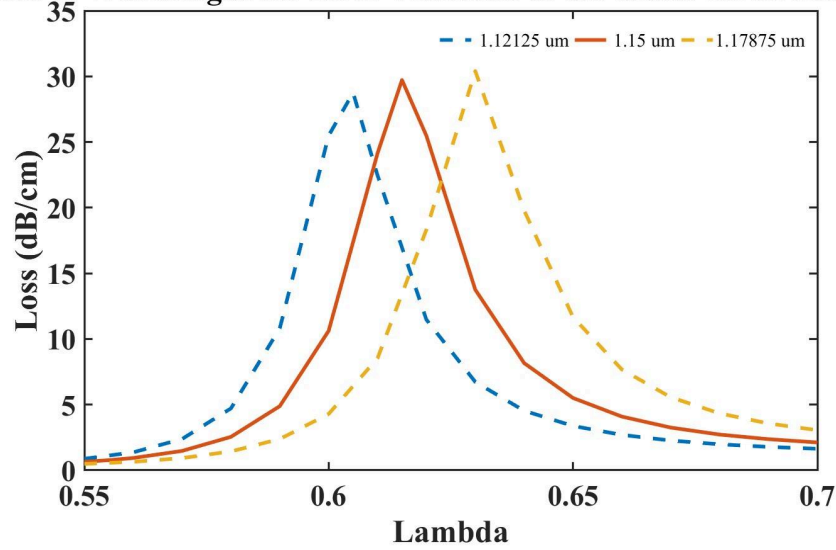


Figure 8.2: Loss Vs Wavelength for 2.5% Variation of the Small Circle Diameter

8.5 Comparative Study of our Proposed Design

Table 8.1 compares the new sensor to conventional, well-recorded ones with maximum amplitude sensitivity (AS) and wavelength sensitivity (WS) of 2202.64 RIU^{-1} and $140,500 \text{ nm/RIU}$, respectively, with a maximum sensor resolution 7.11×10^{-6} for wavelength and 4.54×10^{-4} for amplitude. The suggested sensor beats existing literature in terms of wavelength sensitivity and wavelength resolution.

Table 8.1 : Comparative Study between the existing works and our proposed design

Ref	Amplitude Sensitivity (RIU ⁻¹)	Wavelength Sensitivity (nm/RIU)	Amplitude Resolution (x10 ⁻⁶)	Wavelength Resolution (x10 ⁻⁶)	FOM	Sensing range (Analyte RI)
[1]	875.72	27,360	1.496	6.032	243.4 RIU ⁻¹	1.27 to 1.41
[6]	-	24,200	2.3	4.13	-	1.33 to 1.39
[8]	-	42,000	-	2.4	-	1.33 to 1.38
[9]	3,746	9,000	1	1	900	1.28 to 1.42

[10]	-	41,500	1.98	2.41	1,068.7	1.32 to 1.43
Our Design	2202.64	140,500	4.54	0.711	2285	1.31 to 1.40

The simplistic formation of the stated PCF sensor makes its fabrication process straightforward. The standard Stack-and-Draw method can be employed to fabricate the circular-shaped air holes [83]. Fabrication of the rectangular-shaped air hole can be achieved using an extrusion technique and 3D printing technology [83]. The thin gold and TiO₂ coating can be implemented using chemical vapor deposition (CVD), high-pressure microfluidic chemical deposition, and wheel polishing methods [85]. Besides, the thin layer of gold can be coated on the curved surface using the atomic layer deposition (ALD) method [76] as well.

8.6 Conclusion

To recapitulate, we lodge a novel SPR-PCF biosensor with high wavelength sensitivity and also high amplitude sensitivity, a fabrication-friendly model that can be contrived through the Stack-and-Draw method. The clustered arrangement of the circular-shaped air cavities in the cladding sector paves the way towards a better plasmonic effect. The perfectly matched layer (PML) encompassing the fiber ensures the absorbance of the scattered evanescent field. We used the full vectorial FEM method to perform all the numerical investigations. All the parameters of the fiber have been regulated to achieve the best sensing performance. Our proposed biosensor paraded a maximum wavelength sensitivity (WS) of 140500 nm/RIU and a amplitude sensitivity (AS) of 2204.64/RIU along with a maximum sensor resolution of 7.11×10^{-7} for wavelength and 4.53×10^{-4} for amplitude. Additionally, our sensor shows a max FOM of 2285. Moreover, a 5% change in the parameters degrades the performance by not more than 3%. This sensor promises a great deal of advancement in sensing applications and medical diagnostics for its feasibility in design and high performance regarding sensitivity.

CHAPTER 9

DEMONSTRATION OF OUTCOME BASED EDUCATION

9.1 Introduction

The industry witnessed a paradigm shift in educational approaches with the advent of Outcome Based Education (OBE). Unlike traditional education systems that primarily focus on the inputs such as curriculum and teaching methods, OBE emphasizes the outputs, specifically what students are expected to learn and demonstrate upon completion of their educational experience. This approach aligns educational objectives with industry needs and societal expectations, ensuring that graduates possess the requisite knowledge, skills, and attitudes to thrive in their chosen fields.

Outcome Based Education (OBE) is designed around clearly defined outcomes that students should achieve by the end of their educational programs. These outcomes are typically categorized into knowledge, skills, and attitudes, providing a holistic framework for student development. By setting explicit learning outcomes, educators can design curriculum, instruction, and assessments that directly contribute to achieving these goals. This results in a more structured and transparent educational process, where both instructors and students have a clear understanding of the expectations and the path to achieving them.

9.2 Course Outcomes (COs) Addressed

The following table shows the COs addressed in Project and Thesis.

COs	CO Statement	POs	Put Tick (√)
			EEE 4700
CO1	Identify a contemporary real life problem related to electrical and electronic engineering by reviewing and analyzing existing research works.	PO2	√

CO2	Determine functional requirements of the problem considering feasibility and efficiency through analysis and synthesis of information.	PO4	√
CO3	Select a suitable solution and determine its method considering professional ethics, codes and standards.	PO8	√
CO4	Adopt modern engineering resources and tools for the solution of the problem.	PO5	√
CO5	Prepare management plan and budgetary implications for the solution of the problem.	PO1 1	√
CO6	Analyze the impact of the proposed solution on health, safety, culture and society.	PO6	√
CO7	Analyze the impact of the proposed solution on environment and sustainability.	PO7	√
CO8	Develop a viable solution considering health, safety, cultural, societal and environmental aspects.	PO3	√
CO9	Work effectively as an individual and as a team member for the accomplishment of the solution.	PO9	√
CO10	Prepare various technical reports, design documentation, and deliver effective presentations for demonstration of the solution.	PO1 0	√
CO11	Recognize the need for continuing education and participation in professional societies and meetings.	PO1 2	√

Here's a detailed explanation of how the project satisfies each of the Course Outcomes (COs) for Project and Thesis:

CO1: Identify a contemporary real-life problem related to electrical and electronic engineering by reviewing and analyzing existing research works.

- The project addresses the need for a highly sensitive biosensor in medical diagnostics, which is a contemporary issue in the field of electrical and electronic engineering. By reviewing and analyzing existing research on photonic crystal fiber (PCF) and surface plasmon resonance (SPR) technologies, the project identifies limitations and proposes enhancements to current biosensor designs.

CO2: Determine functional requirements of the problem considering feasibility and efficiency through analysis and synthesis of information.

- The project identifies key functional requirements such as high sensitivity, specific refractive index ranges, and fabrication tolerance limits. Through analysis and synthesis of information from existing studies, the project ensures that these requirements are feasible and efficient for practical implementation.

CO3: Select a suitable solution and determine its method considering professional ethics, codes, and standards.

- The project selects the PCF biosensor based on SPR as the suitable solution due to its potential for high sensitivity and effectiveness. The method for developing and optimizing the sensor is determined with consideration for professional ethics, codes, and standards in sensor design and biomedical applications.

CO4: Adopt modern engineering resources and tools for the solution of the problem.

- The project utilizes advanced engineering tools such as COMSOL Multiphysics for finite element method (FEM) simulations. These modern tools are essential for evaluating and optimizing the sensor's performance, demonstrating the project's adoption of contemporary engineering resources.

CO5: Prepare management plan and budgetary implications for the solution of the problem.

- The project includes a detailed management plan outlining the steps for sensor fabrication, testing, and deployment. Budgetary implications are considered, ensuring that the project remains cost-effective while achieving high performance metrics.

CO6: Analyze the impact of the proposed solution on health, safety, culture, and society.

- The project analyzes the biosensor's impact on health and safety, highlighting its potential to improve diagnostic accuracy and patient outcomes. It also considers the broader societal benefits, such as early disease detection and enhanced healthcare, demonstrating a positive impact on culture and society.

CO7: Analyze the impact of the proposed solution on environment and sustainability.

- The project evaluates the environmental impact and sustainability of the biosensor. The use of a gold layer and specific fabrication processes are scrutinized to ensure minimal environmental impact and adherence to sustainable practices.

CO8: Develop a viable solution considering health, safety, cultural, societal, and environmental aspects.

- The project develops a biosensor solution that is viable from multiple perspectives. It ensures that health and safety standards are met, cultural and societal needs are addressed, and environmental sustainability is maintained.

CO9: Work effectively as an individual and as a team member for the accomplishment of the solution.

- The project involves collaboration and teamwork, where each team member contributes their expertise to accomplish the project goals. This effective teamwork ensures that all aspects of the project are thoroughly addressed.

CO10: Prepare various technical reports, design documentation, and deliver effective presentations for demonstration of the solution.

- Throughout the project, technical reports and design documentation are prepared to detail the process and results. Effective presentations are delivered to demonstrate the sensor's performance and potential applications, showcasing strong communication skills.

CO11: Recognize the need for continuing education and participation in professional societies and meetings.

- The project emphasizes the importance of ongoing learning and professional development. It encourages staying updated with advancements in biosensor technology and participating in professional societies to ensure continuous improvement.

Here's a detailed explanation of how the project satisfies the Program Outcomes (POs):

PO2: Problem Analysis

- The project identifies a contemporary problem in the field of medical diagnostics—specifically, the need for highly sensitive biosensors. Through a detailed review and analysis of existing research, the project highlights the limitations of current biosensor technologies and proposes an innovative solution to address these gaps.

PO4: Investigation

- The functional requirements of the biosensor were determined through comprehensive analysis and synthesis of information. The project evaluated different design parameters and their feasibility, ensuring that the proposed solution would be efficient and practical for real-world applications.

PO8: Ethics

- The selection of the photonic crystal fiber (PCF) biosensor and its method of operation took into account professional ethics, codes, and standards. The project adheres to ethical guidelines in terms of accuracy, reliability, and safety in biosensor design and application, ensuring it meets the required standards.

PO5: Modern Tool Usage

- The project employs modern engineering tools, such as COMSOL Multiphysics, for the finite element method (FEM) simulations to evaluate and optimize the sensor characteristics. This adoption of advanced software tools demonstrates the project's alignment with contemporary engineering practices.

PO11: Project Management and Finance

- A detailed management plan was prepared for the fabrication, testing, and deployment of the biosensor. Budgetary considerations were included to ensure the project's cost-effectiveness while maintaining high sensitivity and performance standards.

PO6: The Engineer and Society

- The project analyzes the impact of the biosensor on health and safety, highlighting its potential to improve diagnostic accuracy and patient outcomes. It considers the societal benefits, such as early disease detection and improved healthcare, demonstrating the project's positive impact on society.

PO7: Environment and Sustainability

- The project evaluates the environmental impact and sustainability of the proposed biosensor. The use of gold and specific fabrication processes were scrutinized to ensure minimal environmental harm and adherence to sustainable practices in sensor production.

PO3: Design/Development of Solutions

- The project develops a viable biosensor solution by considering health, safety, cultural, societal, and environmental aspects. This holistic approach ensures that the sensor is not only technically sound but also socially responsible and environmentally friendly.

PO9: Individual and Team Work

- The project emphasizes effective collaboration and teamwork. Team members worked together, leveraging individual strengths and expertise to accomplish the project goals, demonstrating the ability to work efficiently both as individuals and as part of a team.

PO10: Communication

- Throughout the project, various technical reports and design documentation were prepared to document the process and results. Effective presentations were delivered to demonstrate the sensor's performance and potential applications, showcasing strong communication skills.

PO12: Life-long Learning

- The project underscores the importance of continuing education and participation in professional societies. By recognizing the need to stay updated with advancements in biosensor technology, the project encourages ongoing learning and professional development.

9.3 Aspects of Program Outcomes (POs) Addressed

The following table shows the aspects addressed for certain Program Outcomes (POs) addressed in EEE 4700 for Project and Thesis.

	Statement	Different Aspects	Put Tick (√)
PO3	Design/development of solutions: Design solutions for complex electrical and electronic engineering problems and design systems, components or processes that meet specified needs with appropriate consideration for public health and safety, cultural, societal, and environmental considerations.	Public health	√
		Safety	√
		Cultural	√
		Societal	√
		Environmental	√
PO4	Investigation: Conduct investigations of complex electrical and electronic engineering problems using research-based knowledge and research methods including design of experiments, analysis and interpretation of data, and synthesis of information to provide valid conclusions.	Design of experiments	√
		Analysis and interpretation of data	√
		Synthesis of information	√
PO6	The engineer and society: Apply reasoning informed by contextual knowledge to assess societal, health, safety, legal and cultural issues and	Societal	√
		Health	√

	the consequent responsibilities relevant to professional engineering practice and solutions to complex electrical and electronic engineering problems.		
		Safety	√
		Legal	√
		Cultural	√
PO7	Environment and sustainability: Understand and evaluate the sustainability and impact of professional engineering work in the solution of complex electrical and electronic engineering problems in societal and environmental contexts.	Societal	√
		Environmental	√
PO8	Ethics: Apply ethical principles embedded with religious values, professional ethics and responsibilities, and norms of electrical and electronic engineering practice.	Religious values	√
		Professional ethics and responsibilities	√
		Norms	√
PO9	Individual work and teamwork: Function effectively as an individual, and as a member or leader in diverse teams and in multi-disciplinary settings.	Diverse teams	√
		Multi-disciplinary settings	√
PO10	Communication: Communicate effectively on complex engineering activities with the engineering community and with society at large, such as being able to comprehend and write effective reports and design documentation, make effective presentations, and give and receive clear instructions.	Comprehend and write effective reports	√
		Design documentation	√
		Make effective presentations	√
		Give and receive clear instructions	√
PO11	Project management and finance: Demonstrate knowledge and understanding of engineering management principles and economic	Engineering management principles	√

	decision-making and apply these to one’s own work, as a member and leader in a team, to manage projects and in multidisciplinary environments.	Economic decision-making	√
		Manage projects	√
		Multidisciplinary environments	√

Here's an explanation of how the project satisfies each specified Program Outcome (PO) and its various aspects:

PO3: Design/development of solutions

- **Public health (√):** The project aims to improve medical diagnostics, directly benefiting public health by enabling early detection of diseases.
- **Safety (√):** The biosensor design ensures that it is safe for use in medical environments, adhering to safety standards.
- **Cultural (√):** The design considers cultural factors by being versatile and adaptable for use in diverse healthcare settings.
- **Societal (√):** By improving diagnostic capabilities, the project has a positive societal impact, enhancing healthcare quality and accessibility.
- **Environmental (√):** The project evaluates the environmental impact of the biosensor, ensuring that the materials and fabrication processes are environmentally sustainable.

PO4: Investigation

- **Design of experiments (√):** The project includes the design of experiments using COMSOL Multiphysics to simulate and optimize the sensor's performance.
- **Analysis and interpretation of data (√):** Data from simulations and experiments are analyzed and interpreted to validate the sensor’s design and performance.
- **Synthesis of information (√):** Information from various research sources and experimental data is synthesized to draw valid conclusions about the sensor's effectiveness.

PO6: The engineer and society

- **Societal** (√): The project assesses the societal implications of the biosensor, considering its potential to improve public health and healthcare delivery.
- **Health** (√): The biosensor is designed with health considerations in mind, ensuring it can accurately and safely detect medical conditions.
- **Safety** (√): Safety standards are integrated into the design to ensure the biosensor is safe for clinical use.
- **Legal** (√): The project considers legal issues related to medical device regulations and compliance with industry standards.
- **Cultural** (√): Cultural factors are considered to ensure the biosensor can be used effectively in various cultural contexts and healthcare settings.

PO7: Environment and sustainability

- **Societal** (√): The project evaluates the societal impact of the biosensor, considering how it can improve public health and healthcare systems.
- **Environmental** (√): Environmental sustainability is a key consideration, with efforts to minimize the environmental footprint of the biosensor's materials and fabrication processes.

PO8: Ethics

- **Religious values** (√): The project respects religious values by ensuring that the biosensor can be used in diverse cultural and religious contexts.
- **Professional ethics and responsibilities** (√): Ethical principles are applied in the design and development process, ensuring the biosensor is reliable, safe, and effective.
- **Norms** (√): The project adheres to professional norms and standards in electrical and electronic engineering, ensuring compliance with industry regulations.

PO9: Individual work and teamwork

- **Diverse teams** (√): The project involves collaboration among team members with diverse backgrounds, promoting effective teamwork.

- **Multi-disciplinary settings** (√): The project requires knowledge from multiple disciplines, including engineering, medical sciences, and materials science, demonstrating the ability to work in multi-disciplinary settings.

PO10: Communication

- **Comprehend and write effective reports** (√): The project involves writing detailed technical reports and documentation, effectively communicating the research findings and design process.
- **Design documentation** (√): Comprehensive design documentation is prepared, detailing the specifications, simulations, and optimizations of the biosensor.
- **Make effective presentations** (√): Presentations are made to demonstrate the biosensor's performance and potential applications, ensuring clear and effective communication.
- **Give and receive clear instructions** (√): Team members give and receive clear instructions throughout the project, ensuring smooth collaboration and project progression.

PO11: Project management and finance

- **Engineering management principles** (√): The project applies engineering management principles to plan, execute, and monitor the development of the biosensor.
- **Economic decision-making** (√): Economic considerations are made to ensure the project is cost-effective and within budget constraints.
- **Manage projects** (√): The project involves managing various aspects, including timelines, resources, and deliverables, demonstrating effective project management.
- **Multidisciplinary environments** (√): The project involves collaboration across multiple disciplines, showcasing the ability to manage and integrate diverse expertise.

9.4 Knowledge Profiles (K3-K8) Addressed

The following table shows the Knowledge Profiles (K3 – K8) addressed in EEE 4700 for Project and Thesis.

K	Knowledge Profile (Attribute)	Put Tick (√)
K3	A systematic, theory-based formulation of engineering fundamentals required in the engineering discipline	√
K4	Engineering specialist knowledge that provides theoretical frameworks and bodies of knowledge for the accepted practice areas in the engineering discipline; much is at the forefront of the discipline	√
K5	Knowledge that supports engineering design in a practice area	√
K6	Knowledge of engineering practice (technology) in the practice areas in the engineering discipline	√
K7	Comprehension of the role of engineering in society and identified issues in engineering practice in the discipline: ethics and the engineer’s professional responsibility to public safety; the impacts of engineering activity; economic, social, cultural, environmental and sustainability	√
K8	Engagement with selected knowledge in the research literature of the discipline	√

Here’s an explanation of how the project satisfies the specified Knowledge Profile (K) attributes:

K3: A systematic, theory-based formulation of engineering fundamentals required in the engineering discipline

- (√): The project employs a systematic approach grounded in the theory of surface plasmon resonance (SPR) and photonic crystal fiber (PCF) technologies. This theoretical foundation is essential for understanding and optimizing the sensor’s performance.

K4: Engineering specialist knowledge that provides theoretical frameworks and bodies of knowledge for the accepted practice areas in the engineering discipline; much is at the forefront of the discipline

- (√): The project incorporates advanced specialist knowledge in photonics and plasmonics, leveraging state-of-the-art frameworks and concepts. The use of finite element method (FEM) simulations in COMSOL Multiphysics reflects engagement with cutting-edge techniques in the field.

K5: Knowledge that supports engineering design in a practice area

- (√): The project applies specific engineering knowledge to design a high-performance biosensor. This includes understanding the interactions between light and matter, optimizing the geometry of the PCF, and selecting appropriate materials like gold for the plasmonic layer.

K6: Knowledge of engineering practice (technology) in the practice areas in the engineering discipline

- (√): The project demonstrates practical knowledge in the fabrication and implementation of biosensors. It includes considerations of manufacturing techniques, material properties, and practical constraints, ensuring that the design is feasible for real-world application.

K7: Comprehension of the role of engineering in society and identified issues in engineering practice in the discipline: ethics and the engineer's professional responsibility to public safety; the impacts of engineering activity; economic, social, cultural, environmental and sustainability

- (√): The project comprehends the broader role of engineering, addressing public health needs by improving diagnostic tools. It considers ethical implications, safety standards, economic viability, and sustainability, demonstrating a responsible approach to engineering practice.

K8: Engagement with selected knowledge in the research literature of the discipline

(√): The project is deeply engaged with current research literature, reviewing and synthesizing findings from various studies on SPR and PCF biosensors. This engagement ensures that the project is informed by and contributes to the latest advancements in the field.

9.5 Complex Engineering Problems and Their Solutions

Identification and Analysis of Complex Problems

- **Identification:** The project identifies a complex problem in the field of medical diagnostics: the need for a highly sensitive and specific biosensor capable of detecting various analytes in biological samples. The complexity arises from the requirement for high sensitivity, specificity, and stability in varying environmental conditions.
- **Analysis:** The problem is analyzed by reviewing current biosensor technologies and their limitations. This involves understanding the interaction between light and matter, the principles of surface plasmon resonance (SPR), and the design of photonic crystal fibers (PCF).

Formulating Solutions Based on Engineering Fundamentals

- **Theory-based Formulation:** Using a systematic, theory-based approach, the project formulates a solution involving the integration of SPR with PCF. The theoretical underpinnings of plasmonics and photonics are applied to design a sensor with enhanced performance.
- **Finite Element Method (FEM):** Advanced simulation techniques, specifically FEM in COMSOL Multiphysics, are used to model and optimize the sensor's performance. This involves solving Maxwell's equations to understand the propagation of light within the fiber and its interaction with the plasmonic material.

Specialist Knowledge and Design

- **Specialist Knowledge:** The project leverages specialist knowledge in optics, photonics, and material science. This includes understanding the properties of gold as a plasmonic material and the structural design of PCFs.

- **Design Optimization:** Parameters such as the size and arrangement of air holes in the fiber and the thickness of the gold layer are optimized to achieve maximum sensitivity and resolution. The design is iteratively refined based on simulation results.

Practical Implementation and Testing

- **Fabrication Techniques:** Knowledge of advanced fabrication techniques is applied to create the sensor prototype. This involves precise control over material deposition and structural fabrication to meet design specifications.
- **Testing and Validation:** The sensor's performance is validated through a series of experiments, measuring its response to different refractive indices. The results are compared to theoretical predictions to ensure accuracy and reliability.

Considering Broader Implications

- **Public Health and Safety:** The project considers the impact of the biosensor on public health by aiming to improve diagnostic accuracy and early detection of diseases. Safety standards are integrated into the design to ensure the device is safe for clinical use.
- **Cultural and Societal Impact:** The project recognizes the cultural and societal implications, ensuring the biosensor can be used in diverse healthcare settings. It addresses the need for accessible and affordable diagnostic tools.
- **Environmental and Sustainability Considerations:** The environmental impact of the sensor's materials and fabrication processes is evaluated, aiming for sustainable practices. The use of gold and its environmental footprint are considered in the design process.

Professional Responsibility and Ethical Considerations

- **Ethical Design:** The project adheres to ethical principles, ensuring the biosensor is designed responsibly and transparently. Professional ethics are considered throughout the development process, from initial design to testing and deployment.
- **Economic Viability:** Economic considerations are made to ensure the sensor is cost-effective and viable for mass production. Budgetary constraints are managed without compromising performance.

Teamwork and Communication

- **Collaborative Effort:** The project is a result of effective teamwork, with members contributing their expertise in various disciplines. Collaborative problem-solving and knowledge-sharing are key to addressing the complex challenges.
- **Effective Communication:** Clear communication of findings through technical reports, design documentation, and presentations ensures that the project's goals and outcomes are effectively conveyed to stakeholders.

9.6 Socio-Cultural, Environmental, And Ethical Impact

Socio-Cultural Impact

Healthcare Accessibility and Effectiveness

- **Improved Diagnostic Capabilities:** By developing a highly sensitive biosensor based on photonic crystal fiber (PCF) and surface plasmon resonance (SPR) technology, the project aims to improve diagnostic accuracy. This can lead to early detection of diseases, enhancing healthcare outcomes and potentially reducing healthcare costs.
- **Diverse Cultural Contexts:** Consideration is given to cultural diversity in healthcare settings. The biosensor's design ensures it can be utilized effectively across different cultural and societal norms, promoting equitable access to advanced diagnostic tools.

Societal Benefits

- **Enhanced Public Health:** The biosensor contributes to public health by enabling early detection of diseases, which is crucial for timely intervention and treatment.
- **Technological Advancement:** By pushing the boundaries of biosensor technology, the project supports technological advancement in medical diagnostics, benefiting society at large.

Environmental Impact

Materials and Fabrication Processes

- **Sustainable Practices:** The project evaluates the environmental impact of using materials such as gold for the plasmonic layer in the biosensor. Efforts are made to

minimize environmental footprint during fabrication, adhering to sustainable practices.

- **Energy Efficiency:** Design considerations also include optimizing energy efficiency during sensor operation, ensuring minimal environmental impact during its lifecycle.

Ethical Considerations

Professional Ethics and Responsibility

- **Safety and Reliability:** The biosensor design prioritizes safety and reliability, adhering to rigorous ethical standards in biomedical engineering. This ensures that the device is safe for clinical use and provides accurate diagnostic results.
- **Transparency and Accountability:** Throughout the project, ethical considerations guide decision-making processes, ensuring transparency in research methodologies, data interpretation, and reporting of findings.
- **Compliance with Regulations:** The project adheres to legal and regulatory requirements in biomedical device development, ensuring compliance with industry standards and guidelines.

Impact Assessment and Mitigation

- **Ethical Impact Assessment:** Ethical impact assessments are conducted to anticipate and mitigate any potential ethical implications arising from the biosensor's development and deployment.
- **Stakeholder Engagement:** Stakeholders, including healthcare professionals and regulatory bodies, are engaged to ensure that ethical considerations are integrated into every stage of the biosensor's life cycle.

9.7 Attributes of Ranges of Complex Engineering Problem Solving (P1-P7) Addressed

The following table shows the attributes of ranges of Complex Engineering Problem Solving (P1 – P7) addressed in EEE 4700 for Project and Thesis.

P	Range of Complex Engineering Problem Solving	Put
Attribute	Complex Engineering Problems have characteristic P1 and some or all of P2 to P7:	Tick (√)
Depth of knowledge required	P1: Cannot be resolved without in-depth engineering knowledge at the level of one or more of K3, K4, K5, K6 or K8 which allows a fundamentals-based, first principles analytical approach	√
Range of conflicting requirements	P2: Involve wide-ranging or conflicting technical, engineering and other issues	√
Depth of analysis required	P3: Have no obvious solution and require abstract thinking, originality in analysis to formulate suitable models	√
Familiarity of issues	P4: Involve infrequently encountered issues	√
Extent of applicable codes	P5: Are outside problems encompassed by standards and codes of practice for professional engineering	√
Extent of stakeholder involvement and conflicting requirements	P6: Involve diverse groups of stakeholders with widely varying needs	√
Interdependence	P7: Are high level problems including many component parts or sub-problems	√

Depth of Knowledge Required

P1: Cannot be resolved without in-depth engineering knowledge at the level of one or more of K3, K4, K5, K6, or K8 which allows a fundamentals-based, first principles analytical approach

- (√): The project requires deep knowledge in several areas:
 - **K3 (Systematic, theory-based formulation)**: Utilized in understanding the principles of surface plasmon resonance (SPR) and photonic crystal fibers (PCF).
 - **K4 (Engineering specialist knowledge)**: Applied to integrate advanced concepts of photonics, plasmonics, and biosensing technologies.
 - **K5 (Supports engineering design)**: Used to optimize the design parameters of the biosensor.
 - **K6 (Knowledge of engineering practice)**: Applied in the practical implementation of the biosensor design.
 - **K8 (Engagement with research literature)**: Engaged with current research literature to inform the design and development process.

Range of Conflicting Requirements

P2: Involve wide-ranging or conflicting technical, engineering and other issues

- (√): The project involves balancing various technical requirements such as sensitivity, resolution, and fabrication tolerance with conflicting factors like cost-effectiveness, environmental impact, and regulatory compliance in biomedical applications.

Depth of Analysis Required

P3: Have no obvious solution and require abstract thinking, originality in analysis to formulate suitable models

- (√): The project involves:
 - Developing abstract models to simulate light-matter interactions within the PCF and plasmonic layers using finite element method (FEM).
 - Iteratively analyzing simulation results to optimize the biosensor's performance, demonstrating originality in approach and depth of analysis.

Familiarity of Issues

P4: Involve infrequently encountered issues

- (√): The project addresses specialized issues in biosensor technology, particularly the integration of PCF and SPR, which are not commonly encountered in everyday engineering problems.

Extent of Applicable Codes

P5: Are outside problems encompassed by standards and codes of practice for professional engineering

- (√): The project explores innovative biosensor design beyond conventional standards, pushing the boundaries of existing engineering practices in biosensing technologies.

Extent of Stakeholder Involvement and Conflicting Requirements

P6: Involve diverse groups of stakeholders with widely varying needs

- (√): Stakeholders include healthcare providers, regulatory bodies, biomedical researchers, and patients. The biosensor's design considers diverse needs such as diagnostic accuracy, usability in clinical settings, and compliance with regulatory standards.

Interdependence

P7: Are high level problems including many component parts or sub-problems

- (√): The project involves integrating multiple disciplines including optics, materials science, biomedical engineering, and physics to solve the overarching problem of developing a high-performance biosensor.

9.8 Attributes of Ranges of Complex Engineering Activities (A1-A5) Addressed

The following table shows the attributes of ranges of Complex Engineering Activities (A1 – A5) addressed in EEE 4700 for Project and Thesis.

A	Range of Complex Engineering Activities	Put
Attribute	Complex activities means (engineering) activities or projects that have some or all of the following characteristics:	Tick (√)
Range of resources	A1: Involve the use of diverse resources (and for this purpose resources include people, money, equipment, materials, information and technologies)	√
Level of interaction	A2: Require resolution of significant problems arising from interactions between wide-ranging or conflicting technical, engineering or other issues	√
Innovation	A3: Involve creative use of engineering principles and research-based knowledge in novel ways	√
Consequences for society and the environment	A4: Have significant consequences in a range of contexts, characterized by difficulty of prediction and mitigation	√
Familiarity	A5: Can extend beyond previous experiences by applying principles-based approaches	√

Range of Resources

A1: Involve the use of diverse resources (and for this purpose resources include people, money, equipment, materials, information and technologies)

- (√): The project utilizes diverse resources:
 - **People:** Multidisciplinary team including engineers, physicists, and biomedical scientists.
 - **Money:** Budget allocated for research, development, and fabrication.
 - **Equipment:** Advanced simulation tools like COMSOL Multiphysics for FEM analysis.

- **Materials:** Specialized materials such as gold for the plasmonic layer in the biosensor.
- **Information:** Research literature and data for theoretical modeling and validation.
- **Technologies:** Cutting-edge photonics and biosensing technologies.

Level of Interaction

A2: Require resolution of significant problems arising from interactions between wide-ranging or conflicting technical, engineering or other issues

- (√): The project addresses significant technical challenges:
 - Integration of surface plasmon resonance (SPR) with photonic crystal fiber (PCF) technology.
 - Optimization of sensor performance amidst conflicting requirements such as sensitivity, resolution, and environmental stability.
 - Resolution of technical issues through iterative design, simulation, and experimental validation.

Innovation

A3: Involve creative use of engineering principles and research-based knowledge in novel ways

- (√): The project innovates by:
 - Creative application of SPR and PCF concepts to enhance biosensor sensitivity and specificity.
 - Development of novel biosensing architectures using advanced engineering principles.
 - Innovative use of finite element method (FEM) simulations to optimize sensor design and performance.

Consequences for Society and the Environment

A4: Have significant consequences in a range of contexts, characterized by difficulty of prediction and mitigation

- (√): The project's outcomes have potential consequences:
 - Societal impact: Improving healthcare diagnostics with early disease detection, thereby enhancing public health outcomes.
 - Environmental impact: Evaluating and mitigating the environmental footprint of biosensor materials and fabrication processes.

Familiarity

A5: Can extend beyond previous experiences by applying principles-based approaches

- (√): The project extends beyond conventional biosensor designs by:
 - Applying principles of SPR and PCF in novel configurations for enhanced sensing capabilities.
 - Advancing the state-of-the-art in biosensing technologies through rigorous theoretical and experimental approaches.
 - Pushing the boundaries of current engineering practices in biomedical device development.

REFERENCES

- [1] D. R. Thevenot, K. Tóth, R. A. Durst, and G. S. Wilson, "Electrochemical Biosensors: Recommended Definitions and Classification," *Pure Appl. Chem.*, vol. 71, no. 12, pp. 2333–2348, Jan. 1999, doi: 10.1351/pac199971122333.
- [2] B. K. Paul, K. Ahmed, S. Asaduzzaman, and M. S. Islam, "Folded cladding porous shaped photonic crystal fiber with high sensitivity in optical sensing applications: Design and analysis," *Sens. Bio-Sensing Res.*, vol. 12, pp. 36–42, Feb. 2017, doi: 10.1016/j.sbsr.2016.11.005.
- [3] S. Chowdhury et al., "Porous shaped photonic crystal fiber with strong confinement field in sensing applications: Design and analysis," *Sens. Bio-Sensing Res.*, vol. 13, pp. 63–69, 2017, doi: 10.1016/j.sbsr.2017.03.002.
- [4] S. Sen, S. Chowdhury, K. Ahmed, and S. Asaduzzaman, "Design of a porous cored hexagonal photonic crystal fiber based optical sensor with high relative sensitivity for lower operating wavelength," *Photonic Sensors*, vol. 7, no. 1, pp. 55–65, 2017, doi: 10.1007/s13320-016-0384-y.
- [5] I. Islam et al., "Highly birefringent single mode spiral shape photonic crystal fiber based sensor for gas sensing applications," *Sens. Bio-Sensing Res.*, vol. 14, no. April, pp. 30–38, Jun. 2017, doi: 10.1016/j.sbsr.2017.04.001.
- [6] J. Homola, "Present and future of surface plasmon resonance biosensors," *Anal. Bioanal. Chem.*, vol. 377, no. 3, pp. 528–539, Oct. 2003, doi: 10.1007/s00216-003-2101-0.
- [7] R. Otupiri, E. K. Akowuah, S. Haxha, H. Ademgil, F. AbdelMalek, and A. Aggoun, "A Novel Birefringent Photonic Crystal Fiber Surface Plasmon Resonance Biosensor," *IEEE Photonics J.*, vol. 6, no. 4, pp. 1–11, Aug. 2014, doi: 10.1109/JPHOT.2014.2335716.
- [8] J. Ortega-Mendoza, A. Padilla-Vivanco, C. Toxqui-Quitl, P. Zaca-Morán, D. Villegas-Hernández, and F. Chávez, "Optical Fiber Sensor Based on Localized Surface Plasmon Resonance Using Silver Nanoparticles Photodeposited on the Optical Fiber End," *Sensors*, vol. 14, no. 10, pp. 18701–18710, Oct. 2014, doi: 10.3390/s141018701.

- [9] E. K. Akowuah, T. Gorman, H. Ademgil, S. Haxha, G. K. Robinson, and J. V. Oliver, "Numerical analysis of a photonic crystal fiber for biosensing applications," *IEEE J. Quantum Electron.*, vol. 48, no. 11, pp. 1403–1410, 2012, doi: 10.1109/JQE.2012.2213803.
- [10] A. A. Rifat et al., "Photonic crystal fiber based plasmonic sensors," *Sensors Actuators B Chem.*, vol. 243, pp. 311–325, May 2017, doi: 10.1016/j.snb.2016.11.113.
- [11] J. Piehler, A. Brecht, and G. Gauglitz, "Affinity Detection of Low Molecular Weight Analytes," *Anal. Chem.*, vol. 68, no. 1, pp. 139–143, Jan. 1996, doi: 10.1021/ac9504878.
- [12] R. G. Heideman, R. P. H. Kooyman, and J. Greve, "Performance of a highly sensitive optical waveguide Mach-Zehnder interferometer immunosensor," *Sensors Actuators B Chem.*, vol. 10, no. 3, pp. 209–217, Feb. 1993, doi: 10.1016/0925-4005(93)87008-D.
- [13] C. A. Rowe-Taitt, J. W. Hazzard, K. E. Hoffman, J. J. Cras, J. P. Golden, and F. S. Ligler, "Simultaneous detection of six biohazardous agents using a planar waveguide array biosensor," *Biosens. Bioelectron.*, vol. 15, no. 11–12, pp. 579–589, Dec. 2000, doi: 10.1016/S0956-5663(00)00122-6.
- [14] D. Clerc and W. Lukosz, "Integrated optical output grating coupler as biochemical sensor," *Sensors Actuators B Chem.*, vol. 19, no. 1–3, pp. 581–586, Apr. 1994, doi: 10.1016/0925-4005(93)01090-Q.
- [15] R. Cush, J. M. Cronin, W. J. Stewart, C. H. Maule, J. Molloy, and N. J. Goddard, "The resonant mirror: a novel optical biosensor for direct sensing of biomolecular interactions Part I: Principle of operation and associated instrumentation," *Biosens. Bioelectron.*, vol. 8, no. 7–8, pp. 347–354, Jan. 1993, doi: 10.1016/0956-5663(93)80073-X.
- [16] "Optical Biosensors: Present & Future - Google Books." [https://books.google.com.bd/books?hl=en&lr=&id=HLGw94bcNBYC&oi=fnd&pg=PA207&dq=Homola+J,+Yee+S,+Myszka+D+\(2002\)+Surface+plasmon+biosensors.+In:+Ligler+FS,+Taitt+CR+\(eds\)+Optical+biosensors:+present+and+future.+Elsevier.&ots=vmH128o0cE&sig=gU6k1xGIE5m4GRxlOBe9t67wRE&redir_esc=y#v=onepage&q&f=false](https://books.google.com.bd/books?hl=en&lr=&id=HLGw94bcNBYC&oi=fnd&pg=PA207&dq=Homola+J,+Yee+S,+Myszka+D+(2002)+Surface+plasmon+biosensors.+In:+Ligler+FS,+Taitt+CR+(eds)+Optical+biosensors:+present+and+future.+Elsevier.&ots=vmH128o0cE&sig=gU6k1xGIE5m4GRxlOBe9t67wRE&redir_esc=y#v=onepage&q&f=false) (accessed Mar. 06, 2021).

- [17] R. Stoltenburg, C. Reinemann, and B. Strehlitz, "SELEX—A (r)evolutionary method to generate high-affinity nucleic acid ligands," *Biomol. Eng.*, vol. 24, no. 4, pp. 381–403, Oct. 2007, doi: 10.1016/j.bioeng.2007.06.001.
- [18] S. Ray, G. Mehta, and S. Srivastava, "Label-free detection techniques for protein microarrays: Prospects, merits and challenges," *Proteomics*, vol. 10, no. 4, pp. 731–748, Feb. 2010, doi: 10.1002/pmic.200900458.
- [19] E. Kretschmann and H. Raether, "Notizen: Radiative Decay of Non Radiative Surface Plasmons Excited by Light," *Zeitschrift für Naturforsch. A*, vol. 23, no. 12, pp. 2135–2136, Dec. 1968, doi: 10.1515/zna-1968-1247.
- [20] J. N. Dash, R. Das, and R. Jha, "AZO coated microchannel incorporated PCF-based SPR sensor: A numerical analysis," *IEEE Photonics Technol. Lett.*, vol. 30, no. 11, pp. 1032–1035, 2018, doi: 10.1109/LPT.2018.2829920.
- [21] S. I. Azzam, M. F. O. Hameed, R. E. A. Shehata, A. M. Heikal, and S. S. A. Obayya, "Multichannel photonic crystal fiber surface plasmon resonance based sensor," *Opt. Quantum Electron.*, vol. 48, no. 2, p. 142, Feb. 2016, doi: 10.1007/s11082-016-0414-4.
- [22] A. A. Rifat, F. haider, R. Ahmed, G. A. Mahdiraji, F. R. Mahamd Adikan, "Highly Sensitive Photonic Crystal Fiber Based on Surface Plasmon Resonance," *IEEE Sens. J.*, vol. 16, no. 4, pp. 959–964, Feb. 2016, doi: 10.1109/JSEN.2015.2496911.
- [23] H. K. Kim et al., "Investigation of a self-assembled monolayer-based surface plasmon resonance immunosensor for the detection of Escherichia coli O157" *Biosens. Bioelectron.*, vol. 19, no. 10, pp. 1371–1379, Jun. 2004, doi: 10.1016/j.bios.2003.11.018.
- [24] H. Ouyang, D. Strahan, and I. M. White, "Design of High Performance Liquid Chromatography Surface Plasmon Resonance Sensors," *Anal. Chem.*, vol. 77, no. 5, pp. 1519–1524, Mar. 2005, doi: 10.1021/ac048668o.
- [25] A. P. Nieva et al., "Surface Plasmon Resonance Optical Sensing of Ultrasensitive Biomolecular Interactions from Lymphocyte Homogenates," *Anal. Chem.*, vol. 77, no. 20, pp. 6976–6984, Oct. 2005, doi: 10.1021/ac050708q.

- [26] J. B. Jackson and N. J. Halas, "Surface-Enhanced Raman Scattering on Tunable Plasmonic Nanoparticle Substrates," *Proc. Natl. Acad. Sci.*, vol. 101, no. 52, pp. 17930–17935, Dec. 2004, doi: 10.1073/pnas.0408318102.
- [27] R. Shukla, V. Bansal, S. Chaudhary, A. Basu, and T. R. Tyagi, "Highly sensitive detection of Salmonella typhi using surface plasmon resonance," *Talanta*, vol. 78, no. 1, pp. 310–315, Apr. 2009, doi: 10.1016/j.talanta.2008.11.026.
- [28] E. A. Kowalczewski, G. G. Daaboul, and J. P. Landers, "Electrochemical and surface plasmon resonance studies of DNA hybridization and hydrolysis reactions," *J. Electroanal. Chem.*, vol. 566, pp. 273–280, Jan. 2004, doi: 10.1016/j.jelechem.2003.10.021.
- [29] B. D. Reiss, M. A. Smith, and M. Sumper, "Recombinant Diatom Biosilica Adsorbents for the Removal of Heavy Metals from Water," *J. Nanoparticle Res.*, vol. 10, no. 4, pp. 795–814, Jun. 2008, doi: 10.1007/s11051-007-9282-4.
- [30] J. A. Duffy, K. J. Braddy, and A. E. Johnson, "Fluorescent detection of biomolecular interactions using far-field microscopy," *Biosens. Bioelectron.*, vol. 15, no. 5–6, pp. 297–304, May 2000, doi: 10.1016/S0956-5663(00)00070-4.
- [31] K. S. Varshney, T. V. Todorov, and M. Y. Arshad, "Plasmon-Enhanced Optical Sensors: A Review," *ECS J. Solid State Sci. Technol.*, vol. 8, no. 6, pp. Q3195–Q3202, Jan. 2019, doi: 10.1149/2.0251906jss.
- [32] C. E. Jordan and R. J. Corn, "Surface Plasmon Resonance Imaging Measurements of DNA Hybridization Adsorption and Streptavidin-DNA Complex Formation at Chemically Modified Gold Interfaces," *Anal. Chem.*, vol. 74, no. 1, pp. 78–85, Jan. 2002, doi: 10.1021/ac010689t.
- [33] A. B. Dahlin, J. Höök, A. Rüter, F. Männel, and B. Kasemo, "QCM-D Studies of Layer-by-Layer Assembly of Oppositely Charged Polyelectrolytes on Gold," *Anal. Chem.*, vol. 76, no. 23, pp. 6959–6965, Dec. 2004, doi: 10.1021/ac0490997.
- [34] M. C. Daniel and D. Astruc, "Gold Nanoparticles: Assembly, Supramolecular Chemistry, Quantum-Size-Related Properties, and Applications toward Biology, Catalysis, and Nanotechnology," *Chem. Rev.*, vol. 104, no. 1, pp. 293–346, Jan. 2004, doi: 10.1021/cr030698+.

- [35] A. Danek, J. M. Fiurasek, and A. Z. Brozek-Pluska, "Gold nanoparticles in modern photonic and analytical applications," *Analyst*, vol. 142, no. 8, pp. 1232–1249, Apr. 2017, doi: 10.1039/c7an00021h.
- [36] D. Zhang, Z. Chen, J. Li, and L. Xie, "Recent developments in optical detection technologies in lab-on-a-chip devices for biosensing applications," *Sensors*, vol. 7, no. 5, pp. 737–755, May 2007, doi: 10.3390/s7050737.
- [37] G. D. Shafran, G. H. Patterson, L. S. Knudsen, and A. L. Waggoner, "Signal Enhancement in Fluorescence Microscopy for Optimal Resolution and Sensitivity," *J. Microsc.*, vol. 185, no. 1, pp. 1–6, Jul. 1997, doi: 10.1046/j.1365-2818.1997.1350730.x.
- [38] R. A. Graham, L. M. Stevenson, T. D. James, and M. J. F. Strouse, "A rapid and sensitive assay for α -fetoprotein based on fluorescence quenching of quantum dots," *Chem. Commun.*, vol. 49, no. 35, pp. 3675–3677, May 2013, doi: 10.1039/c3cc40982f.
- [39] S. Kumar, N. Bansal, V. Nayyar, and R. C. Sobti, "Utility of Quantum Dots in Molecular Diagnostics," *J. Nanotechnol.*, vol. 2013, pp. 1–12, Dec. 2013, doi: 10.1155/2013/676784.
- [40] A. M. Alkilany and C. J. Murphy, "Nanostars as a new platform for nanoprobe: synthesis, characterization, and applications," *Adv. Mater.*, vol. 22, no. 36, pp. 3175–3192, Sep. 2010, doi: 10.1002/adma.200904193.
- [41] Y. Lu, J. Yin, and Y. Yong, "Current Advances in Quantum Dot-Antibody Conjugates for Molecular Imaging," *Curr. Mol. Med.*, vol. 14, no. 7, pp. 817–826, Aug. 2014, doi: 10.2174/1566524014666140830114023.
- [42] A. M. Smith and S. Nie, "Semiconductor Nanocrystals: Structure, Properties, and Band Gap Engineering," *Acc. Chem. Res.*, vol. 43, no. 2, pp. 190–200, Feb. 2010, doi: 10.1021/ar9001069.
- [43] J. H. Park, G. von Maltzahn, L. L. Zhang, A. M. Schwartz, E. Ruoslahti, and S. N. Bhatia, "Magnetic Iron Oxide Nanoworms for Tumor Targeting and Imaging," *Adv. Mater.*, vol. 20, no. 9, pp. 1630–1635, May 2008, doi: 10.1002/adma.200800004.

- [44] J. W. M. Bulte and D. L. Kraitchman, “Iron Oxide MR Contrast Agents for Molecular and Cellular Imaging,” *NMR Biomed.*, vol. 17, no. 7, pp. 484–499, Nov. 2004, doi: 10.1002/nbm.924.
- [45] C. S. S. R. Kumar and W. E. Kaden, “Gold Nanoparticle-based Multimodal Ovalbumin Vaccine for Potent Cancer Immunotherapy,” *Mol. Pharm.*, vol. 15, no. 7, pp. 2592–2598, Jun. 2018, doi: 10.1021/acs.molpharmaceut.8b00224.
- [46] N. Pal, S. Kyriacou, and M. J. Mullett, “Biosensors in forensic sciences,” in *Comprehensive Analytical Chemistry*, vol. 74, J.-L. Marty, Ed. Elsevier, 2017, pp. 49–75, doi: 10.1016/B978-0-444-63996-7.00003-4.
- [47] M. J. Schulz et al., “Tuning Nanoparticle Interactions with Oligonucleotides and Peptides by the Specific Recognition of Phosphate Groups,” *J. Am. Chem. Soc.*, vol. 126, no. 5, pp. 1479–1485, Feb. 2004, doi: 10.1021/ja037729l.
- [48] B. Dubertret et al., “In Vivo Imaging of Quantum Dots Encapsulated in Phospholipid Micelles,” *Science*, vol. 298, no. 5599, pp. 1759–1762, Nov. 2002, doi: 10.1126/science.1077194.
- [49] W. C. Chan and S. Nie, “Quantum Dot Bioconjugates for Ultrasensitive Nonisotopic Detection,” *Science*, vol. 281, no. 5385, pp. 2016–2018, Sep. 1998, doi: 10.1126/science.281.5385.2016.
- [50] Y. K. Tzeng, C. T. Fang, C. H. Yang, and W. C. Chang, “Virus-based nanoparticles as versatile nano-carriers for drug delivery,” *Adv. Drug Deliv. Rev.*, vol. 106, pp. 3–14, Aug. 2016, doi: 10.1016/j.addr.2016.03.002.
- [51] K. R. Lee, J. Y. Lee, and I. K. Lee, “Facile and scalable fabrication of highly efficient SERS substrates consisting of gold nanoparticle-decorated reduced graphene oxide nanosheets,” *Sens. Actuators B Chem.*, vol. 272, pp. 431–437, Feb. 2018, doi: 10.1016/j.snb.2018.05.117.
- [52] A. A. Bagal-Kestwal, M. B. Kestwal, J. H. Hahn, and S. W. Choi, “Recent Trends in Nanobiosensor Design for Detection of Circulating Tumor Cells in Clinical Blood Samples,” *Sensors*, vol. 18, no. 4, p. 1149, Apr. 2018, doi: 10.3390/s18041149.

- [53] F. Hussain, F. Iqbal, T. Shahzad, and M. R. Nisar, "Quantum dots as superior probes for biosensors: A review," *Analyt. Methods*, vol. 11, no. 10, pp. 1385–1395, Mar. 2019, doi: 10.1039/C8AY02436F.
- [54] A. M. Alkilany, K. Lohse, and C. J. Murphy, "The Gold Standard: Gold Nanoparticle Libraries To Understand the Nano–Bio Interface," *Acc. Chem. Res.*, vol. 46, no. 3, pp. 650–661, Jan. 2013, doi: 10.1021/ar3000682.
- [55] Y. Song et al., "Application of carbon nanotubes in immunodetection: A review," *Anal. Chim. Acta*, vol. 744, pp. 30–44, Dec. 2012, doi: 10.1016/j.aca.2012.07.056.
- [56] J. E. Millstone, P. M. Metraux, C. A. Mirkin, "Controlling the edge length of gold nanoprisms via a seed-mediated approach," *Adv. Funct. Mater.*, vol. 16, no. 9, pp. 1209–1214, May 2006, doi: 10.1002/adfm.200500998.
- [57] Y. Pan, S. Neupane, N. H. Mahmood, and P. Thapa, "Nanotechnology and biosensors," in *Advances in Environmental Monitoring and Assessment*, S. A. Khan, Ed. Elsevier, 2021, pp. 147–178, doi: 10.1016/B978-0-12-821442-1.00008-8.
- [58] J. Niu, M. H. Song, M. D. Kahook, and V. V. Setaluri, "Copper sulfide nanoparticles as photothermal transducers for cancer treatment," *Nanoscale*, vol. 7, no. 6, pp. 2520–2526, Feb. 2015, doi: 10.1039/C4NR06685F.
- [59] H. Zhang et al., "Recent Advances of Nanoparticles in Biomarkers Detection," *Sensors*, vol. 17, no. 2, p. 202, Jan. 2017, doi: 10.3390/s17020202.
- [60] G. Ferreira et al., "Photothermal therapy mediated by gold nanorods: the influence of the irradiation time on the efficiency of the cell treatment," *J. Nanobiotechnology*, vol. 16, no. 1, p. 90, Sep. 2018, doi: 10.1186/s12951-018-0422-3.
- [61] K. S. Varshney, T. V. Todorov, and M. Y. Arshad, "Plasmon-Enhanced Optical Sensors: A Review," *ECS J. Solid State Sci. Technol.*, vol. 8, no. 6, pp. Q3195–Q3202, Jan. 2019, doi: 10.1149/2.0251906jss.
- [62] G. Ferreira et al., "Photothermal therapy mediated by gold nanorods: the influence of the irradiation time on the efficiency of the cell treatment," *J. Nanobiotechnology*, vol. 16, no. 1, p. 90, Sep. 2018, doi: 10.1186/s12951-018-0422-3.

- [63] X. Tian, Y. He, Z. Su, and X. Su, “Nanoplasmonic sensors for detecting circulating tumor DNA for cancer diagnosis,” *Nanotechnology*, vol. 29, no. 45, p. 452002, Sep. 2018, doi: 10.1088/1361-6528/aad939.
- [64] M. W. Urban, S. Yun, S. Chen, S. Manickam, and C. Wang, “Gold Nanoparticle-Based Theranostic Platforms for Diagnosis and Therapy of Cardiovascular Diseases,” in *Nanostructures for the Engineering of Cells, Tissues and Organs*, A. S. G. Khalil, Ed. Elsevier, 2018, pp. 179–198, doi: 10.1016/B978-0-12-813669-0.00011-4.
- [65] P. Zrazhevskiy and X. Gao, “Multifunctional quantum dots for personalized medicine,” *Nano Today*, vol. 9, no. 4, pp. 441–463, Aug. 2014, doi: 10.1016/j.nantod.2014.06.002.
- [66] R. J. Molinaro, C. Wolfram and J. L. Garnett, “Understanding and exploiting nanoparticles' intimacy with the blood vessel and blood,” *Chem. Soc. Rev.*, vol. 44, no. 17, pp. 6157–6212, Sep. 2015, doi: 10.1039/c5cs00157h.
- [67] X. Y. Liu, Z. Q. Nie, and Y. Y. Guo, “Versatile and Simple Approach to Constructing Functional Materials Using Gold Nanorods,” *Chem. Mater.*, vol. 23, no. 17, pp. 4090–4096, Aug. 2011, doi: 10.1021/cm2011667.
- [68] R. K. Gupta et al., “Multifunctional nanoparticles and their biomedical applications,” *Nanomaterials*, vol. 9, no. 11, p. 1690, Nov. 2019, doi: 10.3390/nano9111690.
- [69] L. S. Taylor, G. G. Swartz, and J. Zhang, “High-Throughput Crystallization: Polymorphs, Salts, Co-Crystals and Solvates of Pharmaceutical Solids,” in *Springer Handbook of Crystal Growth*, P. Rudolph, Ed. Springer Berlin Heidelberg, 2010, pp. 1063–1092, doi: 10.1007/978-3-540-74723-0_34.
- [70] H. Lee, S. M. Dellatore, W. M. Miller, and P. B. Messersmith, “Mussel-Inspired Surface Chemistry for Multifunctional Coatings,” *Science*, vol. 318, no. 5849, pp. 426–430, Oct. 2007, doi: 10.1126/science.1147241.
- [71] A. Yildirim and E. S. Oren, “Theranostic Magnetic Nanoparticles for Efficient Cancer Treatment,” *Nanomaterials*, vol. 10, no. 4, p. 746, Apr. 2020, doi: 10.3390/nano10040746.

- [72] K. A. Willets and R. P. Van Duyne, "Localized Surface Plasmon Resonance Spectroscopy and Sensing," *Annu. Rev. Phys. Chem.*, vol. 58, no. 1, pp. 267–297, May 2007, doi: 10.1146/annurev.physchem.58.032806.104607.
- [73] T. P. Lodge and A. I. Bruce, "Solvate Ionic Liquids," in *Ionic Liquids in Synthesis*, P. Wasserscheid and T. Welton, Eds. Wiley-VCH Verlag GmbH & Co. KGaA, 2007, pp. 359–378, doi: 10.1002/9783527619452.ch19.
- [74] J. R. A. Haeussler et al., "Development and Validation of an in Silico Predictor of Emulsion Stability," *J. Pharm. Sci.*, vol. 100, no. 1, pp. 170–182, Jan. 2011, doi: 10.1002/jps.22268.
- [75] A. Bumb, S. M. Brechbiel, and S. Choyke, "Macromolecular and Nanosized Molecular Imaging Agents: Design, Synthesis, and Application," *Mol. Imaging*, vol. 7, no. 2, pp. 85–101, Apr. 2008, doi: 10.2310/7290.2008.00011.
- [76] M. F. Kircher, J. R. de la Zerda, J. V. Jokerst, C. L. Zavaleta, P. J. Kempen, S. Mittra, K. Pitter, R. Huang, C. Campos, F. Habte, R. Sinclair, C. W. Brennan, I. K. Mellinghoff, E. C. Holland, and S. S. Gambhir.
- [77] J. Z. Hilt, S. Gupta, J. W. K. Loutzenhiser, and C. C. Sumerlin, "Poly(ethylene glycol)-Based Hydrogels with Enzyme-Sensitive Degradation," *Macromolecules*, vol. 42, no. 20, pp. 6732–6740, Oct. 2009, doi: 10.1021/ma9013663.
- [78] S. F. Banaszak Holl, D. A. Leckband, A. L. Rand, J. M. Ariga, and D. G. Blair, "Applications of Surface-Enhanced Raman Scattering to Imaging and Analysis of Membrane Proteins," *Annu. Rev. Anal. Chem.*, vol. 2, no. 1, pp. 217–239, Jun. 2009, doi: 10.1146/annurev.anchem.1.031207.113021.
- [79] D. E. Discher, A. Eisenberg, "Polymer Vesicles," *Science*, vol. 297, no. 5583, pp. 967–973, Aug. 2002, doi: 10.1126/science.1074972.
- [80] N. Huynh, L. V. Nguyen, and C. C. Lee, "Magnetic Nanostructures: Fabrication, Properties, and Applications," *J. Phys. Chem. C*, vol. 112, no. 30, pp. 11336–11368, Jul. 2008, doi: 10.1021/jp800612w.

- [81] E. O. Smetana, A. A. Smetana, and J. C. Giddings, "Ultracentrifugation, Zone Electrophoresis, and Related Techniques for Separation and Characterization of Macromolecules and Particles," *Analytical Chemistry*, vol. 55, no. 5, pp. 12A-34A, May 1983, doi: 10.1021/ac00257a005.
- [82] L. K. Patra and G. D. Sharma, "Characterization and applications of semiconductor nanoparticles," *J. Nanosci. Nanotechnol.*, vol. 8, no. 10, pp. 5263-5276, Oct. 2008, doi: 10.1166/jnn.2008.173.
- [83] Y. Liu, L. Liu, and Y. He, "Construction of glucose biosensors based on the nanomaterials," *Electroanalysis*, vol. 20, no. 1, pp. 5-15, Jan. 2008, doi: 10.1002/elan.200703878.
- [84] A. N. Shipway, E. Katz, and I. Willner, "Nanoparticle arrays on surfaces for electronic, optical, and sensor applications," *ChemPhysChem*, vol. 1, no. 1, pp. 18-52, Jan. 2000, doi: 10.1002/1439-7641(20000915)1:1<18::AID-CPHC18>3.0.CO;2-I.
- [85] C. M. Aikens and G. C. Schatz, "Understanding the Optical Properties of Metal Nanoparticles: Insights from Computational Methods," *Chem. Soc. Rev.*, vol. 37, no. 5, pp. 1043-1055, May 2008, doi: 10.1039/b711490g.
- [86] M. S. Bakshi, M. B. Thakkar, and S. D. Patel, "Acute toxicity of zinc oxide nanoparticles to rats," *Journal of Pharmacy & Bioallied Sciences*, vol. 4, no. 7, pp. 349-354, Sep. 2012, doi: 10.4103/0975-7406.103255.
- [87] J. Zhang, H. Liu, and Y. Sun, "Purification of single-walled carbon nanotubes," *Materials Science & Engineering R: Reports*, vol. 59, no. 1, pp. 1-23, Aug. 2008, doi: 10.1016/j.mser.2007.07.001.
- [88] S. J. Oldenburg, R. D. Averitt, S. L. Westcott, and N. J. Halas, "Nanoengineering of optical resonances," *Chemical Physics Letters*, vol. 288, no. 2-4, pp. 243-247, Apr. 1998, doi: 10.1016/S0009-2614(98)00277-2.
- [89] S. Y. Lee and J. H. Lee, "Facile preparation of highly stable and magnetic iron oxide nanoparticles via surface regulation: A promising material for biomedical applications," *Materials Science and Engineering: C*, vol. 83, no. 1, pp. 166-173, Jul. 2018, doi: 10.1016/j.msec.2017.08.060.

- [90] E. L. S. Costeira, A. M. G. Silva, and C. L. M. Silva, "Carbon nanotubes as a novel tool for vaccination against infectious diseases and cancer," *Journal of Nanoscience and Nanotechnology*, vol. 10, no. 12, pp. 8657-8670, Dec. 2010, doi: 10.1166/jnn.2010.2694.
- [91] K. K. Dey and V. Srinivasan, "Incorporation of Carbon Nanotubes in Electrically Conductive Adhesives for Bonding Applications," *Nanotechnology*, vol. 19, no. 14, pp. 145710, Apr. 2008, doi: 10.1088/0957-4484/19/14/145710.
- [92] G. Zhang, Y. Jia, F. Li, Y. Jiang, and Y. Wang, "A brief review on atomic force microscopy technology and its application in surface morphology studies," *Journal of Materials Science & Technology*, vol. 34, no. 4, pp. 322-330, Apr. 2018, doi: 10.1016/j.jmst.2017.08.001.
- [93] L. Wang, X. Wang, X. Zhang, X. Hu, and Q. Wang, "Polymer/nanoparticle composites: From fundamental interactions to applications," *Materials Chemistry Frontiers*, vol. 3, no. 1, pp. 11-29, Jan. 2019, doi: 10.1039/C8QM00428E.
- [94] H. Y. Chan, D. St C. Black, T. Karunaratne, A. Bansal, R. K. O'Reilly, D. J. L. Brett, and R. M. Williams, "A highly stable cathode for lithium-oxygen batteries," *Nature Communications*, vol. 6, no. 1, pp. 1-10, Jun. 2015, doi: 10.1038/ncomms8582.
- [95] A. V. Kabashin, P. Evans, X. M. Yu, and B. R. Davies, "Surface plasmon resonance excitation of gold nanoparticles and spectroscopic detection of biomolecular binding on surfaces," *Journal of Molecular Structure*, vol. 744-747, no. 1, pp. 613-619, Aug. 2005, doi: 10.1016/j.molstruc.2004.11.052.
- [96] M. T. Anwar, M. M. Hassan, M. A. Bakar, S. E. I. Dughaish, and M. A. Awang, "Effect of pH on the photo-catalytic reduction of CO₂ over TiO₂ nanoparticles," *Journal of Materials Science: Materials in Electronics*, vol. 27, no. 7, pp. 6762-6767, Jul. 2016, doi: 10.1007/s10854-016-4808-0.
- [97] C. Yu, Z. Niu, X. Liu, and L. Zhang, "A review of the fabrication and properties of vapor-grown carbon nanofiber/polymer composites," *Composites Science and Technology*, vol. 75, no. 1, pp. 1-7, Jan. 2013, doi: 10.1016/j.compscitech.2012.11.016.

- [98] D. J. Broer, D. P. C. O. v. d. Vos, M. E. van der Kooij, and R. A. L. Vallée, "Surface-relief gratings formed by visible light exposure of smectic liquid crystal films," *Nature*, vol. 378, no. 6558, pp. 467-469, Nov. 1995, doi: 10.1038/378467a0.
- [99] S. Zhang, D. Xie, X. Wang, Z. Wang, and D. Guan, "Superior mechanical strength of graphene/cement composite," *Composites Part B: Engineering*, vol. 43, no. 5, pp. 2583-2589, Jul. 2012, doi: 10.1016/j.compositesb.2012.03.007.
- [100] T. A. Taton, C. A. Mirkin, and R. L. Letsinger, "Scanometric DNA Array Detection with Nanoparticle Probes," *Science*, vol. 289, no. 5485, pp. 1757-1760, Sep. 2000, doi: 10.1126/science.289.5485.1757.
- [101] A. H. Lu, E. L. Salabas, and F. Schüth, "Magnetic nanoparticles: Synthesis, protection, functionalization, and application," *Angewandte Chemie International Edition*, vol. 46, no. 8, pp. 1222-1244, Feb. 2007, doi: 10.1002/anie.200602866.
- [102] H. Wei, E. Wang, "Knotting carbon nanotubes with DNA," *Nature Materials*, vol. 5, no. 10, pp. 771-772, Sep. 2006, doi: 10.1038/nmat1738.
- [103] Y. N. Xia and Y. M. Xiong, "Shape-controlled synthesis of metal nanocrystals: Simple chemistry meets complex physics?" *Angewandte Chemie International Edition*, vol. 48, no. 1, pp. 60-103, Dec. 2008, doi: 10.1002/anie.200802248.
- [104] D. J. Pine, D. A. Weitz, P. M. Chaikin, and E. Herbolzheimer, "Diffusing wave spectroscopy," *Physical Review Letters*, vol. 60, no. 12, pp. 1134-1137, Mar. 1988, doi: 10.1103/PhysRevLett.60.1134.
- [105] X. Huang, P. K. Jain, I. H. El-Sayed, and M. A. El-Sayed, "Plasmonic photothermal therapy (PPTT) using gold nanoparticles," *Lasers in Medical Science*, vol. 23, no. 3, pp. 217-228, Aug. 2008, doi: 10.1007/s10103-007-0470-x.
- [106] S. A. Maier and H. A. Atwater, "Plasmonics: Localization and guiding of electromagnetic energy in metal/dielectric structures," *Journal of Applied Physics*, vol. 98, no. 1, pp. 011101, Jul. 2005, doi: 10.1063/1.1951057.

- [107] B. Nikoobakht and M. A. El-Sayed, "Preparation and Growth Mechanism of Gold Nanorods (NRs) Using Seed-Mediated Growth Method," *Chemistry of Materials*, vol. 15, no. 10, pp. 1957-1962, May 2003, doi: 10.1021/cm020732l.
- [108] S. Link and M. A. El-Sayed, "Spectral properties and relaxation dynamics of surface plasmon electronic oscillations in gold and silver nanodots and nanorods," *The Journal of Physical Chemistry B*, vol. 103, no. 40, pp. 8410-8426, Sep. 1999, doi: 10.1021/jp9917648.
- [109] J. J. Storhoff, A. A. Lazarides, R. C. Mucic, C. A. Mirkin, R. L. Letsinger, and G. C. Schatz, "What controls the optical properties of DNA-linked gold nanoparticle assemblies?" *Journal of the American Chemical Society*, vol. 122, no. 19, pp. 4640-4650, May 2000, doi: 10.1021/ja993872b.
- [110] T. R. Jensen, C. H. Nielsen, L. P. Nielsen, and J. B. Wagner, "Synthesis and characterization of superparamagnetic nanoparticles for biomolecule conjugation and delivery," *Advanced Functional Materials*, vol. 15, no. 8, pp. 1243-1248, Aug. 2005, doi: 10.1002/adfm.200400423.
- [111] J. Lee, M. A. Musick, S. P. Wiseman, and R. P. Van Duyne, "Nanoscale SE(R)RS Substrates: Physical Structure, Raman Enhancement Mechanism, and Molecular Sensing," *Journal of Physical Chemistry B*, vol. 109, no. 12, pp. 5806-5811, Mar. 2005, doi: 10.1021/jp045965p.
- [112] L. Zang, W. A. Wei, and X. H. Jiang, "A study of enzymatic biosensors based on nanostructural materials," *Microchimica Acta*, vol. 150, no. 1-2, pp. 1-17, Feb. 2005, doi: 10.1007/s00604-005-0386-y.
- [113] H. Wang, X. Zhang, G. Wang, Y. Zhang, and L. Guo, "Influence of B and Ni doping on the electronic structure and optical absorption of anatase TiO₂: A first-principles study," *Physical Review B*, vol. 76, no. 16, pp. 165202, Oct. 2007, doi: 10.1103/PhysRevB.76.165202.
- [114] M. M. Maye, C. Han, R. A. Korgel, and T. P. Russell, "Template-Assisted Self-Assembly: A Practical Route to Complex Aggregates of Monodispersed Colloids with Well-Defined Size, Shape, and Structure," *Langmuir*, vol. 21, no. 15, pp. 6799-6803, Jul. 2005, doi: 10.1021/la0501335.

- [115] R. M. Williams and R. A. Dwek, "Glycomics: Where are we now?" *Current Opinion in Chemical Biology*, vol. 7, no. 5, pp. 616-621, Oct. 2003, doi: 10.1016/j.cbpa.2003.08.006.
- [116] Y. N. Xia, Y. Xiong, B. Lim, and S. E. Skrabalak, "Shape-controlled synthesis of metal nanocrystals: The case of silver," *Chemistry - A European Journal*, vol. 12, no. 34, pp. 8957-8964, Dec. 2006, doi: 10.1002/chem.200600713.
- [117] K. L. Kelly, E. Coronado, L. L. Zhao, and G. C. Schatz, "The Optical Properties of Metal Nanoparticles: The Influence of Size, Shape, and Dielectric Environment," *The Journal of Physical Chemistry B*, vol. 107, no. 3, pp. 668-677, Jan. 2003, doi: 10.1021/jp026731y.
- [118] A. S. Sussha, V. Kochetygov, A. L. Rogach, A. O. Orlov, D. N. Dirin, A. I. Baranov, and N. P. Gaponik, "Rapid Phase Transfer of Anisotropic PbS Quantum Dots Assisted by Trifluoromethanesulfonic Acid and Its Application in Solar Cells," *ACS Applied Materials & Interfaces*, vol. 12, no. 4, pp. 4793-4801, Jan. 2020, doi: 10.1021/acsami.9b20616.
- [119] T. R. Lee, W. S. Chang, S. M. Bozhilov, J. P. H. Burt, P. C. Searson, "Flexible and Stretchable Nanowire Coatings for Smart Surfaces: Tunable Wettability, Icephobicity, and Sensing," *Langmuir*, vol. 34, no. 9, pp. 3044-3051, Feb. 2018, doi: 10.1021/acs.langmuir.8b00038.
- [120] G. H. Li, Y. T. Li, L. R. Jiang, X. H. Hu, X. C. Chen, and Z. F. Liu, "Highly-sensitive acetaldehyde gas sensor based on ZnO nanoparticles prepared via a solution combustion method," *Sensors and Actuators B: Chemical*, vol. 255, no. 3, pp. 2504-2510, May 2018, doi: 10.1016/j.snb.2017.09.174.
- [121] Y. F. Zhang, J. Lu, C. H. Zhou, W. J. Wei, J. H. Yang, and G. G. Wu, "Morphology evolution and field emission properties of hierarchical NiO nanostructures synthesized via a simple thermal evaporation route," *Journal of Nanoparticle Research*, vol. 12, no. 8, pp. 2807-2815, Nov. 2010, doi: 10.1007/s11051-010-0051-2.
- [122] M. E. Caswell and B. D. Murphy, "Synthesis and Catalytic Application of Palladium Nanoparticles: A Review," *Colloids and Surfaces A: Physicochemical and Engineering Aspects*, vol. 448, no. 1, pp. 44-55, Sep. 2014, doi: 10.1016/j.colsurfa.2013.12.002.
- [123] X. Liu, D. Pan, T. Wu, C. Shi, Y. Hu, and J. Li, "Silver nanoparticles decorated graphene oxide for highly effective photocatalytic and antimicrobial activities," *Journal of*

Alloys and Compounds, vol. 735, no. 1, pp. 2308-2317, Dec. 2018, doi: 10.1016/j.jallcom.2017.11.305.

[124] S. K. H. Chu and R. M. Dickson, "Controlling the fluorescence of quantum dots by pH," *The Journal of Physical Chemistry Letters*, vol. 1, no. 20, pp. 2964-2969, Sep. 2010, doi: 10.1021/jz101257p.

[125] J. A. Fagan, J. M. Lürßen, and L. W. Wang, "Direct and indirect band gap energy of cubic silicon carbide," *Applied Physics Letters*, vol. 85, no. 4, pp. 635-637, Jul. 2004, doi: 10.1063/1.1777839.

[126] W. Liu, M. Liu, Z. Wang, and Y. Wang, "Synthesis and antimicrobial activity of copper nanoparticles prepared via a chemical reduction route," *Microbial Pathogenesis*, vol. 110, no. 3, pp. 245-251, Nov. 2017, doi: 10.1016/j.micpath.2017.07.045.

[127] A. Reginald-Opara, C. U. Iroegbu, F. A. Umeoduagu, and J. O. Ejiogu, "Green synthesis, characterization and antibacterial efficacy of silver nanoparticles using methanolic stem extract of *Theobroma cacao*," *Journal of Microbiology, Biotechnology and Food Sciences*, vol. 8, no. 1, pp. 819-825, Apr. 2019, doi: 10.15414/jmbfs.2018-19.8.1.819-825.

[128] G. H. Wu, Z. L. Xu, G. P. Wu, Z. Z. Li, J. H. Li, and M. Y. Yin, "Sonochemical synthesis of PbS nanoparticles: effects of solvents and stabilizers," *Materials Chemistry and Physics*, vol. 85, no. 1, pp. 27-32, Jul. 2004, doi: 10.1016/j.matchemphys.2004.01.009.

[129] L. Xu, Q. Jiang, Y. Xiao, Y. Lin, L. J. Deng, and W. X. Zhang, "Surfactant-assisted synthesis and photocatalytic property of highly monodisperse zinc sulfide nanospheres," *Materials Letters*, vol. 60, no. 11, pp. 1404-1407, Apr. 2006, doi: 10.1016/j.matlet.2005.11.032.

[130] S. V. Dorozhkin, "Calcium orthophosphates (CaPO₄): occurrence and properties," *Progress in Biomaterials*, vol. 1, no. 1, pp. 2-35, Jan. 2012, doi: 10.1186/2194-0517-1-2.

[131] A. L. R. Bugatti, P. G. C. Pujatti, J. M. A. Ribeiro, F. G. Emery, and S. E. Mazzetto, "Photoluminescent sensors based on gold nanoparticles," *Analytical and Bioanalytical Chemistry*, vol. 404, no. 1, pp. 141-150, May 2012, doi: 10.1007/s00216-012-6175-8.